# UNIVERSITY OF GAZİANTEP
# GRADUATE SCHOOL OF
# NATURAL & APPLIED SCIENCES

# DESIGN OF CRACK-FREE, DURABLE AND DUCTILE CONCRETE FOR SUSTAINABLE HIGHWAY RIGID PAVEMENT OVERLAYS

## Ph. D. THESIS
## IN
## CIVIL ENGINEERING

## BY
## HASAN ERHAN YÜCEL
## APRIL 2013

# Design of Crack–Free, Durable and Ductile Concrete for Sustainable Highway Rigid Pavement Overlays

**Ph.D. Thesis**
**In**
**Civil Engineering**
**University of Gaziantep**

**Supervisor**
**Assoc. Prof. Dr. Mustafa ŞAHMARAN**

**Co-Supervisor**
**Assoc. Prof. Dr. Murat GÜLER**

**by**
**Hasan Erhan YÜCEL**
**April 2013**

T.C.
UNIVERSITY OF GAZİANTEP
GRADUATE SCHOOL OF
NATURAL & APPLIED SCIENCES
CIVIL ENGINEERING DEPARTMENT

Name of the thesis: Design of Crack-Free, Durable and Ductile Concrete for
Sustainable Highway Rigid Pavement Overlays

Name of the student:  Hasan Erhan YÜCEL
Exam date:            24.04.2013

Approval of the Graduate School of Natural and Applied Sciences

Assoc. Prof. Dr. Metin BEDİR
Director

I certify that this thesis satisfies all the requirements as a thesis for the degree of
Doctor of Philosophy.

Prof. Dr. Mustafa GÜNAL
Head of Department

This is to certify that we have read this thesis and that in our opinion it is fully
adequate, in scope and quality, as a thesis for the degree of Doctor of Philosophy.

Assoc. Prof. Dr. Murat GÜLER          Assoc. Prof. Dr. Mustafa ŞAHMARAN
Co-Supervisor                         Supervisor

Examining Committee Members                     Signature

Prof. Dr. Mustafa ÖZAKÇA
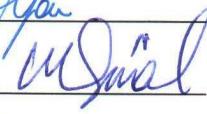
Prof. Dr. İsmail Özgür YAMAN

Prof. Dr. Mustafa GÜNAL

Assoc. Prof. Dr. Erdoğan ÖZBAY

Assoc. Prof. Dr. Mustafa ŞAHMARAN

I hereby declare that all information in this document has been obtained and presented in accordance with academic rules and ethical conduct. I also declare that, as required by these rules and conduct, I have fully cited and referenced all material and results that are not original to this work.

Hasan Erhan YÜCEL

To my wife and my little son…

**ABSTRACT**

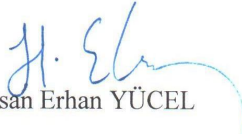**Design of Crack-Free, Durable and Ductile Concrete for Sustainable Highway Rigid Pavement Overlays**

YÜCEL, Hasan Erhan
Ph.D. in Civil Engineering
Supervisor: Assoc. Prof. Dr. Mustafa ŞAHMARAN
Co-Supervisor: Assoc. Prof. Dr. Murat GÜLER
April 2013, 143 pages

The superior ductility with high strength and improved durability characteristics suggest that the Engineered Cementitious Composites (ECC) could be used as an alternative to conventional concrete overlay materials. In this thesis, the research program was divided into two phases. In the first phase, an experimental program was performed to understand the dependence of the composite properties on its mixture composition governed by mineral admixture types and maximum aggregate size and amount. In the second phase, two different ECC-overlay mixture designs were selected from the first phase: one with high strength and moderate ductility, and the other with moderate strength and high ductility. The performance of two selected ECC mixture as an overlay material was investigated by laboratory experiments. Micro-silica concrete (MSC) was also prepared as a reference mixture. The layered composite specimens' flexural strength, reflective cracking characteristics and bond properties were investigated as performance criteria. The test results show that, layered ECC beams have significantly increased both load carrying capacity and deformability and shows better crack width control in comparison with MSC composite beam. Also, ECC increases bond strength, eliminates the reflective cracking and delamination failure in repaired systems and ECC overlay with 35 mm thickness is superior to MSC overlay with 50 mm thickness for rehabilitating concrete pavements. The superior performance of ultra-thin ECC overlay system under mechanical loading will be expected to prolong the service life of the structure under traffic loading and to reduce the costs in the rehabilitation work.

***Keywords:*** Engineered Cementitious Composites (ECC); Reflective cracking; Bond strength; Rigid pavement overlay.

# ÖZ

## Sürdürülebilir Karayolu Rijit Üstyapı Kaplamaları İçin Çatlaksız, Dayanıklı ve Sünek Beton Tasarımı

YÜCEL, Hasan Erhan
Doktora Tezi, İnşaat Mühendisliği Bölümü
Tez Yöneticisi: Doç. Dr. Mustafa ŞAHMARAN
Yardımcı Tez Yöneticisi: Doç. Dr. Murat GÜLER
Nisan 2013, 143 sayfa

Yüksek dayanım ile yüksek süneklik ve gelişmiş dayanıklılık özellikleri, Tasarlanmış Çimento Esaslı Kompozitler (ECC)'in beton kaplama malzemelerine bir alternatif olarak kullanılabilirliğini akla getirmektedir. Bu tezde araştırma programı iki safhaya ayrılmıştır. Birinci safhada, maksimum tane boyutu ve agrega miktarının kompozitlerin özellikleri ile olan ilişkisini saptamak amacıyla bir deney program yapılmıştır. İkinci safhada, biri yüksek dayanım ve orta sünekliliğe, diğeri ise orta dayanım ve yüksek sünekliliğe sahip iki farklı ECC-kaplama karışımı seçilmiştir. Seçilen iki ECC karışımının kaplama malzemesi olarak performansları laboratuvar deneyleriyle incelenmiştir. Ayrıca mikro-silika betonu (MSB) referans karışımı olarak hazırlanmıştır. Tabakalı kompozit numunelerin eğilme dayanımı, yansıma çatlağı ve bağ özellikleri performans kriterleri olarak incelenmiştir. Deney sonuçları göstermektedir ki, tabakalı ECC kirişlerinin MSB'ye göre daha yüksek yük taşıma kapasitesi ve şekil değiştirebilme özelliklerine sahiptir ve daha iyi çatlak genişliği kontrolü göstermektedir. Ayrıca, ECC bağ dayanımını arttırmış, onarılmış sistemdeki yansıma çatlağı ve ayrılarak kırılmayı ortadan kaldırmış, ve beton üstyapıların iyileştirilmesinde 35 mm kalınlığındaki ECC kaplama 50 mm kalınlığındaki MSB kaplamaya göre daha üstün olmuştur. Mekanik yükleme altındaki üstün performansı ile ultra-ince ECC kaplama sisteminin trafik yükleri altındaki yapının kullanım ömrünü uzatması ve onarım maliyetini düşürmesi beklenmektedir.

**Anahtar Kelimeler:** Tasarlanmış Çimento Esaslı Kompozitler (ECC); Yansıma çatlağı; Bağ dayanımı; Rijit üstyapı kaplaması.

# ACKNOWLEDGEMENT

# TABLE OF CONTENTS

# LIST OF FIGURES

xvii

# LIST OF TABLES

# LIST OF SYMBOLS/ABBREVIATIONS

| | |
|---|---|
| A | Aggregate |
| ACP | Asphalt concrete pavement |
| AEA | Air-entrained admixture |
| ASR | Alkali-silica reaction |
| AWI | Aggregate wear index |
| B | Binder |
| C | Portland cement |
| CH | Calcium hydroxide |
| $d_f$ | Fiber diameter |
| DOT | Department of transportation |
| $e^{f\phi}$ | Accounts for the changes in bridging force for fibers crossing at an inclined angle to the crack plane |
| $E_m$ | Elastic modulus of the mortar matrix |
| ECC | Engineered cementitious composites |
| f | Snubbing coefficient |
| $f\left(\dfrac{a}{W}\right)$ | Geometric calibration factor |
| F-T | Freeze-thaw cycle |
| F_ECC | Selected ECC with fly ash |

| | |
|---|---|
| FA | Fly ash |
| FRC | Fiber reinforced concrete |
| GGBFS | Ground granulated blast furnace slag |
| HPFRCC | High performance fiber reinforced cementitious composites |
| HRWR | High range water reducing admixture |
| $J'_b$ | Complimentary energy |
| $J_{tip}$ | Fracture energy of the mortar matrix |
| $K_m$ | Fracture toughness of the mortar matrix |
| $L_f$ | Fiber length |
| LVDT | Linear variable displacement transducer |
| MAS | Maximum aggregate size |
| MDOT | Michigan department of transportation |
| MIP | Mercury intrusion porosimetry |
| MOR | Modulus of rupture |
| MS | Microsilica |
| MSC | Micro silica concrete |
| $P_Q$ | Applied load |
| $P(\delta)$ | Pullout load versus displacement relation of a single fiber aligned normal to the crack plane |
| $p(\phi)$, $p(z)$ | Probability density functions |
| PCCP | Portland cement concrete pavement |

| PE | Polyethylene |
|----|--------------|
| PVA | Polyvinyl-alcohol fibers |
| RCPT | Rapid chloride permeability test |
| RH | Relative humidity |
| S | Slag |
| S_ECC | Selected ECC with slag |
| SEM | Scanning electron microscope |
| SUBC | Substrate concrete |
| T | Bond strength |
| UPV | Ultrasonic pulse velocity |
| $V_f$ | Fiber volume fraction |
| W | Water |
| W/B | Water to binder ratio |
| W/C | Water to cement ratio |
| z | Centroidal distance of a fiber from the crack plane |
| $\sigma_0$ | Maximum crack bridging stress of the mortar matrix |
| $\sigma_{fc}$ | First cracking strength of the mortar matrix |
| $\delta_0$ | Crack opening |
| $\phi$ | Orientation angle of the fiber |

## CHAPTER I

## INTRODUCTION

### 1.1 General

The use of rigid concrete pavements has become increasingly popular for places subjected to moderate and heavy traffic loads, such as bridge deck, highway and airport pavements and industrial floor rehabilitation, due to their high load carrying capacity and low maintenance requirement compared to asphalt concrete pavements (Zhang and Li, 2002). Several hundred thousand kilometers of rigid concrete pavements had been built around the world in the past decades. At present, most of those concrete pavements are either approaching the end of their design lives or in need of repair (Emmanuel et al., 1998). For pavements subjected to moderate and heavy traffic loads, the most common rehabilitation method is to place an overlay on the existing pavement. Asphalt concrete and Portland cement concrete are the most prevalent materials to form the overlays, which protect the structure of existing pavement, reduce the pavement deterioration rate, provide a smooth riding surface and strengthen the existing pavement, thus extending the pavement service life (Emmanuel et al., 1998). Depending on the application, traffic requirements and condition of the pavement structure, an overlay may be as thin as 50 mm (ultra-thin) or as thick as 150 mm or more (Fwa and Paramasivam, 1990; Risser et al., 1993; Cable and Hart, 1998). Although, this is a good solution for pavement improvement, some problems can still appear such as reflective cracking, which occurs when the existing cracks in the underlying pavements reflect into the newly constructed overlay under shrinkage and/or temperature change, and traffic loads. Cracking in overlay slabs allows water and other aggressive agents, such as deicing salts, to enter into the coating layer, thereby, leading to corrosion and rupture of the reinforcing bar and hence decreasing the structural capacity of pavement.

Cracks in the top layer of a pavement may also cause pumping of soil particles through the cracks, thus reducing the soil load bearing capacity (Sikdar et al., 1999).

1

Also, severely spalled and wide cracks will increase the roughness of the pavement and reduce its serviceability level and discomfort for users, finally leading to service termination. In addition to the reflective cracking, due to the change in deformation behavior between new constructed overlay and old pavement under mechanical and environmental loading, a certain delamination along the interface of overlay and old pavement starting from the existing cracks will take place (Zhang and Li, 2002). Therefore, the prevention of overlay delamination and reflective cracking in overlaid slabs are crucial.

The quasi-brittle nature of plain concrete under mechanical and environmental loading is one of its major obstacles to the successful overlay applications. Cracks can spread instantly to result in failure at a low ultimate strain (around 0.01% ultimate tensile strain) without sign of deterioration through the brittle nature of concrete. During the last decade concrete technology has been undergoing rapid development. The effort to improve the brittle behavior of plain cementitious materials has resulted in modern concepts of high performance fiber reinforced cementitious composites (HPFRCC) that show pseudo-ductile behavior under uniaxial tension load. In plain concrete, after the first crack there is no load carrying capacity. In conventional fiber reinforced cementitious composites, matrix cracking is followed by a reduction in load carrying capacity known as residual strength. For HPFRCC, the fibers themselves are able to carry the additional load, after the formation of the first through crack. On further loading, multiple micro-cracks will form along the member, leading to a significant increase in strain. The tensile stress-strain curve will hence exhibit a post-cracking hardening branch similar to that of ductile materials.

Engineered Cementitious Composites (ECC) is a special class of HPFRCC with extremely high tensile ductility. It is designed to strain harden in tension based on micromechanical principles, which permits optimization of the composite for high performance represented by extreme ductility while minimizing the amount of reinforcing fibers, typically less than 2% by volume (Li, 1998; Li, 2003 and Li et al., 2001). The most distinctive characteristic separating ECC from conventional concrete and fiber reinforced concrete (FRC) is an ultimate tensile strain potential between 2 to 4%, contingent on the definite ECC mixture design. Along with tensile

ductility, the unique crack development within ECC is critical to its durability. Different from normal concrete and most fiber reinforced concretes, ECC displays self-controlled crack widths under loading. Crack widths of ECC remain tight, less than 100 μm, even at high imposed deformation. ECC represents a new concrete material that offers an important potential to resolving the durability problem of concrete structures, with high tensile ductility and inherently narrow crack width.

ECC promises to be used in a variety of civil engineering constructions, as explained in Japan Concrete Institute (JCI, 2002) and by Kunieda and Rokugo (2006). The repair application, using over an existing concrete, is one of the most successful areas of practice of this material (Zhang and Li, 2002; Lim and Li, 1997; Kamada and Li, 2000). Experimental testing of ECC overlays reveals important developments in system ductility and load-carrying capacity compared to conventional concrete or steel fiber reinforced concrete overlays (Qian, 2007). Along a specific ''kinking-and-trapping'' mechanism, the material's ductility efficaciously intercepts substrate cracks from reflecting along an ECC overlay. It was also seen that the normal failure phenomenon of delamination or spalling in maintained concrete overlays were extinguished with the use of ECC. Microcracks occupied from the edges of cracks on the ECC/concrete interface were kinked into and immediately captured in the ECC mixture. Therefore, the superficial crack wideness and interface delamination could be both miniaturized with the use of ECC. Moreover, reflective cracking could be consumed when ECC is applied for maintenance material (Zhang and Li, 2002).

## 1.2 Research Objectives and Scope

In this thesis, the research program was divided into two phases. In the first phase, an experimental program was performed to understand the dependence of the composite mechanical and durability properties on its mixture composition governed by mineral admixture types and replacement level, and maximum aggregate size and amount. As mentioned before, cracking in ECC is fundamentally different from that which occurs in concrete or reinforced concrete. ECC develops multiple micro-cracking in a strain-hardening response as a result of mechanical loading. Due to multiple micro-cracking, it is important to test the pre-cracked ECC under freeze-thaw cycles, which is of great importance for critical assessment of the durability of ECC under comprehensive conditions. Since no information is currently available on these

subjects. The objective of the first phase is intended to fill this knowledge gap.

Although lower life cycle costs are obtained due to reduced maintenance requirements, the current high cost of ECC may not justify their use (Kendall et al., 2008 and Zhang et al., 2008). It is necessary to optimize the overlay thickness in order to obtain optimum performance at lowest possible cost to facilitate the extended use of ECC in pavement construction (especially in developing countries). This is the main objective of the second phase of this thesis. Regarding the overlay materials, the type of supplementary cementitious material used in ECC production was varied to control its ductility and strength. Therefore, two different mixtures of ECC with fly ash and ground granulated blast furnace slag were used for the comparison of overlay performances. Layered ECC/concrete beams will be cast with three different ECC layer thicknesses, namely 25, 35 and 50 mm. After measuring the basic mechanical properties of monolithic overlay specimens (compressive strength, flexural strength, drying and restrained shrinkage), layered ECC_concrete beam in which a layer of ECC is applied beneath a layer of substrate concrete under four point-bending tests were performed to determine the reflective cracking and flexural performances. The influence of ECC's strength and ductility, and layer thickness on the strength and ductility of the layered beam are discussed in experimental aspects. Also, the bond properties of ECC mixtures are considered as a performance criteria. During the experimental study, microsilica concrete, one of the most commonly used overlay mixtures, was also cast and tested as a reference overlay material.

This thesis is organized into five chapters as follows: Chapter 1 describes introduction for the research, objectives of the research, and scope of the study. In Chapter 2, (i) Pavements and pavement types in general, and the most important problems about these pavements (ii) Proposed material solution for sustainable rigid pavement overlay (iii) Background of Engineered Cementitious Composites (ECC) (iv) Mechanical and environmental performance in pavement and cost of ECC are discussed in detail. In Chapter 3, experimental program, material properties and tests applied on the specimens are discussed. The results of the experimental studies are presented and discussed in Chapter 4. The conclusions of the research are presented in Chapter 5.

# CHAPTER II

## LITERATURE REVIEW AND BACKGROUND

### 2.1 Introduction

Pavement is the durable surface coating material laid down on a specific area desired to sustain traffic. The basic role of the pavement construction is to distribute wheel loads over a large area of the ground. In general, there are two types of pavements as concrete (rigid) and asphalt (flexible) (Figure 2.1). While rigid concrete pavements distribute the wheel loads nearly uniform over the subgrade, asphalt concrete pavements display a cone-shaped stress distribution under the wheel as seen in Figure 2.1 (Atkinson, 2003).
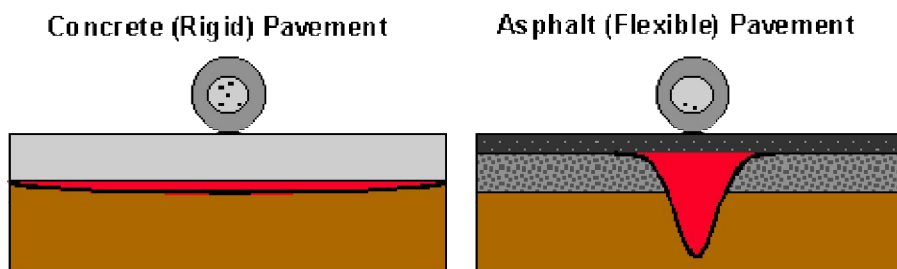


Figure 2.1 Pavement types (Atkinson, 2003)

There are several distresses that determine the serviceability performance of rigid and flexible pavements caused by repeated heavy traffic loads, temperature and moisture changes resulting in, such as fatigue cracking, bleeding, longitudinal cracking, rutting, faulting and spalling (Figure 2.2). In addition, the most important one of the distresses is reflective cracking (Figure 2.3) (Miller and Bellinger, 2003).

Reflective cracks are defined as fractures in a pavement overlay that are the result of reflecting the cracks or joint patterns from the underlying layer (Sherman, 1982). It especially occurs through the asphalt concrete pavement (ACP) overlays and Portland cement concrete pavement (PCCP) overlays placed over a new PCCP.

Vertical movement of the underlying PCCP at the location of cracks and joints occurs due to heavy traffic loads being applied to the pavement surface. These traffic loads cause shear and bending stresses to occur in the pavement system (Blankenship, 2007). Main cause of this movement in the underlying pavement is due to the poor joint load transfer efficiency. Horizontal movement is caused by the thermal expansion and contraction of the underlying PCCP (Aleis, 2004). Reflective cracks normally occur when the underlying pavement contracts due to a drop in the ambient air temperature. Temperature gradients in the PCCP also cause curling to occur in the underlying pavement (Cleveland et al., 2002). Moisture changes in the subgrade will also increase the movement in the underlying PCCP. While parallel movement of the pavement is not common, it can occur when the pavement exists in laterally unstable conditions (Mukhtar, 1996). These movements cause shear, tensile, and bending stresses to be exerted on the overlay (Von Quintus, 2007). Reflective cracks form due to the ACP overlay's inability to withstand these stresses (Cleveland et al., 2002).

Fatigue and temperature associated reflective cracking cause not only the serviceability loses, but also numerous other problems with the ACP overlays of PCCP. Reflective cracking increases surface roughness and maintenance cost for the pavement (Blankenship, 2007). It also allows water to penetrate into base and subgrade of the pavement system (Kallas, 1983). The water infiltration of the pavement system can cause the pavement to have premature distresses, resulting in spalling at the reflective crack locations, shortening the life of the pavement system, and decreasing the structural strength of the pavement system through loss of support of the base and subgrade (Button, 1989 and Jacob, 1990). Therefore, there is a significant need to develop new overlay materials which can meet mechanical, durability, and constructability demands of concrete pavements.

An asphalt concrete pavement (ACP) can provide advantages during and after construction. It can enable good serviceability with lower initial construction cost than rigid pavements. ACP overlays require less construction time and cost during the construction stage. Although there are several advantages, it has also some disadvantages. It may not be the most economical solution for the long-term rehabilitation. Due to their relatively short service life, ACP overlays will require

maintenance sooner than the other types of overlays, such as rigid overlays (Cho, 1995). Therefore, rigid pavement overlays can be preferred and become a good solution for reflective cracking when the concrete material is improved.



| Fatigue cracking | Bleeding |
| Logitudinal cracking | Rutting |
| Faulting | Spalling |

Figure 2.2 Pavement distresses (Miller and Bellinger, 2003)



Figure 2.3 Reflective cracking (Miller and Bellinger, 2003)

PCCP overlays are increasingly used as a rehabilitation technique for both existing portland cement concrete and ACP. The use of PCCP overlays have an important

advantage when compared with other coating materials about the properties such as extension of the service life, improved structural capacity, reduced repair needs and lower life-cycle costs (Smith et al., 2002).

PCCP overlays are separate into three types as bonded, partially bonded and unbonded state between the new PCCP overlay and the existing pavement. The selection of PCCP overlay type depends largely upon the condition of the existing pavement and on the future traffic levels (Smith et al., 2002).

Bonded PCCP overlays consist of a thin layer of PCCP (typically 76 to 102 mm) that is bonded to the existing pavement. These are used to increase the structural capacity of an existing pavement or to improve its overall ride quality and should be used where the underlying pavement is free of structural distress and in relatively good condition (ACPA, 1990a; McGhee, 1994). The most important construction and performance aspect of bonded PCCP overlays is the achievement of an effective bond between the overlay and the existing pavement. This is needed to create a pavement system that behaves monolithically; if such bonding is not achieved, cracking of the overlay will result due to increased curling and loading stresses (Smith et al., 2002).

Partially bonded PCCP overlays are placed directly on the existing pavement with little, if any, surface preparation. These are used where the question of whether and to what degree bonding takes place is not critical to the performance of the overlay (Lokken, 1981). Partially bonded PCCP overlays are commonly used on airfield pavement where required overlay thicknesses are typically much greater (because of heavy aircraft loads) and where the slabs are more fully restrained. On airfield pavements, partially bonded overlay thicknesses are generally greater than 305 mm, whereas on highway applications thicknesses are generally in the range of 152 to 203 mm (Smith et al., 2002). No special measures are taken to prepare the existing pavement to receive a partially bonded PCCP overlay, other than just sweeping the surface. As a result, varying degrees of bonding will occur, so reflective cracking can potentially be a problem. Consequently, partially bonded overlays should be used when the existing pavement is in sound, well-seated condition and with no measure distresses, distortions or rocking slabs (Lokken, 1981).

An unbonded PCCP overlay involves an interlayer between the existing pavement and the new PCCP overlay. This separation layer causes the behavior of these two slabs independent. Therefore, this phenomena supports the PCCP overlay about resistance to reflective cracking. Unbonded PCCP overlays are typically constructed between about 152 and 305 mm thick (Smith et al., 2002). When the existing pavement has a very high portion of disruption, unbonded PCCP overlays are used (ACPA, 1990b). In unbonded PCCP overlays, the two pavements will be split. Therefore, little overlay maintenance is needed. Nevertheless, it is important that the separator layer must be powerfully provide independent behavior between the two pavements. In general, ACPs (about 25 mm thick) are applied as a separator layer (Smith et al., 2002).

While the overlay is designed, it has to be controlled according to the adopted performance criteria established based on the requirements of the Department of Transportations (DOTs) as well as the available information in literature (Alhassan, 2007). A preliminary set of performance criteria established by DOTs is listed in Table 2.1.

Table 2.1 Adopted performance criteria (Alhassan, 2007)

| Property | | Test Method | Target Performance |
|---|---|---|---|
| **Air content** | | ASTM C231 | $7 \pm 1.5$ % |
| **Unit Weight** | | ASTM C138 | 2.16-2.40 g/ cm$^3$ |
| **Flexural strength** | | ASTM C78 | $\geq 3.10$ MPa at 7 days $\geq 4.48$ MPa at 28 days |
| **Compressive Strength** | | ASTM C39 | $\geq 27.6$ MPa at 7 days $\geq 41.0$ MPa at 28 days |
| **Toughness** | | ASTM C1018 | 30 % of $f_r$, residual strength |
| **Unrestrained drying shrinkage** | | ASTM C157 | $\leq 400$ με at 28 days $\leq 600$ με at 90 days |
| **Direct tensile bond strength** | | Standard Equipment | $\geq 2.07$ MPa at 7 days $\geq 2.76$ MPa at 28 days |
| **Permeability** | | ASTM C1202-97 | $\leq 2000$ coulomb |
| **Air-void parameters** | **Total entrained air** | ASTM C457 | $7 \pm 1.5$ % |
| | **Air-void spacing** | | $\leq 0.0254$ cm |
| | **Specific surface** | | $\geq 197$ cm$^{-1}$ |
| | **Number of voids** | | $\geq 3.15$ voids/cm |

**2.2 The Need for Sustainable Concrete Overlay**

Around the globe, nations struggle with ever increasing challenges of unsustainable development. The consequences of this struggle are often most visible in developing nations with rapidly expanding economies. Often, the backbone of such rapidly expanding economies is infrastructure development in the form of highways, airports, bridges, underground mass transit facilities, dams, wastewater treatment systems, marine structures and buildings, which support trade and encourage outside investment. Therefore, concrete material is, literally, one of the building blocks of economic development.

While essential for the development of economies, the construction and maintenance of these infrastructures often requires large volumes of portland cement and aggregate for use in concrete structures. The production of these materials can result in tremendous public health impacts decades into the future. To illustrate, the production of one tonne of Portland cement releases 6.3 mg of particles less than 10 microns in diameter ($PM_{10}$) into the atmosphere (Marlowe, 2003). Numerous deaths annually have been attributed to atmospheric $PM_{10}$ concentrations as low as 20 mg/m$^3$ (Ostro, 1994). In addition to direct public health concerns, the production of portland cement requires 4 GJ of energy per tonne, and releases into the atmosphere approximately 1 tonne $CO_2$ per tonne of cement, representing in total 7% of worldwide $CO_2$ emissions, and significantly contributing to global warming due to ozone depletion (Malhotra, 1998; Mehta, 1998). A signatory to the Kyoto Protocol, Turkey is committed to reducing its greenhouse gases emissions by about 29% below expected levels by 2012. Furthermore, mining large quantities of raw materials such as limestone and clay, and coal for fuel in the cement kiln, often results in extensive deforestation and topsoil loss. As a case study, Turkey has seen cement production increase from 30 million tonnes in 2001 to more than 51 million tonnes in 2008 (TCMA, 2009). Due to this rise in production, capacity utilization within Turkey has increased from 46% to over 80% from 2001 to 2008 requiring construction of new cement plants in the near future if demand does not fall. Moreover, as in cement production, mining of the aggregates used in concrete production causes significant ecological damage. The overall consequence is an inherently unsustainable system measured by economic, environmental, and social indicators. Sustainability requires

the application of energy efficient materials with low impact on environment and improved durability. Many concrete structures are prone to extensive distress due to improper design, material selection, and construction practices for a given service environment. Therefore, concrete production is a serious concern for global environmental sustainability. In spite of these environmental problems, the global demand for concrete increases at a very rapid pace, largely driven by the construction boom in developing countries; and in less than one century, concrete has become the most widely used construction material in the world. Concrete is now used not only for buildings but also for highways, airports, bridges, underground mass transit facilities, dams, wastewater treatment systems, and marine structures.

In European Design Codes, a service life time of 75+ for concrete structures is now required in large public works (Alexander and Stanish, 2005). But experience has shown that under the combined effects of mechanical loads and environment, many infrastructures start to deteriorate after only 20 or 30 years (Mehta and Burrows, 2001). The short service life of portland cement concrete infrastructures has significant impact due to materials production for repair and replacement of deteriorated infrastructure, along with fuel consumption and vehicle emissions from construction related traffic congestion. The poor durability of reinforced portland cement concrete infrastructure associated with concrete cracking is one of the main reasons for this short service life of concrete infrastructure (Mindess et al., 2003). Cracking is usually a result of various physical, chemical, and mechanical interactions between concrete and its environment, and it may occur at different stages throughout the life of a structure. The formation of cracks coupled with a lack of crack width control in brittle concrete are primarily responsible for two damaging phenomena; reduction of the strength and stiffness of the concrete structure, and acceleration of the ingress of aggressive ions, leading to other types of concrete deterioration such as corrosion, alkali-silica reaction (ASR), freeze/thaw damage and sulphate attack, and resulting in further cracking and disintegration (Mindess et al., 2003; Li and Li, 2007). Therefore, durability is vitally important for all concrete structures, and it can be associated with the brittle nature of concrete.

It is an unfortunate fact that very large amounts of existing concrete structures

worldwide are in a state of deterioration/distress (Vaysburd et al., 2004). Increased $CO_2$ concentrations in the atmosphere are expected to further weaken the chemical stability of concrete in these structures (Engineers Canada, 2008). Maintaining and repairing structures has been a recurring need owing to the natural degradation of materials and infrastructure under the combined effects of mechanical loads and environmental factors. In the past, the practice was to replace old and deficient structures that had deteriorated or that were no longer suited to their original purpose with new ones. In today's nebulous economic climate and high cost of replacement, emphasis has been on repair of existing structures rather than new construction.

Repair, retrofitting and rehabilitation of existing concrete structures have become a large part of the construction activity in both Turkey and Europe. The deterioration of highway pavements, airport runways and bridge decks poses serious problems and requires millions of euros to renovate them. By some estimates, the money spent on repairing of existing structures in recent years has exceeded that spent on new structures (Vecchio and Bucci, 1999). As an example, the costs for the maintenance of bridges are higher than $1 billion per year in Europe (Raupach, 2006). The total costs for maintenance of all types of buildings can be assumed to be higher than about $20 billion per year (Raupach, 2006). A significant part of this cost is spent on repair of concrete structures. In many countries, the amount of work conducted for building new structures is declining; however, the market of repair and protection has been growing considerably as the age of the existing infrastructure is increasing. The concrete overlay industry is thus facing a major challenge: How to stop or slow the decay of the world's infrastructure?

While more and more 'effective' overlay materials have been developed recently, concrete overlay experiences continue to represent a 'mixed bag'. Despite the best efforts of the overlay industry, the failure rate for concrete overlays remains unacceptably high. It has been estimated that almost half of all concrete overlays fail in the field (Mather and Warner, 2003). Concrete overlays are often perceived to lack both early age performance and long-term durability. Therefore, it is of utmost importance and challenge to develop effective, economical, and durable (ultra high performance) overlay materials, which would fundamentally address the underlying concrete deterioration problems and protect the existing concrete from aggressive

environments in the long term. In addition to focusing on effective and durable overlay materials, challenges include the development of more environmentally benign materials and the effective utilization of by-products and waste materials in the production of overlay materials.

## 2.3 Proposed Material Solution for Sustainable Rigid Pavement Overlay

An ideal overlay material, would be volumetrically stable, i.e. it would undergo neither shrinkage nor expansion once installed, and would display compatible modulus of elasticity, strength, creep, shrinkage, thermal expansion, permeability and electrochemical properties to the substrate. Unfortunately, despite the best efforts of product formulators such products do not appear to exist. Therefore, the best that can be hoped for are overlay materials that have a suitable mechanical properties and low volume change capacity that they neither shrink nor expand to the extent that they crack, or impose adequate interfacial shear stress (or direct tensile stress) to lead bond failure.

During the last decade concrete technology has been undergoing rapid development. The effort to modify the brittle behaviour of plain cement materials like concretes, cement pastes and mortars has resulted in modern concepts of high performance fiber reinforced cementitious composites (HPFRCC) that show ductile behaviour under uniaxial tension load. In plain concrete, after the crack there is no load carrying capacity (Figure 2.4). In conventional fiber reinforced cementitious composites, matrix cracking is followed by a reduction in load carrying capacity known as residual strength (lower curve in Figure 2.4). For HPFRCC, after the existence of the first through crack, the fibers themselves are able to carry additional load. On further loading, multiple micro cracks with crack width less than 100 μm will form along the member, spearheading to a significant increase in strain. The tensile stress-strain curve will hence exhibit a post-cracking hardening branch similar to that of ductile materials, such as aluminium (upper curves in Figure 2.4). The quantitative criterion for the achievement of ductility (inelastic straining), in terms of various material and geometric parameters (such as characteristics of fiber, matrix [composite without fiber], fiber-matrix interface, fiber geometry and volume fraction, etc.), was proposed by Li and Leung (1992) and further improved by Li (1993), and Kanda and Li (1999). With proper selection of parameters to fulfill the criterion, ductile composites

with different strengths can be made with fiber volume from 1.5% to 5%. The actual 'ductility' of the HPFRCC, which can be described as the strain at maximum tensile stress, depends on the effectiveness of fibers in transferring stress back into the matrix (which in turn depends on the microstructural parameters) as well as the toughness of the matrix itself (Li, 1997). Normally, the higher the matrix toughness, the lower will be the ductility achieved with a certain fiber volume fraction. Depending on the particular application, the material design can be varied to produce an optimal tensile stress vs. strain relation that satisfies the strength and ductility requirements. In the literature, HPFRCC's have been given different names by various researchers. These include CARDIFRC (Alaee and Karihaloo, 2003), hybrid fiber composites (Markovic et al., 2004) and MSFRCC (Rossi and Parant, 2005), which are the high strength composites with relatively low ductility, as well as HPFRCC (Li, 1993), a highly ductile HPFRCC with moderate fiber volume (tensile failure occurs at 2-5% strain – 200-500 times that of conventional concrete or fiber reinforced concrete) with relatively low strength. This type of HPFRCC is also called as Engineered Cementitious Composites (ECC).
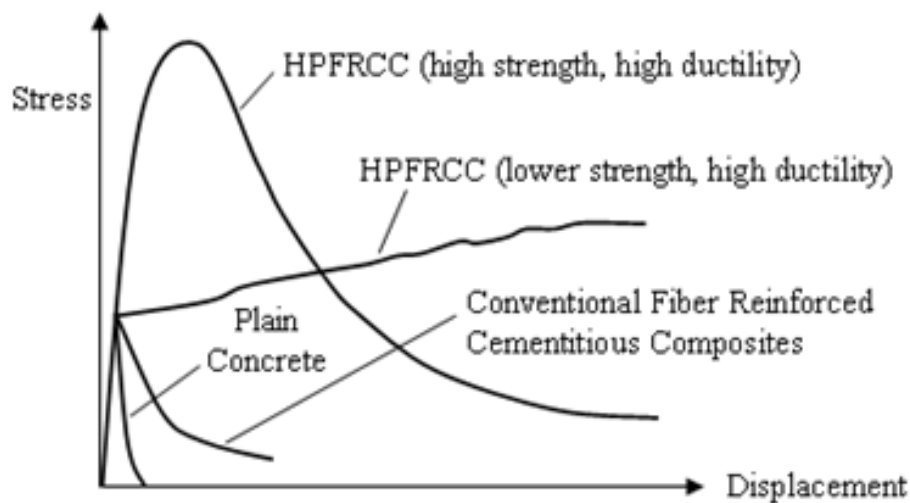


Figure 2.4 Tensile behavior of plain and fiber reinforced cementitious materials

Inelastic straining in the form of micro-crack damage has been demonstrated in ECC. Moreover, when crack width is small, the self-healing of cracks becomes featured. If durability, and eventually sustainability are substantial aims, current construction practice and the codes of recommended practice must undergo a paradigm shift to achieve concrete structures that have tight cracks or are 'crack-free' in preference to high strength. The formation of cracks coupled with a lack of crack width control in

brittle concrete are primarily responsible for distresses that can dramatically reduce the long-term durability performance of concrete. While it is unrealistic to imagine the complete suppression of cracking in concrete, the ability to use robust self-healing functionality as an autogenous mechanism in areas with tight cracks may lead to the realization of such virtually 'crack free' concrete. In 2002, the Concrete Research and Education Foundation also listed such robust self-healing concretes second in its list of 'high priority research topics' for the concrete industry (CREFSDC, 2002). Self-healing is generally attributed to the hydration of previously unhydrated cementitious material, calcite formation, expansion of the concrete in the crack flanks, crystallization and closing of cracks by solid matter in the water (Ramm and Biscoping, 1998). Self-healing of cracks can only be taken into account when crack width is small (generally less than about 150 μm). Self-healed cracks or very tight cracks (less than 0.1 mm) do not pose a durability problem in concrete structures (Sahmaran et al., 2007; Yang et al., 2009).

The ductile behavior and self-healing characteristic of ECC is associated with many other desirable properties for overlay applications. These include (i) high energy absorption, impact resistance and tensile ductility (high inelastic strain), (ii) ability to redistribute localized stresses, thus reducing the sensitivity of the material to stress concentrations, (iii) high deformability, passing ability, and resistance to segregation to secure complete filling of complex formwork and ease of production including self-consolidation casting and shotcreting (iv) high shear strength, (v) high bond strength to steel reinforcement and substrate concrete (high delamination resistance), and (vi) capability to control the opening of cracks, and hence preventing the resulting increase of transport properties that would lead to durability problems. However, three major limitations of ECC are the high cost, environmental issues and high shrinkage of the material. The cost is high because fibers are much more expensive than the basic components of conventional concrete. Currently, poly-vinyl alcohol (PVA), polyethylene (PE), and micro-steel fibers are the most successfully used fibers in the production of ECC. ECC is usually two to three times higher cement content than conventional concrete. Table 2.2 shows the ingredients and percentages of typically conventional structural concrete, PE-ECC (Li, 1997) and PVA-ECC (Li et al., 2002) mixtures. The high cement content of ECC is a result of rheology control for easy distribution of fiber, and more fundamentally, the control

of the matrix toughness for strain hardening behavior. To obtain a high ductility, fracture toughness should be limited in case cracking may occur before it reaches the maximum bridge stress. Therefore, restriction of the use of large aggregates in the mixture, resulting in a higher cement content in comparison with normal concrete. Actually, the ECC materials formed as a matrix of cement paste or mortar by using fine sand and has typically 800 to 1200 kg/m$^3$cement content. Undesirable high heat of hydration as well as high cost of materials and high drying shrinkage are the results of the use of high cement content. Cement production creates 7% of global greenhouse gas emissions generated by human activity (Malhotra, 1998; Mehta, 1998).Moreover, ECC could generate relatively large shrinkage strain compared to conventional concrete due to relatively high cement content, low water-cement ratio and lack of coarse aggregate, thus increasing cracking potential of the concrete. However, the presence of fibers can control the crack width such that deterioration is not an issue.

Table 2.2 Typical mixture proportions of concrete and ECCs

(Li, 1997; Li et al., 2002)

| Material (kg/m$^3$) | PVA-ECC | PE-ECC | Conventional Concrete |
|---|---|---|---|
| Portland Cement | 832 | 1205 | 390 |
| Water | 366 | 314 | 166 |
| Aggregates | 832 | 603 | 1717 |
| Fiber | 26 | 17 | - |
| Superplasticizer | 17 | 12 | 2 |

## 2.4 Engineered Cementitious Composites (ECC)

## 2.4.1 Background of Engineered Cementitious Composites

As a new class of HPFRCC materials, Engineered Cementitious Composites (ECC) is a ductile fiber reinforced cementitious composite micromechanically designed to achieve high damage tolerance under severe loading and high durability under normal service conditions (Li, 1998; Li et al., 2001; Li, 2003a). The most obvious

16

feature that separates ECC from Conventional concrete and fiber-reinforced concrete (FRC) is the certain contingency between 3 to 5% higher tensile strain capacity. The strain capacity of more than 300 times that of a normal concrete, allowing for the formation of microcracks is placed very closely. This increased load-bearing after the formation of cracks, as many ductile metals, allows to show hardening the material.

Although similar to a typical ECC, FRC component, verify the characteristics of the interface between components (i.e., aggregate, cement and fibers) with microcracking components by means of micromechanical strain hardening is carried out by means of tailoring (Li, 1998; Lin et al., 1999; Li et al., 2001; Li, 2003a). Fracture properties of cement are carefully controlled through the mixing ratios. Strength, elastic modulus and fiber properties, such as aspect ratio, the ECC has been customized for the user. In addition, the fiber-matrix interface between the properties of this material have been optimized for use in cooperation with the manufacturer.

Although, the main reason of HPFRCCs high performance is according to high fiber content in the mixture, ECC uses moderate quantity (about 2% by volume) of fiber content. This low fiber volume permits flexibility in construction execution. To date, ECC materials have been engineered for self-consolidation casting (Kong et al., 2003), extrusion (Stang and Li, 1999), shotcreting (Kim et al., 2003), and conventional mixing in a gravity mixer or conventional mixing truck (Lepech and Li, 2008).

Figure 2.5 shows uniaxial tensile stress-strain curve for a typical ECC containing 2% poly-vinyl-alcohol (PVA) fiber. The characteristic strain-hardening behavior after first cracking is accompanied by multiple microcracking. Figure 2.5 also shows the development of the microcrack width during inelastic straining. Even at ultimate load, crack widths are smaller than 80 microns. This compound tight crack width to be used in combination with traditional reinforcement or self-reinforcement ratio is controlled and independent feature of the material. On the contrary, normal concrete and fiber-reinforced concrete rely on steel reinforcement to control crack width. Under severe bending loads, the ECC beam has been deformed ductile plastic deformation similar to a metal plate (Figure 2.6). In compression, ECC materials exhibit compressive strengths similar to high strength concrete (e.g. greater than 60 MPa) (Lepech and Li, 2008).
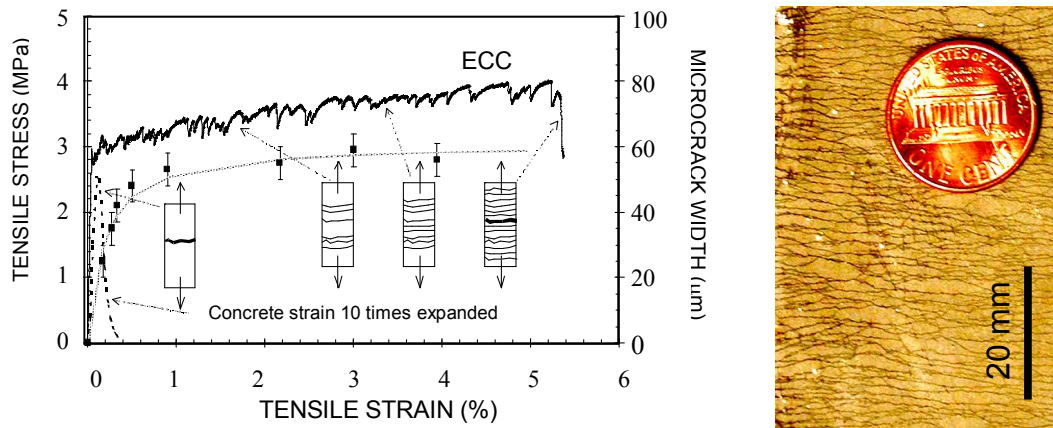
Figure 2.5 Typical tensile stress-strain curve and crack width development of ECC
(Weimann and Li, 2003a)
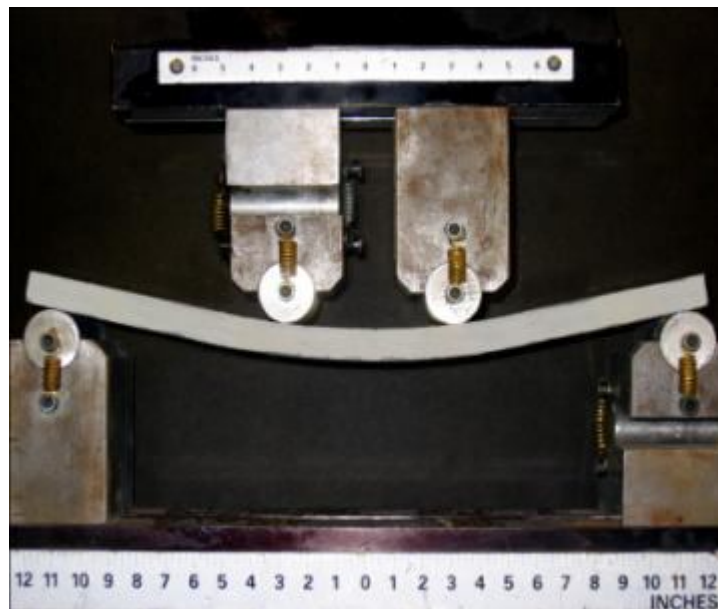


Figure 2.6 Response of ECC under flexural loading (Weimann and Li, 2003a)

### 2.4.2 Design of Engineered Cementitious Composites

In ECC material design, the first priority is to provide the formation of multiple cracks and deformation hardening behavior under load. This allows the formation of micro-cracks distributed over multiple large deformations. Firstly, Marshall and Cox (1988) characterized steady-state crack propagation in multiple micro-cracking and strain hardening of ECC. After that, Li and Leung (1992) and Lin et al (1999) studied extended fiber reinforced cementitious composites. Instead of the typical strain softening fiber reinforced cementitious material to expand during the spread of the Griffith-type cracks again, while advancing crack width to maintain a constant steady-state "flat cracks" by creating multiple micro-cracks in ECC saturate the

18

sample material exhibited strain-hardening going through extreme stress during deformation. The interaction between cracking stress and crack width manages the multiple steady-state cracking texture. Inequality seen in Equation-2.1 must be implemented to obtain this circumstance.

$$J_b^{'} = \sigma_0 \delta_0 - \int_0^{\delta_0} \sigma(\delta)d\delta \geq J_{tip} \approx \frac{K_m^2}{E_m} \quad (2.1)$$

where $J_b^{'}$ is the complimentary energy shown in Figure 2.7, $\sigma_0$ and $\delta_0$ are the maximum crack bridging stress and corresponding crack opening, $J_{tip}$ is the fracture energy of the mortar matrix, $K_m$ is the fracture toughness of the mortar matrix, and $E_m$ is the elastic modulus of the mortar matrix. A strength criterion seen in Equation-2.2 must be implemented, additionally to the fracture energy criterion.

$$\sigma_0 > \sigma_{fc} \quad (2.2)$$
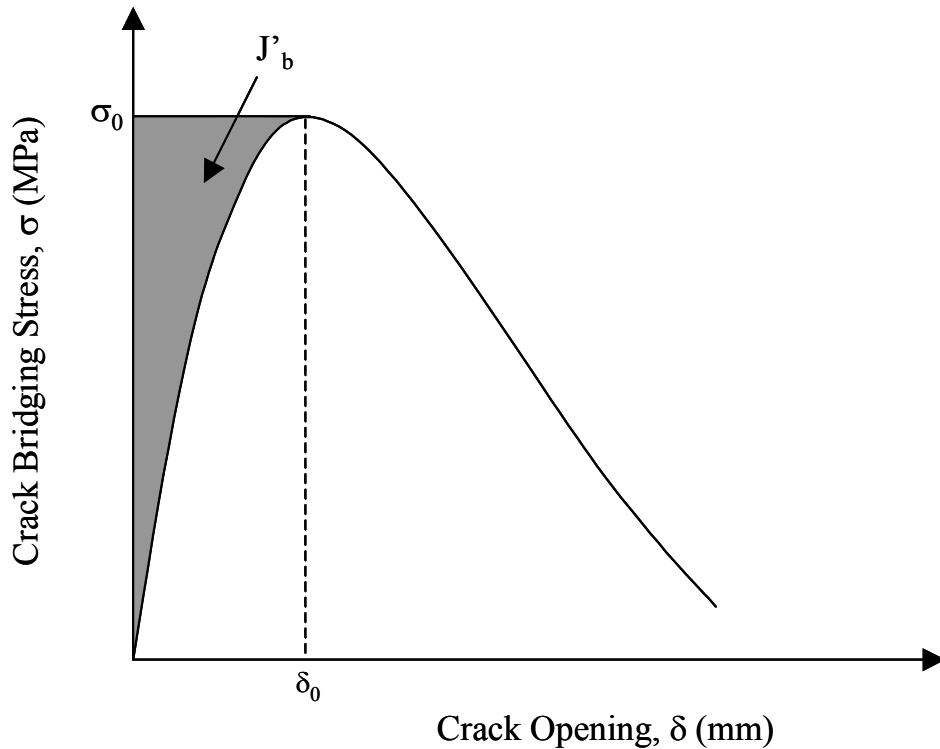


Figure 2.7 Crack opening versus crack bridging stress relation

where, $\sigma_{fc}$ is the first cracking strength and $\sigma_0$ is the maximum crack bridging stress

of the mortar matrix. Wang and Li (2004) found that Equation-2.2 must be implemented for saturated multiple cracking at each potential crack plane, where $\sigma_{fc}$ is perceived as the cracking stress on that crack plane.

The generation of multiple steady-state cracks, and strain-hardening behavior, can be achieved, if an ECC mixture is chosen according to the criteria above. Also, the mixture must be designed to produce crack widths below the 100 µm threshold limit. This can be obtained from the Equation-2.1 that identifies the relation between the crack opening and crack bridging. The maximum steady state crack width exhibited during ECC multiple cracking can be assumed to be $\delta_0$, the crack width corresponding to the maximum crack bridging stress, $\sigma_0$, as shown in Figure 2.7. The crack bridging stress would start to decrease, if the crack width were to grow beyond $\delta_0$, in which case the crack would localize and multiple crack formation would cease. The ECC material can suggest strain hardening performance and multiple cracking by holding $\delta_0$ under the 100 µm threshold limit.

The formulation of the crack opening versus crack bridging stress relationship based on summing the bridging force contribution of fibers that cross a given crack plane, was laid out by Lin et al. (1999). This relevance is represented in Equation-2.3.

$$\sigma(\delta) = \frac{4V_f}{\pi d_f^2} \int_{\phi=0}^{\pi/2} \left( \int_{z=0}^{(L_f/2)\cos\phi} P(\delta)e^{f\phi} p(\phi) p(z) dz \right) d\phi \quad (2.3)$$

where $V_f$ is the fiber volume fraction, $d_f$ is the fiber diameter, $L_f$ is the fiber length, $\phi$ is the orientation angle of the fiber, z is the centroidal distance of a fiber from the crack plane, f is a snubbing coefficient, and $p(\phi)$ and $p(z)$ are probability density functions of the fiber orientation angle and centroidal distance from the crack plane. Lin et al. (1999) defined $P(\delta)$ which is the pullout load versus displacement relation of a single fiber aligned normal to the crack plane. The factor $e^{f\phi}$ calculates for changing in bridging loads for the fibers cross from the crack plane of the oblique angle.

Using these basic micromechanical models to adapt the ECC material, due to a large crack widths of the composite without sacrificing the low permeability, at most a few

percent, can be designed to exhibit large deformations. Implementation of material design procedures, allows materials engineers to select material properties, like low permeability and strain capacity, for specific construction needs.

## 2.5 Use of ECC as an Overlay Material

The most usual deformations like separation of scaling and maintenance regions in rehabilitated infrastructures can be prevented by trapping mechanism of the ECC overlay system. Moreover, a large amount of energy absorption capacity and high ultimate strength with large deflection capacity can be anticipated. The ultimate refraction method has been changed from the interface crack extension towards the flexural strength of the maintenance material. Immediate improvement of strength, displacement, the ultimate failure mode and energy absorption capacity is not practical without the capture mechanism with regard to interface mechanism and design of the ECC material. Also, this overlay model could provide very low water permeability in improved infrastructures.

ECC overlays are designed to improve the durability into two ways, first, 'greener' ECC materials work together with industrial remaining materials like ground granulated blast furnace slag (GGBFS), fly ash and waste foundry sands and carbon residue in order to decrease the environmental effects of material production. Green material design is carefully guided by fundamental micromechanics in order to sustain pseudo-strain hardening material behavior under uniaxial tension. This ductile behavior is critical to the second mechanism for sustainability enhancement. Through a different storm, premature overlay failure, cracking is eliminated by ECC ductility very well. So life-cycle maintenance reduces and durability increases. Green material and overlay design approaches are verified by experimental and theoretical analysis. Without decreasing critical mechanical performance characteristics, over 70% of ECC virgin parts have been replaced with incorporating industrial wastes. Combination of environmentally friendly raw materials, have cause a 50% decrease in pavement overlay thickness, and have increased twice as compared with concrete overlays from the point of the service life. Therefore, significant sustainable developments have been achieved.

## 2.5.1 Mechanical and Environmental Performance of ECC in Pavement Applications

Researchers have studied about durability and long-term performance tests to determine the performance of ECC under characteristic mechanical loads associated with transporting and environmental loads.The tests are related to shrinkage, fatigue and overlay bond characteristics, freeze-thaw and salt scaling resistance, abrasion and wear, early age strength, long term strain capacity and accelerated weathering. All of these test results show that ECC can be successfully used as an overlay material for the rigid highway practices.

### 2.5.1.1 Shrinkage

Restrained ring tests (AASHTO PP-34) were performed for both ECC and normal Portland cement concrete to determine the restrained shrinkage behavior of ECC. Noticeably higher free shrinkage deformation is exposed, analogized to normal concrete, owing to the high cement content of ECC (Weimann and Li, 2003b). However, restrained shrinkage tests display that crack widths in ECC stay below 50 μm (50% relative humidity, RH, for 100 days), analogized to concrete crack widths of approximately 1 mm (Figure 2.8), although hygral deformation may be higher. While all shrinkage deformation in concrete localizes at a single crack, ECC permits the shrinkage deformation to be dissipated over a large number of small cracks. Moreover, lower interfacial stresses due to the large deformability of ECC prevent the appearance of shrinkage cracks at ECC/concrete interfaces.

### 2.5.1.2 Fatigue Testing and Overlay Bond Characteristics

The performance of ECC has been explored in high fatigue plans, like rigid pavement overlay rehabilitation. In these overlay practices, reflective cracking through the new overlay is of greatest concern. Existing cracks and locally reduced load capacity in the substrate pavement can result in flexural fatigue within the overlay structure. To evaluate ECC performance as a rigid pavement overlay material, both ECC/concrete and concrete/concrete overlay specimens were tested in flexural fatigue (Zhang and Li, 2002). Test results display that the load carrying capacity of ECC/concrete overlay samples was double that of concrete/concrete overlay samples, the deformability of ECC / concrete  samples was significantly
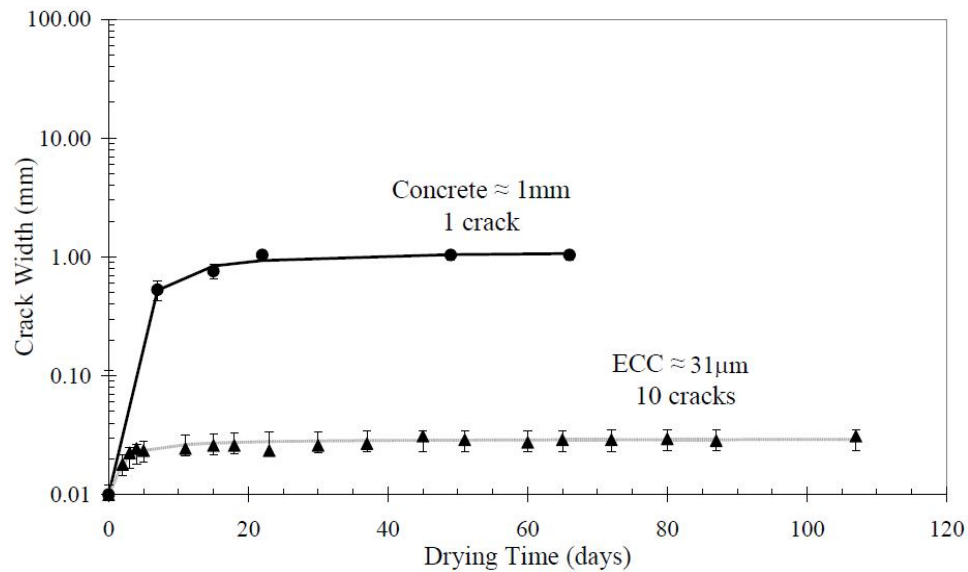
Figure 2.8 Crack width development as a function of drying time
(RH=50%) (Weimann and Li, 2003b).

higher, and the fatigue life was expanded by various orders of magnitude. In addition, the microcracking deformation system of ECC effectively eliminated reflective cracking. Similar advantages in the fatigue resistance of ECC have also been found in comparison to polymer cement mortars (Suthiwarapirak et al., 2002). Fatigue resistance of ECC for repair of viaducts subjected to train loading was studied by Inaguma et al. (2005). In fatigue-prone concrete infrastructure, the application of ECC materials may be able to significantly lengthen service-life, reduce maintenance events, and life cycle costs.

In addition to crack resistance and fatigue performance, the bond properties of ECC/concrete composites were determined. The spall processes and delamination, normally seen in many concrete/concrete repairs, were eliminated by using ECC as an overlay material. The energy absorption and load capacity of the ECC/concrete overlay was increased over concrete/concrete system through a unique kinking-and-trapping crack formation process. At first, cracks spread indistinctly along the bond interface, but then, they are directed into the ECC overlay and the high ECC toughness (34 kJ/m$^2$) instantly avoid the cracks (Maalej et al., 1995). Independent to interfacial debonding, the kinking-and-trapping procedure reiterates until the ECC finally fails in flexure. In addition, the effect of surface preparation on bonding was determined. Tests results show that in any case of a rough or smoothened interface, the bond capacity of an ECC/concrete composite is superior to that of a

23

concrete/concrete composite (Li, 2003b). The bond properties of ECC/concrete maintenance uses verify to be far better than update concrete/concrete maintenance types.

### 2.5.1.3 Freeze-Thaw and Salt Scaling Resistance

It is well known that the freeze-thaw cycles and the use of de-icing salts during winter are two of the major causes of rapid degradation in concrete pavements, bridge decks, parking structures, and similar structures. ECC used for this kind of structures must be resistant to freezing and thawing, and the effects of de-icing agents. It is known that a proper air-void system is generally needed in normal concrete to avoid internal cracking due to freeze-thaw cycles and scaling due to freezing in the presence of deicer salts.

In accordance with ASTM C666, durability of non-air-entrained ECC samples was tested by exposure to cycles of freezing thawing testing (Li et al., 2003). Non-air-entrained concrete samples were also tested as reference samples. Non-air-entrained samples were used as control since no air entrainment was added to the ECC mixtures. As stipulated by the testing standard, the concrete samples had seriously disintegrated after 110 cycles, behooving removal from the freeze-thaw apparatus. But, all ECC samples existed during the test of 300 cycles with no deterioration of dynamic modulus. Figure 2.9 shows the typical surface condition of the after 300 freeze-thaw cycles and fog room cured prismatic ECC specimens. As determined according to ASTM C666, this behavior results in a durability factor of 10 for concrete compared to 100 for ECC (1991). In uniaxial tension tests acted on wet cured and freeze-thaw subjected ECC tensile coupons at the same age after 300 cycles, no important change in strain capacity was observed. Freeze thaw and wet cured samples displayed a strain capacity of approximately 3%.

Numerous laboratory test data in accordance with ASTM C672 (2001) have indicated that air entrained concretes incorporating high volume fly ash often perform unsatisfactorily when exposed to freezing and thawing cycles in the presence of de-icing salts. For the production of ECC, as much as two-thirds of the portland cement is substituted by fly ash. Due to the high volume fly ash content, it is important to test the performance of ECC exposed to freezing and thawing cycles
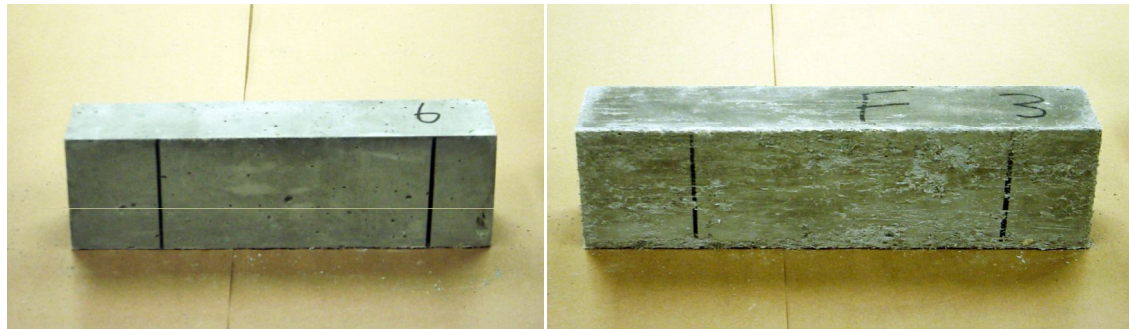
(a) fog room curing                    (b) after 300 freeze-thaw cycles

Figure 2.9 ECC specimen surface appearance after (a) normal curing and (b) freeze-thaw cycles (Li et al., 2003)

in the presence of de-icing salt. In accordance with ASTM C672, Şahmaran and Li (2009a) determined salt scaling resistance of mechanically pre-loaded (cracked) ECC and non-air-entrained sound (uncracked) samples. Non-air-entrained mortar specimens with and without fly ash were also tested as reference samples. The total mass of the scaling residue and surface condition visual rating for ECC samples remains within acceptable limits of ASTM C672, after 50 freeze-thaw cycles in the presence of de-icing salt (Figure 2.10). This level of durability holds true even for ECC samples pre-loaded to high deformation levels and displaying extensive microcracking. In comparison, reference mortar samples under same testing situations deteriorated seriously. In addition, the replacement of fly ash with cement in mortar further exacerbated deterioration due to freezing and thawing cycles in the presence of de-icing salt. To compare residual tensile strength and ductility of reloaded ECC samples, in a separate test, both pre-loaded (cracked) and sound ECC coupon samples were exposed to freeze-thaw cycles in the presence of de-icing salts for 25 and 50 cycles. The reloaded samples showed negligible loss of ductility, and retained the multiple micro-cracking behavior and tensile strain capacity of more than 3%. It was also discovered that micro-cracks due to mechanical loading will heal sufficiently under freezing and thawing cycles in the presence of salt solutions, restoring them to nearly the original stiffness. These results verify that ECC, both sound and micro-cracked, remains durable despite exposure to freezing freeze-thaw cycles in the presence of de-icing salts.

### 2.5.1.4 Abrasion and Wear Testing

For bridge deck and pavement surface maintenances, ECC has to supply a sufficient
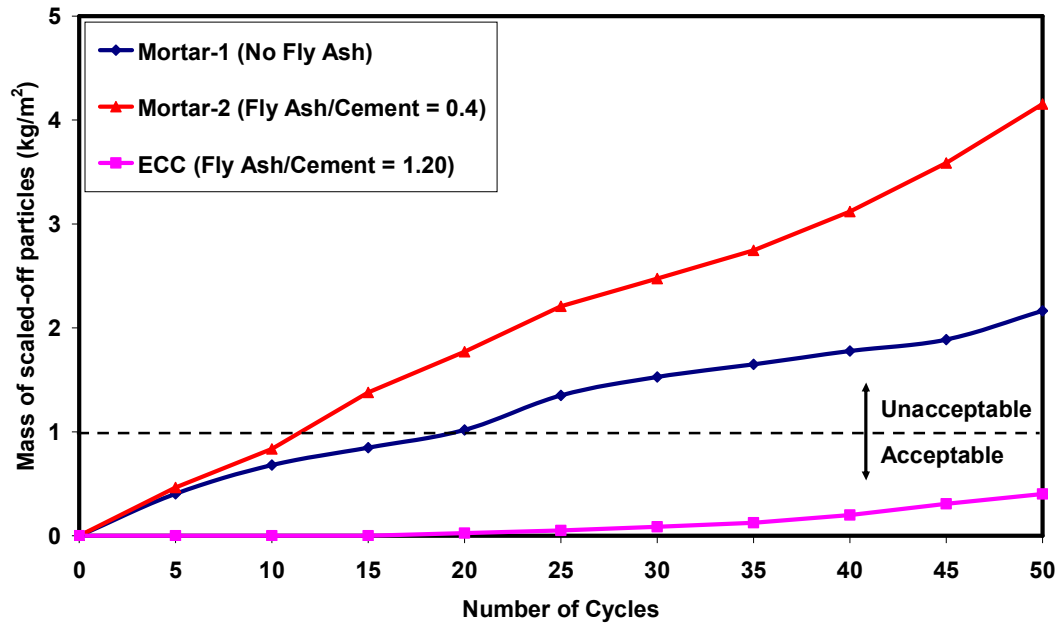
Figure 2.10 Mass of scaled-off particles versus number of freeze thaw cycles for virgin mortar and virgin ECC prisms in presence of de-icing salts (Şahmaran and Li, 2009).

surface for braking and driving, while resisting traffic abrasion. Samples were cured for 28 days and, wear track test and static friction test were applied on these samples according to Michigan Test Method 111 (2009). Initial friction forces between the textured ECC samples and vehicle tires operating at 65 kph were specified using a Michigan Department of Transportation (MDOT) static friction tester. Wet pavement surfaces were used for all static friction tests. ECC samples were exposed to 4 million tire moves to model long period tire wear, after initial friction testing. Following wearing test, friction forces were specified to determine surface polishing or degradation during wearing. These final friction forces equate to an Aggregate Wear Index (AWI) used for long term evaluation of pavement wear. AWI values for the textured ECC specimens tested range from 1.6 kN to 2.3 kN (Li et al., 2003). The found minimum AWI for Michigan trunkline road surfaces is 1.2 kN, importantly lower than all ECC overlays tested, indicating its suitability for highway surface maintenance subject to heavy traffic volumes.

**2.5.1.5 Early Age Strength**

Highway surface maintenance materials must show fast early age strength improvement for infrastructure works. Certainly, the longer a material cures before accomplishing sufficient strength to withstand service loads, the larger an impact the

project will have on traffic over-crowding and postpones. A group of compressive cylinders (10 cm x 20 cm) were examined at different early ages to specify the early age strength improvement of ECC. Tests were applied up to an age of about 100 hours. Tests results show that at 24 hours, ECC displays a compressive strength of 24 MPa, suitable for most maintenance works. The strength has passed 28 MPa after another 5 hours of curing, a normal needed concrete strength in reinforced concrete structures. The ultimate compressive strength of a standard ECC material is 60 MPa, well above most transportation requirements. A curing time of one day is advised for standard maintenance works according to the results. A group of catalysis types have easily been used with ECC to accomplish sufficient compressive strengths after only hours, while the use of hydration catalyst was not involved in this research.

### 2.5.1.6 Long Term Strain Capacity

A series of tensile tests have been conducted to specify long-term strain capacity, to formalize the long-term viability of ECC pavements. The strain capacity of ECC material changes during the maturing application due to the sensitive equilibrium of cement matrix, fiber, and matrix/fiber interface characteristics which must be repaired to accomplish strain hardening. This is showed in a plot of ECC age versus strain capacity (Figure 2.11) (Li and Lepech, 2004). At first, due to the low strength of the matrix, strain capacity is very low. At roughly 10 days aging peak strain capacity is accomplished due to an optimum equilibrium of matrix, fiber, and matrix/fiber interface characteristics for the ECC mix design shown. As hydration continues, a small instability happens and residues over the life of the material resulting in a long-term strain capacity of 3% for ECC material. This long term strain capacity data fits well with the strain capacity displayed by freeze thaw and wet cured tensile samples at 14 weeks, as mentioned before. The long-term strain capacity has asymptotically got about 3%, while long-term tests have only been performed to 180 days.

### 2.4.1.7 Accelerated Weathering Tests

Hot water submersion tests were applied to model the long term effects of hot and humid environments, in contrast to freeze thaw tests which are prepared to model temperature changes in cold climates. Hot water submersion was operated on
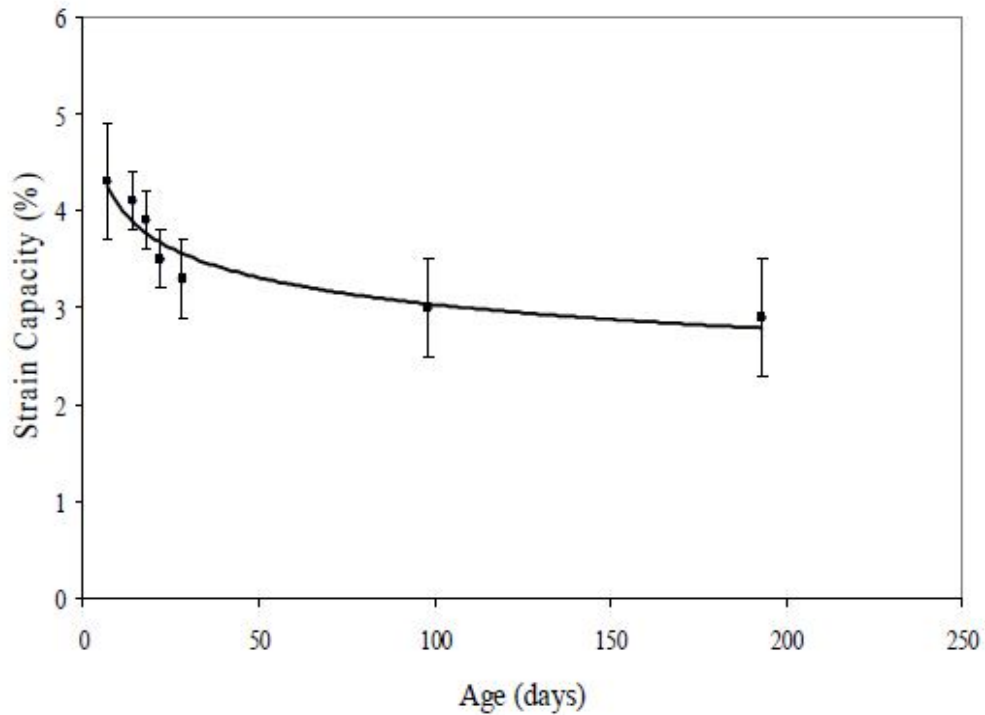
Figure 2.11 Tensile strain capacity improvement of ECC material (Li and Lepech, 2004).

particular fibers, single fibers implanted in ECC matrix, and composite ECC material samples, to investigate the impressions of environmental exposure (Li et al., 2004). Samples for both particular fiber pull-out and composite ECC material were cured for 28 days at room temperature prior to submersion in hot water at 60 ºC for 26 weeks. Little difference was determined in fiber characteristics like fiber strength, fiber modulus of elasticity, and elongation, after 26 weeks in hot water submersion. The tensile strain capacity of the ECC decreased from 4.5% at early age to 2.75%. The 2.75% strain capacity displayed after 26 weeks remains over 250 times that of normal concrete, while quickened hot weather testing does result in lower strain capacity of ECC.

### 2.5.2 Cost of ECC Materials

The funds required for up to date technology compared with present material is very essential to any transportation or infrastructure owner. Normal Portland cement concrete is considered one of the simplest and the most economically useful materials used in designing of infrastructures, with a price of about $99/m$^3$. Just like

we have discussed before, this material has a characterizing lifetime shortage, which make it need more renewal at more duration costs. High strength concretes, which are commonly believed to have a longer lifetime than ordinary concrete, or traditional steel fiber reinforced concrete's price may rise to nearly $199/m^3$. The recent price of PVA-ECC material is nearly $349/m^3$. However, the price of the MDOT fixing materials is about $539/m^3$ in the patch application. On the other hand, the price of ECC might appear higher in when compared to ordinary concrete, it is quite fewer than a lot of polymer concretes generally that are being used in repairing structures, or specific highly strength FRC, which might reach $2000/m^3$-$5000/m^3$ in price. As early noted, it is fundamental for the transportation society to look for basic methods to overcome inconvenient condition of the international infrastructures. Supported by a proof with initiatives, for example Michigan's "Preserve First", the requirement and sources for an enhanced transport infrastructure are found. A designer person must not look at precursors for fixing and renewing initially cost, and look for long lasting material, for instance ECC, that might cost a bit more than other commonly used material do. This highly performing material offers long lasting service life with decreased duration costs incorporated with repeated fixing, renewal, and displacing material. It is essential for transport plan makers and design experts to look to modern "brighter" material for the following generations to develop infrastructures.

# CHAPTER III

# EXPERIMENTAL PROGRAM

## 3.1 General

In this thesis, the experimental program was divided into two phases. In the first phase, compressive strength, fracture thoughness, flexural strength, drying and restrained ring shrinkage and freezing-thawing tests were performed to determine mechanical and durability properties of ECC mixtures. In the second phase, monolithic and layered performances of MSC and ECC mixtures, which were selected according to the literature review and tests results of the first phase, were investigated. Compressive strength, flexural strength, drying and restrained shrinkage, rapid chloride permeability and modulus of elasticity tests were conducted on monolithic specimens, and flexural strength, reflective cracking and bond strength tests were conducted on layered composite specimens to determine overlay performances of MSC and ECC mixtures. The experimental program and materials of both first and second phases are detailed below.

## 3.2 Experimental Program for the Development of Engineered Cementitious Composites (ECC) Mixtures with Locally Available Materials

### 3.2.1 Materials

#### 3.2.1.1 Cement

The cement used in all mixtures was a normal Portland cement CEM I 42.5R (C), similar to ASTM Type I cement. It had a specific gravity of 3.06 and Blaine fineness of 325 $m^2$/kg. Chemical composition and physical properties of cement are presented in Table 3.1. The particle size distributions of Portland cement, procured by a laser scattering technique, is given in Figure 3.1. Portland cement was analyzed with a scanning electron microscope (SEM) to identify morphological characteristics. Figure 3.2 illustrates the particle morphology of Portland cement.

Table 3.1 Chemical composition and physical properties of Portland cement, fly ash, slag and microsilica

| Chemical Composition | Cement | Fly Ash | Slag | Microsilica |
|---|---|---|---|---|
| CaO (%) | 61.43 | 1.64 | 34.48 | 0.62 |
| $SiO_2$ (%) | 20.77 | 56.22 | 38.40 | 91.96 |
| $Al_2O_3$ (%) | 5.55 | 25.34 | 10.96 | 1.20 |
| $Fe_2O_3$ (%) | 3.35 | 7.65 | 0.81 | 0.84 |
| MgO (%) | 2.49 | 1.80 | 7.14 | 1.02 |
| $SO_3$ (%) | 2.49 | 0.32 | 1.48 | 0.12 |
| $K_2O$ (%) | 0.77 | 1.88 | 0.86 | 1.16 |
| $Na_2O$ (%) | 0.19 | 1.13 | 0.18 | 0.67 |
| Loss of ignition (%) | 2.20 | 2.10 | 3.00 | 1.86 |
| $SiO_2+Al_2O_3+Fe_2O_3$ | 29.37 | 89.21 | 50.17 | 94.00 |
| **Physical properties** | | | | |
| Specific gravity | 3.06 | 2.31 | 2.79 | 0.60 |
| Blaine fineness ($m^2$/kg) | 325 | 290 | 425 | - |
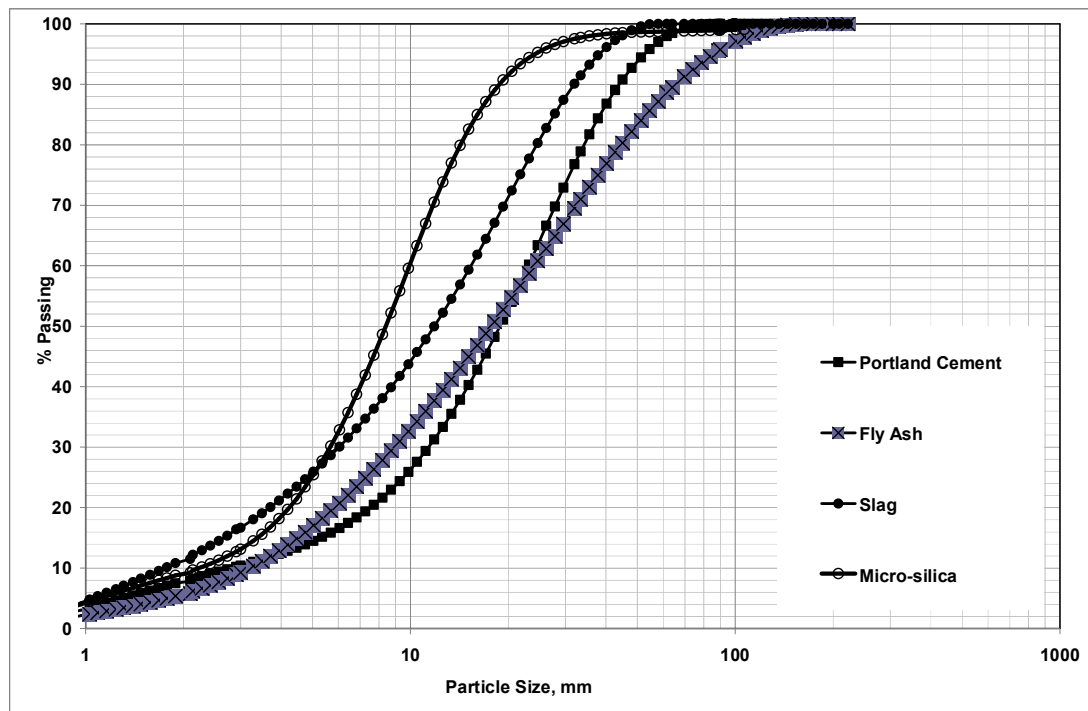


Figure 3.1 Particle size distributions of Portland cement, fly ash, slag and microsilica
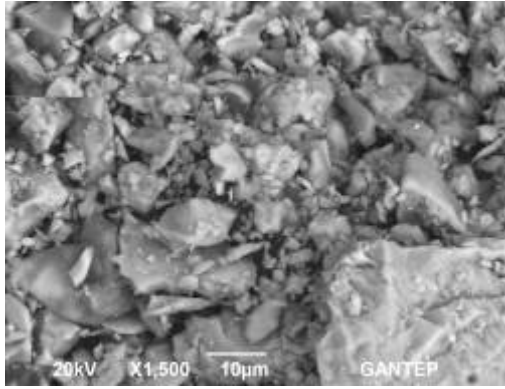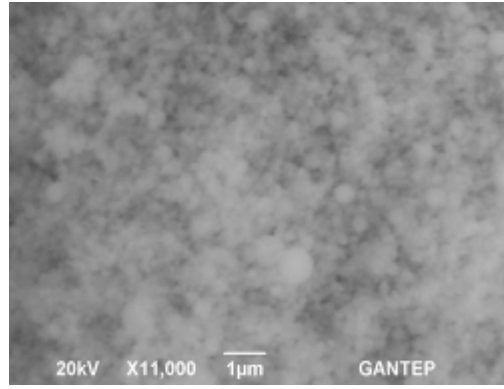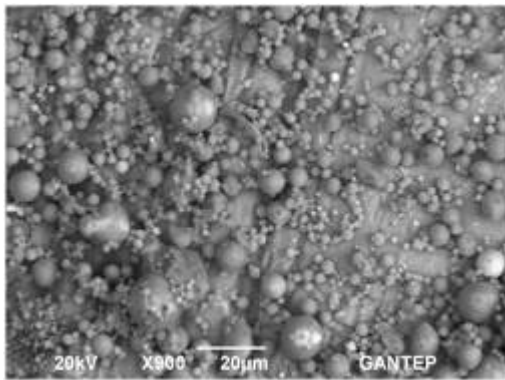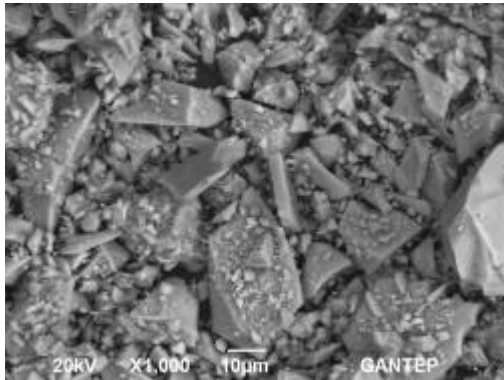
|  | |
|---|---|
| Portland Cement | Microsilica |
| Fly Ash | Slag |

Figure 3.2 Particle morphology of Portland cement, microsilica, fly ash and slag analyzed by SEM

### 3.2.1.2 Fly Ash

Class-F fly ash (FA) conforming to ASTM C 618 (2003) requirements with a lime content of 1.64% obtained from Sugözü Thermal Power Plant was used. The chemical composition and physical properties of FA are given in Table 3.1. The specific gravity and Blaine fineness of FA are 2.31 and 290 $m^2$/kg, respectively. The particle size distribution of FA is provided in Figure 3.1. Figure 3.2 illustrates the particle morphology of FA. The SEM image showed that the particles of FA had significantly smooth spherical particles in comparison to slag.

### 3.2.1.3 Ground Granulated Blast Furnace Slag

Ground granulated blast furnace slag (hereafter slag – S) was supplied from Iskenderun Iron–Steel Factory in Turkey. Table 3.1 summarizes its chemical oxide composition. The specific gravity of slag was 2.79. The slag was ground granulated in Iskenderun Cement Factory to have a Blaine specific surface area about 425 $m^2$/kg. The slag used was classified as a category 80 slag according to ASTM C 989

32

(2009) hydraulic activity index. Particle size distribution of slag obtained by using the laser diffraction is shown in the Figure 3.1. To identify morphological characteristics of slag, it was analyzed with SEM and the resulting photograph is presented in Figure 3.2.

### 3.2.1.4 Aggregates

According to micro-mechanic based design of ECC, exhibiting ductile and showing a large crack number, but small in width, of cementitious composites, a low toughness of the matrix is required. However, with the increasing of maximum grain size of aggregate, increase in toughness of the matrix is appeared and as a result, to obtain suitable ECC, aggregate grain size is limited (Li et al.,1995). Therefore, so far, ECC has been produced successfully with an average grain size of about 110 μm and maximum grain size of about 200 μm (Li et al.,1995). Using high volumes of industrial by-product in the production of ECC decreases matrix toughness and provides freedom of changing aggregate size. It is very important to produce ECC from normal size local sources of aggregate in terms of widespread application for both literature and our country. For this purpose, in the production of ECC, fine quartz with two maximum aggregate sizes (MAS) of 400 μm and 1000 μm was obtained from local sources in our country's resources. Water absorption capacity and specific gravity of quartz aggregate used is 0.3% and 2.60, respectively. The grain size distribution curves for these aggregates and image under digital camera are shown in Figure 3.3 and Figure 3.4, respectively.

### 3.2.1.5 Chemical Admixtures

To develop the workability of ECC mixtures, Glenium 51, high range water reducing admixture (HRWR – polycarboxylate ether as an active ingredient with 1.1 specific gravity and 40% solid content) produced by BASF Construction Chemicals was used.

### 3.2.1.6 Polyvinyl Alcohol (PVA) Fiber

PVA fiber was used in this study (see Figure 3.5), although several kinds of fibers have been used in the production of ECC. The use of PVA fiber was decided based on micromechanical principals and PVA-ECC represents the most practical ECC
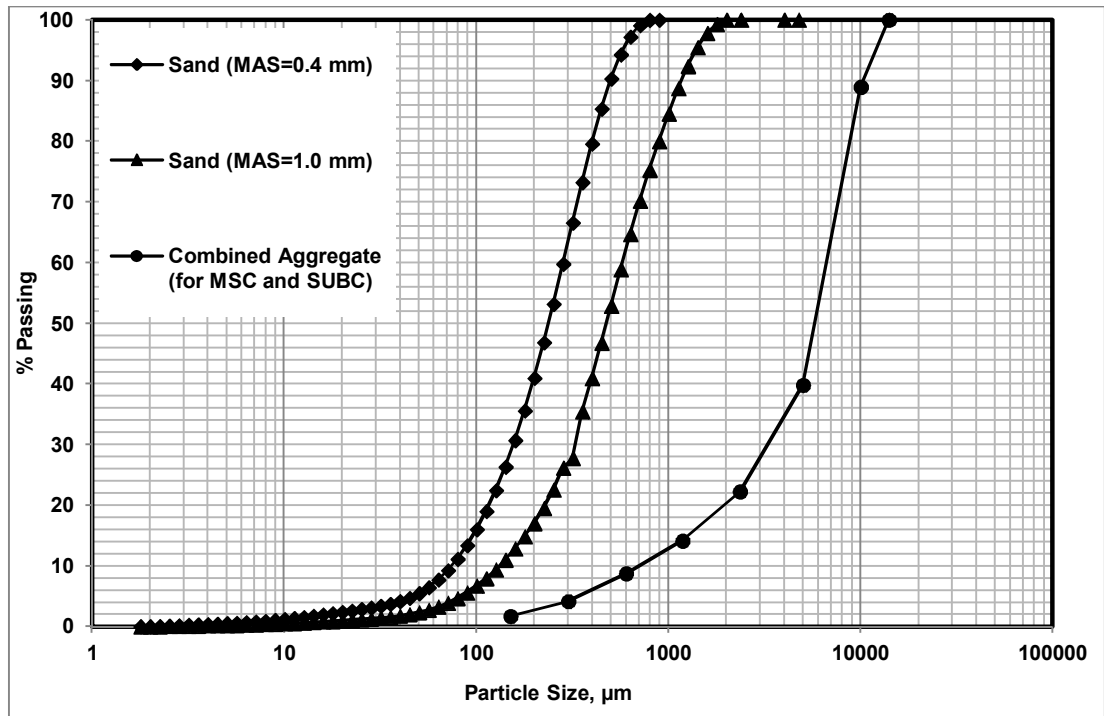
Figure 3.3 The grain size distribution curves for the aggregates used in this study



Figure 3.4 Fine quartz sand used in the production of ECC

used in the field (Li et al., 2001; Kunieda and Rokugo, 2006) at the present. PVA fibers have attracted most attention due to the outstanding composite performance and economics consideration. The dimensions of the PVA fiber are 8 mm in length and 39 µm in diameter. The density of the fiber is 1300 kg/m$^3$ and the nominal tensile strength of the fiber is 1620 MPa. The mechanical and geometric properties of

(a)



5 mm

200 μm
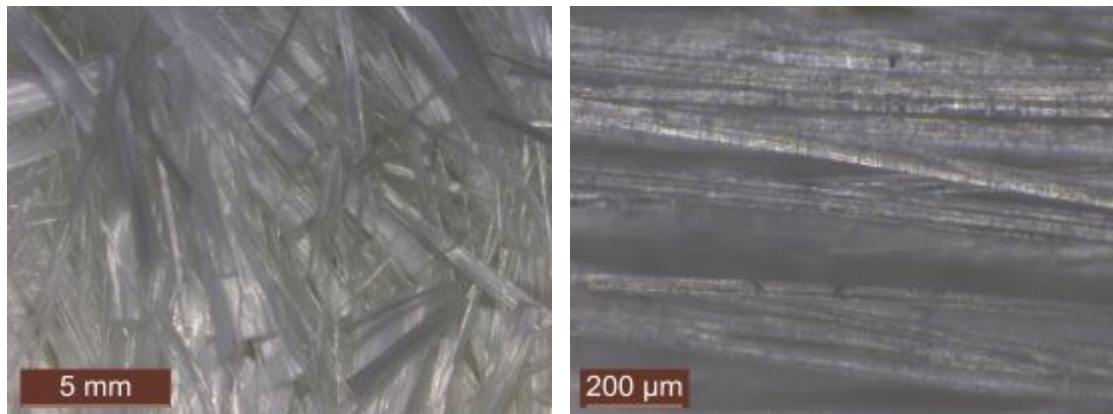
(b)

Figure 3.5 PVA fiber used in the production of ECC under

(a) digital-camera image (b) macroscope image

PVA fibers are summarized in Table 3.2. In order to decrease the fiber/matrix interfacial bond strength, the surface of PVA fiber is coated by hydrophobic oil (1.2% by weight). A fiber content of 2% by volume in excess of the calculated critical fiber content has been typically used in the mix design, to consider material inhomogeneity. These determinations were made according to ECC micromechanics material design theory and had been empirically proved to produce good ECC characteristics in previous researches (Li et al., 2001; Kong et al., 2003).

### 3.2.2 Mixing and Specimen Preparation

The experimental program was based on a 2 (MAS) × 3 (aggregate/binder ratio) × 2

Table 3.2 Mechanic and geometric properties of PVA fibers

| Fiber Type | Nominal Strength (MPa) | Apparent Strength (MPa) | Diameter (µm) | Length (mm) | Young Modulus (GPa) | Strain (%) | Specific Weight kg/ m³ |
|---|---|---|---|---|---|---|---|
| PVA | 1620 | 1092 | 39 | 8 | 42.8 | 6.0 | 1300 |

(mineral admixture types) × 2 (mineral admixture replacement rate). In total twenty-four mixtures with two different aggregate sizes (0.4 and 1.0 mm MAS), three aggregate contents ( 0.36, 0.45 and 0.55 aggregate-binder ratios ), two mineral admixture types (FA and slag), and two mineral admixture replacement rate (1.2 and 2.2 FA or S – C ratio) were considered in this study. Details of this factorial design and designation of mixtures are presented in Table 3.3. In all mixtures the water/binder ratio (W/B) were the same. To obtain approximately similar workability and uniform disperse of fibers, the HRWR content was varied from mix to mix. As seen from Table 3.3, the ECC mixture with the lowest slag content (S/C ratio of 1.2) had the highest HRWR demand, but as part of the cement was replaced by FA or slag replacement rate was increased, the HRWR content of mixtures decreased. The smooth surface characteristics and spherical shape of the FA improved the workability characteristics of ECC mixtures, so that similar workability properties at constant W/B ratio were achieved by using a lower HRWR content at higher FA replacement level (please see Figure 3.2).

As shown in Table 3.3, the ECC mixtures are denominated such that the ingredients are identifiable from their Mix IDs. The first letter in the mixture designations indicates the mineral admixture type (FA = fly ash, S = slag). The numbers after the letter indicate the mineral admixture (FA or S) – cement ratio, aggregate/binder (A/B) ratio and maximum aggregate size, respectively. The mix proportion of a standard ECC mixture, FA1.2_0.36_400 (M45) (Table 3.3), is used as a reference in the ECC mix design (Wang and Li, 2007).

In this study, a Hobart type mixer (Figure 3.6) with 20-liter capacity was used in the production of all ECC mixtures. Solid ingredients, such as cement, mineral admixture (FA or S), and aggregate, were first mixed at 100 rpm for one minute. Water and HRWR admixture were then poured in the dry mixture and mixed at 150 rpm for one minute and then at 300 rpm for another two minutes to produce a

Table 3.3 ECC mixture proportions containing fly ash and slag by weight

| Mix ID. | Cement | W/B | Aggregate/Binder | | FA/C | S/C | HRWR |
| | | | 0-400 μm | 0-1000 μm | | | kg/m$^3$ |
|---|---|---|---|---|---|---|---|
| FA1.2_0.36_400 (M45) | 1 | 0.27 | 0.36 | - | 1.2 | - | 5.1 |
| FA1.2_0.45_400 | 1 | 0.27 | 0.45 | - | 1.2 | - | 5.1 |
| FA1.2_0.55_400 | 1 | 0.27 | 0.55 | - | 1.2 | - | 5.0 |
| FA1.2_0.36_1000 | 1 | 0.27 | - | 0.36 | 1.2 | - | 4.9 |
| FA1.2_0.45_1000 | 1 | 0.27 | - | 0.45 | 1.2 | - | 5.0 |
| FA1.2_0.55_1000 | 1 | 0.27 | - | 0.55 | 1.2 | - | 5.0 |
| FA2.2_0.36_400 | 1 | 0.27 | 0.36 | - | 2.2 | - | 3.0 |
| FA2.2_0.45_400 | 1 | 0.27 | 0.45 | - | 2.2 | - | 3.0 |
| FA2.2_0.55_400 | 1 | 0.27 | 0.55 | - | 2.2 | - | 3.0 |
| FA2.2_0.36_1000 | 1 | 0.27 | - | 0.36 | 2.2 | - | 3.0 |
| FA2.2_0.45_1000 | 1 | 0.27 | - | 0.45 | 2.2 | - | 3.0 |
| FA2.2_0.55_1000 | 1 | 0.27 | - | 0.55 | 2.2 | - | 3.0 |
| S1.2_0.36_400 | 1 | 0.27 | 0.36 | - | - | 1.2 | 5.8 |
| S1.2_0.45_400 | 1 | 0.27 | 0.45 | - | - | 1.2 | 5.9 |
| S1.2_0.55_400 | 1 | 0.27 | 0.55 | - | - | 1.2 | 6.0 |
| S1.2_0.36_1000 | 1 | 0.27 | - | 0.36 | - | 1.2 | 4.9 |
| S1.2_0.45_1000 | 1 | 0.27 | - | 0.45 | - | 1.2 | 5.0 |
| S1.2_0.55_1000 | 1 | 0.27 | - | 0.55 | - | 1.2 | 5.0 |
| S2.2_0.36_400 | 1 | 0.27 | 0.36 | - | - | 2.2 | 4.7 |
| S2.2_0.45_400 | 1 | 0.27 | 0.45 | - | - | 2.2 | 4.1 |
| S2.2_0.55_400 | 1 | 0.27 | 0.55 | - | - | 2.2 | 4.3 |
| S2.2_0.36_1000 | 1 | 0.27 | - | 0.36 | - | 2.2 | 3.5 |
| S2.2_0.45_1000 | 1 | 0.27 | - | 0.45 | - | 2.2 | 3.6 |
| S2.2_0.55_1000 | 1 | 0.27 | - | 0.55 | - | 2.2 | 4.0 |

*HRWR: High range water reducing admixture, C: Cement, FA: Fly Ash, S: Slag*

Mixing of solid ingredients

Water addition

HRWR addition

Fiber addition

Figure 3.6 Production of ECC by using Hobart Type mixer

uniform ECC matrix (without PVA fiber). Lastly, PVA fiber was added and mixed at 150 rpm for an extra three minutes.

At least six specimens of each ECC mixture were tested under each type of loading condition for each testing age (7, 28, 90 and 180 days). 50-mm cubic samples were produced for the compressive strength test, $360 \times 50 \times 75$ mm prism samples were prepared for the four-point bending and fracture toughness tests. Also, for each mixture three $285 \times 25 \times 25$ mm bar specimens and two ring specimens were cast to determine drying shrinkage and restrained shrinkage cracking potential, respectively.

In addition, 400×100×75 mm prism specimens of selected ECC mixtures as FA1.2_0.36_400, FA2.2_0.36_400, S1.2_0.36_400 and S2.2_0.36_400 were prepared for freezing and thawing durability test.

### 3.2.3 Test Procedures

### 3.2.3.1 Compressive Strength

Twenty four cubic samples (6 specimens for each of age) of 50 mm were cast from each ECC mixture. The samples were demolded after 24 hours, and moisture cured in plastic bags at 95±5 % relative humidity, 23±2 $^{o}$C for 7 days (Figure 3.7). The samples were then air cured at 50±5 % relative humidity (RH) , 23±2 $^{o}$C until the day of testing. In accordance with ASTM C39 (2003), the compression test was performed on the cubic samples by using a 3000 kN capacity testing machine (Figure 3.8). ECC cubic specimens were tested for compressive strength measurement at the age of 7, 28, 90 and 180 days.



Figure 3.7 Curing of ECC specimens under sealed condition

### 3.2.3.2 Fracture Toughness

To measure the fracture toughness of ECC matrix (ECC without PVA fiber), eighteen prismatic samples (6 specimens for each age of testing) having dimensions of 360x75x50 mm were prepared. There is no method in the standards in order to measure stress intensity factor of cementing materials. Therefore, in this study to measure stress intensity factor, ASTM E399 (2003) "Linear-Elastic Plane-Strain Fracture Toughness $K_{IC}$ of Metallic Materials," Standard test method was used. This standard test method for cement matrix has been previously implemented in a

Figure 3.8 Compression testing machine and cubic ECC samples

detailed manner and applicability of it to such systems has been verified. Set-up for measuring fracture toughness is presented in Figure 3.9. According to this test method, 6 samples of 360x75x50 mm size, in center of which about 30 mm deep notch was opened (Figure 3.10), were prepared for each age of 28, 90 and 180 day. Then these samples were tested at a three-point bending test at a rate of 0.002 mm/sec. After this test, exact notch depth of samples was measured, and then the toughness of the matrix was calculated.
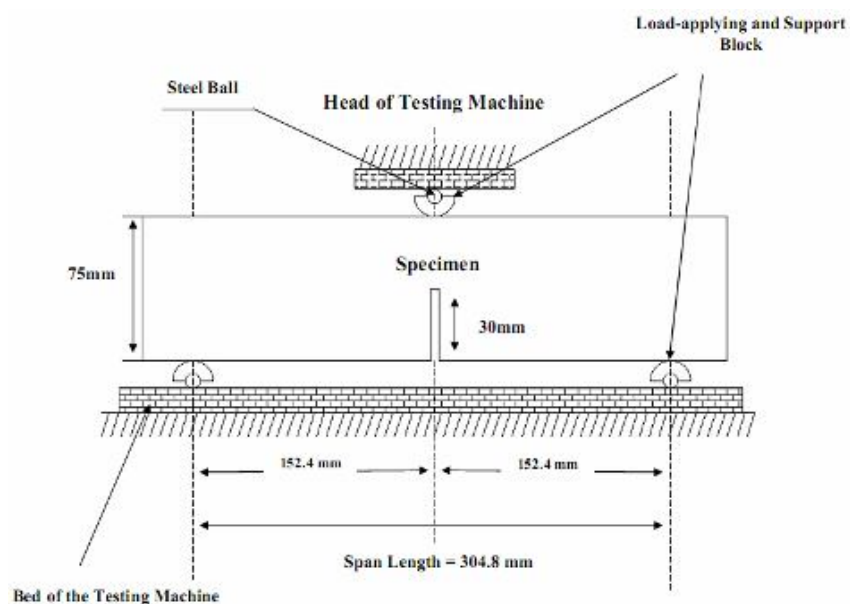


Figure 3.9 Test set-up of determining fracture toughness

Fracture toughness ($K_Q$) of the specimens was calculated in accordance with following Equation (3.1):

$$K_Q = \frac{P_Q S}{BW^{\frac{3}{2}}} \cdot f\left(\frac{a}{W}\right) \tag{3.1}$$

$P_Q$: Applied load, S: Span width, B: Height of the specimen, W: Depth of the specimen, and $f\left(\frac{a}{W}\right)$: geometric calibration factor (varying between 1.91 and 2.18 with respect to determined exact depth of the specimens )



Figure 3.10 Notch opening of a specimen for determining fracture toughness

### 3.2.3.3 Flexural Performance

To measure the flexural performance of ECC mixture, twenty four prismatic samples (6 specimens for each testing age) having dimensions of 360x75x50 mm were cast from each produced ECC mixture. ECC prisms were first cleaned, and then flexural strength under four-point test was performed by using universal testing system (Figure 3.11).

Four point bending test was performed on a closed-loop controlled material testing system at a loading rate of 0.005 mm/s. The capacity of the loading frame was 100 kN (Figure 3.12). To eliminate extraneous deformations like sample rotations and
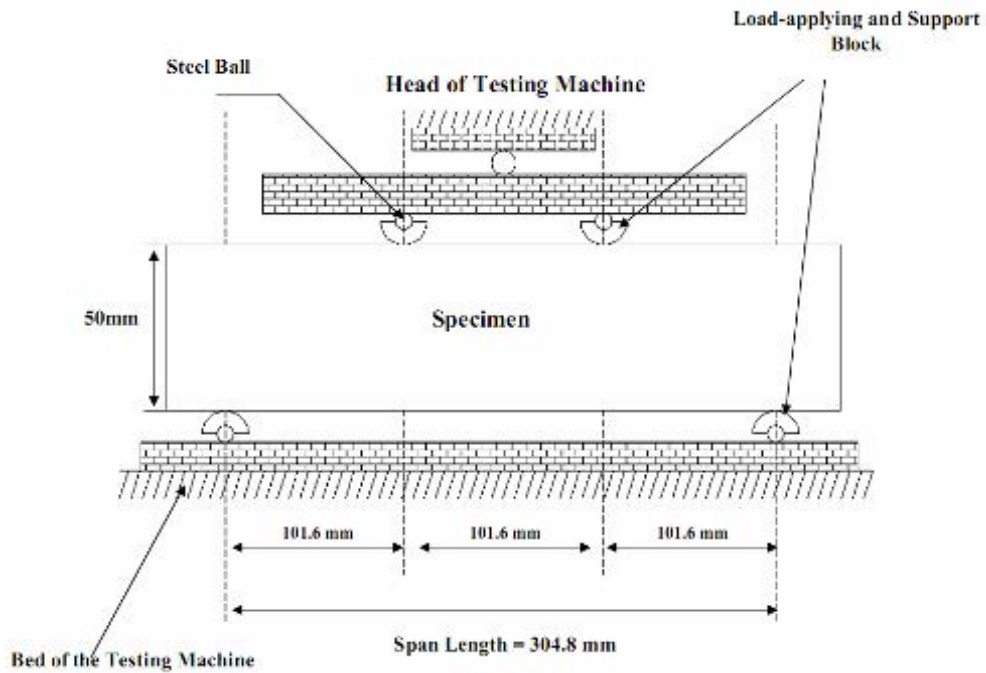
Figure 3.11 Four-point bending test set-up

support settlements, a four point bending loading fixture was improved. The span length of flexural loading was 304 mm with a 101 mm center span length. During the flexural tests, the load and mid-span deflection were written down on data recording system in a computer. Linear variable displacement transducer (LVDT) was fixed on the test set-up to measure the flexural deflection of the specimen. In this study, flexural deflection capacity of ECC prismatic specimens is calculated from the deformation value at the peak flexural stress of the flexural stress-deformation curves. After bending tests, crack widths on the surface of the samples were measured by using a portable and video microscope (Figure 3.13). To evaluate composite performances, microstructural analysis in terms of scanning electron microscopy (SEM) and mercury intrusion porosimetry (MIP) were also conducted. For each FA or slag replacement level, microstructural investigations were only conducted on ECC specimens with 400 μm MAS. Specimens were dried to constant weight at 50 °C prior to testing. An instrument capable of producing pressures up to 414 MPa and presuming a contact angle of 130° was used for pore size distribution analysis by the mercury intrusion method. All tests included at least two identical specimens tested at the same time.

42

Figure 3.12 Four-point flexural strength test
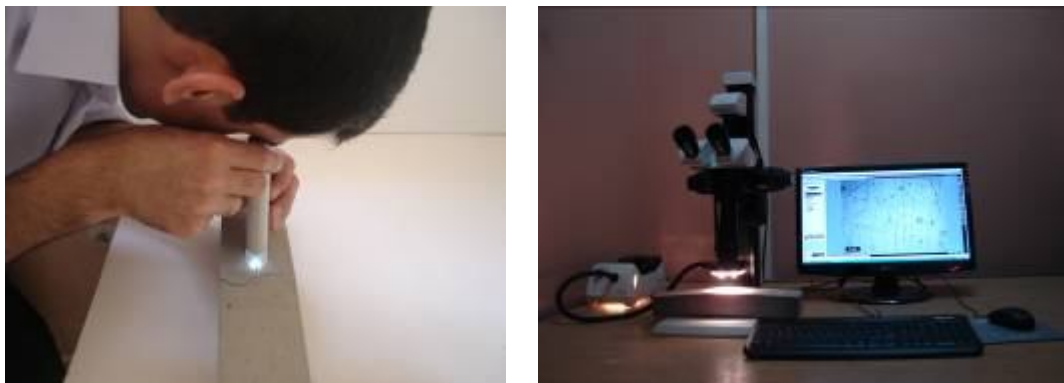


Figure 3.13 Control of crack widths of specimens tested by four-point test

### 3.2.3.4 Drying Shrinkage

In accordance with ASTM C157 (2004), the drying shrinkage of bar specimens was measured up to 180 days after an initial curing of one day in the mould and 27 days in lime saturated water by using three 285×25×25 mm prismatic specimens for all ECC mixtures (Figure 3.14). Gauge studs were inserted in the bar moulds coaxial with the bar before the ECC mixtures was poured in to the moulds. The drying shrinkage specimens were stored in laboratory at 23±2 $^{o}$C, and 50±5% RH.

### 3.2.3.5 Restrained Ring Shrinkage

Several kinds of restrained shrinkage test methods have been performed to determine

43

Figure 3.14 Drying shrinkage device and samples

the shrinkage cracking behavior of concrete (Malhotra, 1970; Kraai, 1985; Carlson and Reading, 1988), although there is no standard test to evaluate cracking due to restrained shrinkage. In this work, ring tests were performed to evaluate the restrained shrinkage cracking potential. Restraining ring was made of ECC ring (140 mm in height) cast around the outer perimeter of a steel ring with 280 mm and 305 mm inner and outer diameters, respectively. A 25.4 mm thick layer of ECC was cast around a 12.5 mm thick steel annulus. For each type of ECC mixture, two rings were cast and cured in the molds for 24 hours. After that, the exterior mold was removed and the top surface of the ring was sealed using a silicone-based sealant. The rings were then placed in an environmental chamber at $50 \pm 5\%$ RH and $23\pm2$ $^{o}$C. Thus, the ring-type concrete started to dry only from the outer. It should be noted that the curing states for the ring tests are different from the free drying shrinkage test. The purpose of the early demolding and short curing time in the ring tests is to simulate the early re-opening conditions in field application. The restrained shrinkage was used to record the onset time of a new crack and the time improvement of the width at the crack mouth. The cracking pattern, crack number and crack width were measured as a function of age with a hand held microscope. Measurements were taken every 24 hour for 28 days at three different locations along each crack and the average value was plotted. Figure 3.15 shows a schematic restrained ring test set-up.

### 3.2.3.6 Freezing and Thawing Test

Four ECC mixtures, that showed good performance according to the test results of mechanical properties, were selected for freezing and thawing test as

44
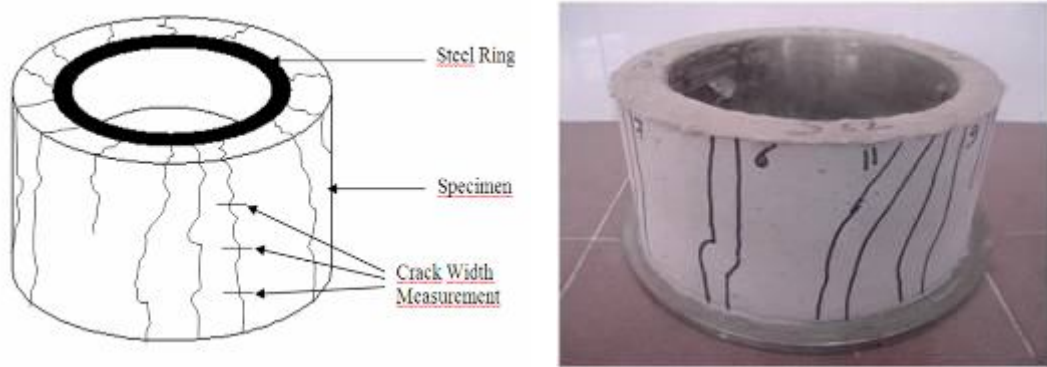
Figure 3.15 Restrained shrinkage test set-up

FA1.2_0.36_400 (FA_1.2), FA2.2_0.36_400 (FA_2.2), S1.2_0.36_400 (S_1.2) and S2.2_0.36_400 (S_2.2). For each ECC mixture, fifteen 400 × 100 × 75 mm prisms for the freeze-thaw test and determination of air-void characteristics were prepared. All samples were cast without any compaction in one layer, demolded at the age of 24 h., and moist cured in lime-saturated water at 23±2°C for 13 days. Fourteen days after casting, from each mixture, six prism samples with a span length of 355 mm and a height of 75 mm were tested under the four-point bending test up to failure, and the average ultimate flexural strength, mid-span beam deflection capacity and flexural stiffness of each mixture were determined. The deflection at which point the bending stress reaches maximum (MOR) was determined as the deflection capacity. At the same age, six prisms were preloaded up to 2.5 mm deformation level and then load released; just after that three of those preloaded beams were reloaded up to failure to observe the effect of damage by preloading. The deflection of 2.5 mm is below ultimate deflection capacity of both groups of mixtures with no localized fracture. Tests were conducted on a closed-loop controlled material test system with 100 kN capacity under displacement control at a rate of 0.005 mm/s. LVDT was fixed on the test set-up to measure the flexural deflection of the specimen. The crack widths were measured just after load released by using a video microscope. The widths of the crack were measured on the tension surface of the beam samples along the span length. Then from each mixture three pristine and three preloaded specimens were transferred into the freeze-thaw chamber according to ASTM C666 Procedure A (1991), and subjected to between five and six freeze-thaw cycles in a 24 h. period (Figure 3.16). Changes in ultrasonic pulse velocity (UPV) and mass loss were measured at each interval of nominally 60 cycles up to 300 cycles. The travel time for the UPV was measured in the longitudinal direction. After completing the

300 freeze-thaw cycles, beam specimens were also loaded up to failure under flexural loading and decrements in flexural properties were determined.



Figure 3.16 Freezing and thawing test

The air-void parameters of ECC mixtures on polished specimens were determined by modified point count method according to ASTM C457 (1998). This measurement is made on the hardened ECC mounted under a microscope at 14 days. Scanning is used along a series of traverse lines to determine air void parameter. Air content, the specific surface and the spacing factor are used to characterize the air voids. A frost resistant concrete in high quality generally needs a specific surface greater than 25 mm$^{-1}$ and a spacing factor less than 0.20 mm.

**3.3 Experimental Program for the Development of Overlay Mixtures**

**3.3.1 Materials**

**3.3.1.1 Cement**

The cement used in overlay mixtures and substrate concrete (SUBC - existing rigid pavement overlay) mixture is the same cement as in ECC mixtures, which was

explained in Section 3.1.1.1.

### 3.3.1.2 Fly Ash

The fly ash used in ECC overlay mixtures is the same fly ash as in ECC mixtures, which was explained in Section 3.1.1.2.

### 3.3.1.3 Slag

The slag used in ECC overlay mixtures is the same slag as in ECC mixtures, which was explained in Section 3.1.1.3.

### 3.3.1.4 Microsilica

Microsilica (MS), which was obtained from Norway (ELKEM), was used to replace cement in the production of microsilica concrete (MSC). Chemical composition and physical properties of microsilica are shown in Table 3.1. The specific gravity of MS is 0.60. Particle size distribution of microsilica obtained by using the laser diffraction can be seen in Figure 3.1. Figure 3.2 illustrates the particle morphology of microsilica.

### 3.3.1.5 Aggregates

Fine quartz was used for ECC overlay mixtures with maximum aggregate sizes (MAS) of 400 μm. It was obtained from local sources in our country's resources as mentioned in Section 3.1.1.4.

An aggregate combination of natural river sand with particle size of 0.1 – 5 mm and crushed natural stone with 12 mm maximum size was used in the production of substrate concrete (SUBC) and microsilica concrete (MSC) mixtures. Water absorption capacity and specific gravity of this aggregate is 0.7% and 2.70, respectively. The grain size distribution curve of this combined aggregate and image under digital-camera are seen in Figure 3.3 and Figure 3.17.

### 3.3.1.6 Chemical Admixtures

To improve the workability of ECC and MSC overlay mixtures and SUBC mixture, Glenium 51, high range water reducing admixture produced by BASF Construction

Figure 3.17 Combined aggregate used in the production of SUBC and MSC

Chemicals was used. To increase the freeze-thaw resistance of MSC and SUBC mixtures, an air-entrained admixture (AEA) called as İKSA-AER was also used as chemical admixture.

### 3.3.1.7 Polyvinyl Alcohol (PVA) Fiber

The PVA fiber used in ECC overlay mixtures is the same slag as in ECC mixtures, which was explained in Section 3.1.1.6.

### 3.3.2 Mixture Proportions and Mixing Procedures of Overlay Materials

As an overlay material, in accordance with the test results, two different ECC-overlay mixture designs are selected from the first section of this study: one with high strength and moderate ductility (S1.2_0.36_400), and the other with moderate strength and high ductility (FA1.2_0.36_400). In addition, microsilica concrete (MSC) was employed as a control overlay mixture. The selection and proportions of MSC mixture were based on the information collected from the literature. Özyıldırım and Gomez (1999), Sprinkel (2000, 2003, 2004), Alhassan (2007) and Mokarem et al. (2008) studied MSC as an overlay material. The mixture proportions and the mechanical and durability properties of concrete mixtures incorporating microsilica for overlay applications were comprehensively discussed in these studies. The test results show that MSC is one of the most effective high performance material for

rigid pavement overlays. Therefore, the three overlay mixtures were: ECC with fly ash - FA1.2_0.36_400 (F_ECC), ECC with ground granulated blast furnace slag - S1.2_0.36_400 (S_ECC) and microsilica concrete (MSC). Table 3.4 shows mixture proportions and main properties of overlay mixtures.

To determine the overlay performances and bond properties of the overlay mixtures, the substrate concrete (SUBC – existing rigid pavement overlay), which is a normal concrete usually used in the construction of rigid pavements, was prepared. The substrate concrete mix was designed to mimic a representative of Michigan Department of Transportation (MDOT) bridge deck mix. According to the Michigan Bridge Design Manual (2009) the bridge deck concrete requirements are shown in Table 3.5. SUBC was designed for 31 MPa compressive strength at 28 days and tested to check requirements (Table 3.5). Mixture proportion of SUBC is shown in Table 3.4.

In this study, a Hobart type mixer (Figure 3.6) with 20-liter capacity was used in preparing F_ECC and S_ECC overlay mixtures as explained in Section 3.1.2. For preparing MSC and SUBC mixtures a laboratory type concrete mixer with 30-liter capacity was used. Solid ingredients, including cement, aggregate, and microsilica, were first poured into the mixer tank and mixed for a minute. After that, water, AEA and HRWR admixtures were added into the dry mixture and mixed for five minutes. During this procedure, the materials were moved from the edge to the center of the mixer tank by trowel for the further of mixing. All of these procedures can be seen in Figure 3.18.

Before testing overlay materials as overlaid specimens (substrate concrete + overlay materials), monolithic specimens of overlay mixtures were prepared. During this procedure, all materials were tested in the freshly mixed state for slump flow and air content in accordance with relevant ASTM standards. Specimens were then prepared for tests in the hardened state. Several Ø100 x 200-mm cylinder specimens were prepared for compression testing, rapid chloride permeability test and modulus of elasticity test, and 400 (length) × 75 (depth) × 80 (height) mm prismatic specimens were prepared for four-point flexural strength and freezing-thawing testing. Also, for each overlay mixture three 285×25×25 mm bar specimens and ring specimens were

cast to determine drying shrinkage and restrained shrinkage cracking potential, respectively

Table 3.4 Mixture proportions and main properties

| Materials (kg/m³) | SUBC | MSC | F_ECC | S_ECC |
|---|---|---|---|---|
| **Portland Cement** | 400 | 454 | 566 | 593 |
| **Micro-silica** | - | 45 | - | - |
| **Fly Ash** | - | - | 680 | - |
| **Slag** | - | - | - | 712 |
| **Water** | 180 | 150 | 331 | 347 |
| **Silica Sand** | - | - | 453 | 474 |
| **Coarse Aggregate** | 920 | 1068 | - | - |
| **Fine Aggregate** | 900 | 699 | - | - |
| **HRWR** | 1.8 | 5.5 | 5.0 | 6.0 |
| **AEA** | 0.43 | 0.43 | - | - |
| **PVA** | - | - | 26 | 26 |
| **Water/Binder** | 0.45 | 0.30 | 0.27 | 0.27 |
| **Slump flow (mm)** | - | - | 815 | 670 |
| **Air content (%)** | 5.3 | 4.7 | 6.9 | 6.4 |
| **28 day Young's modulus (GPa)** | 25.8 | 35.2 | 19.7 | 24.9 |

Table 3.5 MDOT (2009) the bridge deck concrete requirements and properties of SUBC

| REQUIREMENTS | MDOT | SUBC |
|---|---|---|
| **28-day compressive strength (MPa)** | 31 | 31,9 |
| **Minimum cement content (kg/m³)** | 390 | 400 |
| **Entrained Air (%)** | 4,5±1,5 | 5,3 |
| **Slump (mm)** | 25-150 | 65 |
| **28-day flexural strength (MPa)** | 5 | 5,7 |

After that, SUBC specimens were prepared to determine the pavement overlay performance of F_ECC, S_ECC and MSC mixtures related to reflective cracking, flexural properties and bond properties. At this stage, composite (overlay/SUBC) specimens were prepared. The composite specimen preparations were explained in Section 3.2.4.


Solid ingredients


Water addition


HRWR addition


AEA addition


Moving the materials from the edge to the center


Final mixing of all materials

Figure 3.18 Production of MSC and SUBC

### 3.3.3 Test Procedures of Overlay Mixtures

### 3.3.3.1 Compressive Strength

Twenty four cylinder samples (6 specimens for each of age) of 100x200 mm were cast from MSC, F_ECC and S_ECC mixtures. The compression test was performed on the cylinder samples by using a 3000 kN capacity testing machine in accordance with ASTM C39 (Figure 3.19). All of the specimens were tested for compressive strength measurement at the age of 1, 7, 28 and 90 days. Before conducting this test, the top and bottom surfaces of the cylinder samples were capped with sulfur compound.



Figure 3.19 Compressive strength testing machine with a cylinder sample

### 3.3.3.2 Flexural Performance

To measure the flexural performance of ECC mixture, twenty four prismatic samples (6 specimens for each testing age) having dimensions of 400x75x80 mm were cast from each overlay mixtures. Four-point bending test was carried out on a closed-loop controlled material test system at a loading rate of 0.005 mm/s (Figure 3.20). The span length of flexural loading was 350 mm with a 116 mm center span length. In the flexural load–deformation curves, the maximum stress is defined as the flexural strength (modulus of rupture — MOR), and the corresponding deflection is defined as the flexural deformation capacity.

Figure 3.20 Four-point bending test

### 3.3.3.3 Drying Shrinkage

The drying shrinkage of overlay materials was determined up to 180 days after an initial curing of one day in the mold and 27 days in lime saturated water by using three 285×25×25 mm prismatic specimens in accordance with ASTM C157 (2004) (Figure 3.21). Gauge studs were inserted in the bar molds coaxial with the bar before the overlay mixtures was poured in to the molds. The drying shrinkage specimens were stored in laboratory at 23±2 °C, and 50±5% RH. Mass loss and drying shrinkage measurements were done for 1, 2, 3, 4, 5, 7, 14, 21, 28, 56, 112 and 180 days.


Figure 3.21 Drying shrinkage samples of overlay mixtures and device

### 3.3.3.4 Restrained Shrinkage

Restraining ring was made of overlay mixtures ring (140 mm in height) cast around the outer perimeter of a steel ring with 280 mm and 305 mm inner and outer diameters, respectively. A 25.4 mm thick layer of overlay mixture was cast around a 12.5 mm thick steel annulus. For F_ECC, S_ECC and MSC mixtures, three rings were cast and cured in the molds for 24 hours. The exterior mold was removed 24 hour after casting and the top surface of the ring was covered using a silicone-based sealant. The rings were then placed in an environmental chamber at $50 \pm 5\%$ RH and $23 \pm 2$ $^o$C (Figure 3.22). The restrained shrinkage was used to record the onset time of a new crack and the time improvement of the width at the crack mouth. The cracking pattern, crack number and crack width were measured as a function of age.



| MSC | F_ECC | S_ECC |

Figure 3.22 Restraining ring shrinkage samples of overlay mixtures

### 3.3.3.5 Rapid Chloride Permeability Test

The rapid chloride permeability test (RCPT), which is standardized with ASTM C 1202 (1997), is conducted to determine the quantity of electrical current that passes through a spacimen with the dimensions of 50 mm (height) to 100 mm (diameter) in 6 hours. For this test, from each overlay material, the specimen is cut like a disc of a 50x100 mm cylinder. The specimen is placed between two cells, one is filled with 3.0% salt (NaCl) solution and the other is filled with a 0.3 M sodium hydroxide (NaOH) solution. After that, the leads submerged into the cells with a voltage of 60V during the test. A qualitative rating is made of the concrete's permeability according to the charge that passes through the specimen. The test set-up can be seen in Figure 3.23. Chloride ion permeability properties of overlay materials were tested for 28 and 90 days age (Figure 3.24).

Figure 3.23 Rapid chloride permeability test set-up



MSC                    F_ECC                    S_ECC

Figure 3.24 Rapid chloride permeability test samples

### 3.3.3.6 Modulus of Elasticity Test

In accordance with ASTM C 469 (2010), the static modulus of elasticity was measured for F_ECC, S_ECC and MSC overlay mixtures. Cylinder samples of these mixtures were tested in uniaxial compression at a stable rate of loading according to ASTM C39 (2003). A compressometer, which was placed parallel to the direction of the applied load, was used to determine longitudinal strains. The compressometer was fixed at center and mid-height of the sample and the compressive deformation was determined using two LVDTs placed at completely opposite positions on the surface of the sample. The empirical test set-up used to determine the stress–strain characteristics of the mixtures is seen in Figure 3.25.

Figure 3.25 Experimental test set-up of modulus of elasticity

### 3.3.4 Test Procedures of Overlaid (Overlay + SUBC) Specimens

### 3.3.4.1 Flexural Performance of Overlaid Specimens

The first step in layered sample preparation was to cast the 400x75x80 mm base member from SUBC, which represents the old rigid pavement. After demoulding and 28-days basic curing in lime-saturated water, the substrates were left for 5 months in the curing room at a temperature of 23 °C and a relative humidity of 50%. After that, specimens were cut with a diamond saw to catch the thickness of 30 mm. This cut surface procures also the same surface condition of the substrate in each overlay system. Thus, 400x75x30 mm beam specimens were produced to use as concrete substrate. The overlay material was cast on the upper of the substrate material with three different thicknesses: 2.5 cm, 3.5 cm and 5.0 cm thickness (Figure 3.26). A sample consisted of a layer of overlay material on a substrate simulating the structure to be renovated. Three different overlay materials were used (MSC, F_ECC and S_ECC). To determine the flexural performance of layered overlay-substrate

composite beams, four point bending tests were performed with MSC, F_ECC and S_ECC overlay surfaces on the bottom (in tension) and SUBC surface on the top (in compression) as in the field condition (Figure 3.27). In each overlay type, eighteen specimens were cast over the concrete substrate (SUBC) with dimensions of 400x75x30 mm. All samples were demolded after 24 hours, and moisture cured in plastic bags at 95±5 % RH, 23±2 °C for 7 days, and then, air cured at 50±5 % RH, 23±2 °C until the day of testing. Four point bending test was carried out on a closed-loop controlled material testing system at a loading rate of 0.005 mm/s with the composite beams at the age of 1, 7 and 28 days. A four point bending loading fixture was improved to compensate extraneous deformations such as support settlements and sample rotations. The mid-point deflection was recorded and it represents the relative displacement between the top of the beam and the loading fixture. The span length of flexural loading was 350 mm with a 116 mm center span length. During the flexural tests, both loading and mid-span deflection were written down on a computerized data recording system.



Figure 3.26 Layered specimens with different thicknesses for flexural performance

Figure 3.27 Four-point bending test of overlaid specimen

**3.3.4.2 Reflective Cracking Test of Overlaid Specimens**

Overlay is generally used as a surface repair on deteriorated pavements, parking lots, bridge decks, airport pavements and industrial floors for riding quality or strengthening of existing pavement. These deteriorated structures may involve joints or cracks, and these defects can be the starting points of failures in repaired systems. Reflective cracking is one of the most generally observed overlay failure phenomenon in the overlay applications. To simulate the reflective cracking in overlaid pavements, a composite beam, initially used by Lim and Li (1997), Kamada and Li (2000) and, Zhang and Li (2002), is utilized with four-point bending load applied to the beam as a loading condition. The substrate concrete blocks were cut out of concrete beams with size 400x75x30 mm. These concrete beams were cut into the base blocks with a diamond saw. Each such beam was cut into two equal blocks of 30 mm height to form two substrate beams with preinduced joint (or substrate crack) at beam center (see Figure 3.28). Only diamond saw cut surface against the overlay were used in this study. The existing vertical cracks were made by using a smooth water-proof tape along the periphery of each substrate to form a notch prior to casting the overlay materials. After preparation of 30 mm thick smooth SUBC specimens with a vertical crack in the center of the beam, MSC, F_ECC and S_ECC mixtures were cast on these substrate concrete specimen with three different thicknesses, 25 mm, 35 mm and 50 mm. All samples were demoulded after 24 hours,

58

and moisture cured under plastic bags at 95±5 % RH, 23±2 °C for 7 days. The samples were then air cured at 50±5 % RH, 23±2 °C until the day of testing. Four-point bending test, which modelled in Figure 3.29, was performed under displacement control at a loading rate of 0.005 mm/s with these composite specimens at the age of 7 and 28 days. Mid-point deflection was determined by using two linear variable differential transducers (LVDT) that sat on the base part of the bending test fixture. The lengths of interface crack (extension) were measured on both sides of a sample like the distance from an initial notch tip to a propagated crack tip along the interface between the substrate concrete and the overlay material, after the samples' final failure. Six samples were cast for each overlay material type and thickness, and each testing age.


Figure 3.28 SUBC sample preparation for reflective cracking test
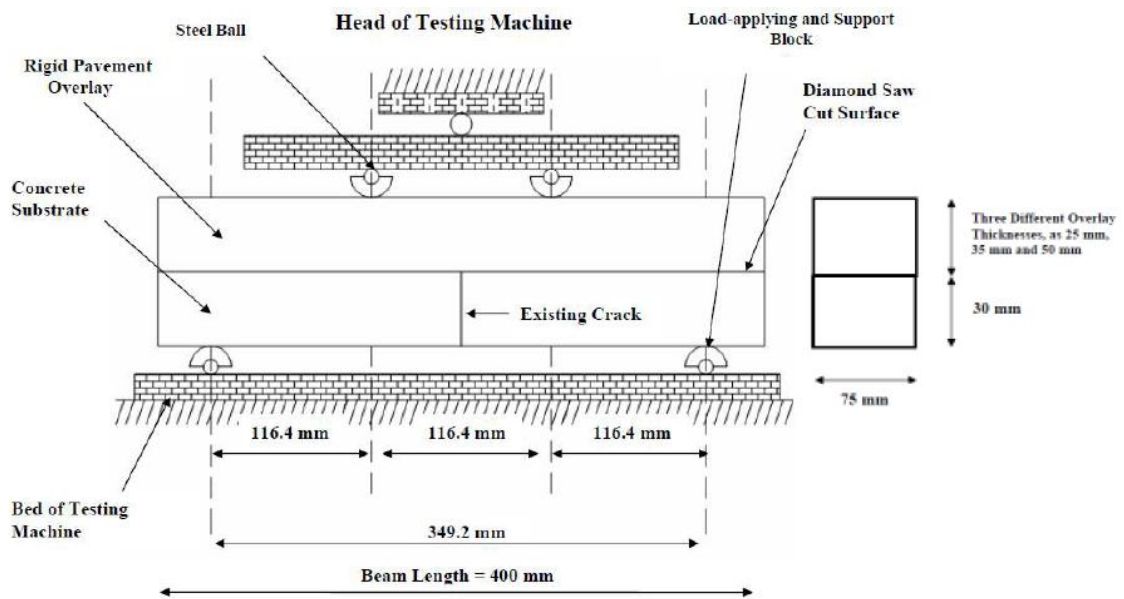

Figure 3.29 Model of four-point bending for reflective cracking test

### 3.3.4.3 Slant Shear Test

The slant shear test (according to ASTM C882, 2012) has become one of the most accepted test methods, and has been adopted by a number of international specifications as a test for determining the bond of repair materials to concrete substrates. The test is also economical and can be easily reproduced. It measures the bond strength under a state of stress that combines shear and compression stresses. In this test, the repair material is bonded to a substrate concrete specimen on a slant elliptical plane inclined at an angle of 30° from the loading axis to form 100×200mm composite cylinder.

The first step in specimen preparation for slant shear test was to cast several cylinder samples with 10 cm in diameter and 20 cm in height (Figure 3.30-a). After demolding, the cylinders were cured in lime-saturated water at 23±2 °C for 4 weeks and in laboratory environment for 5 months. Realizing that in field practice the old concrete had worked for a long time and could be thought to have almost completed chemical reaction and shrinkage. Our previous experiences have demonstrated that the plain concrete specimens cured 28 days under lime saturated water and subjected to drying afterwards for 5 months were almost reached hygral equilibrium state. For this reason, to simulate field practice better, at the time of placing an overlay on the previously prepared substrate concrete, the age difference between overlay and substrate concrete was 6 months. At the end of six months, the base substrate concrete half-cylinders were cut out of whole cylinder specimens. To eliminate mechanical interlock induced by rough bond plane, which affects the measured value of bond strength, a smooth diamond saw bond plane has been used. Figure 3.30-b shows representative substrate halve of the slant shear test specimens with the smooth surface texture. The substrate half concrete cylinders were then placed into plastic molds with the slant side up and were ready for overlay casting (Figure 3.30-c). No bonding agent was used before placing the overlay on any of the substrates. The concrete substrates were also dry when an overlay was placed on top of them. The molds were filled with overlay materials and the composite specimens were demolded after 24 hours, and moisture cured in plastic bags at 95±5 % RH, 23±2 °C, until the age of testing. In each overlay type, eighteen specimens were cast over the concrete substrate. Figure 3.30-d shows complete composite specimens for the slant

60

shear test. After curing, cylinders were tested in compression (according to ASTM C39, 2003) at the age of 1, 7 and 28 days in order to investigate the bond strength of each material. Before testing in compression, both ends of the cylinders were capped with sulfur to ensure parallel surfaces and to dissipate the load evenly. The test setup is shown in Figure 3.31.



(a)                                    (b)



(c)                                    (d)
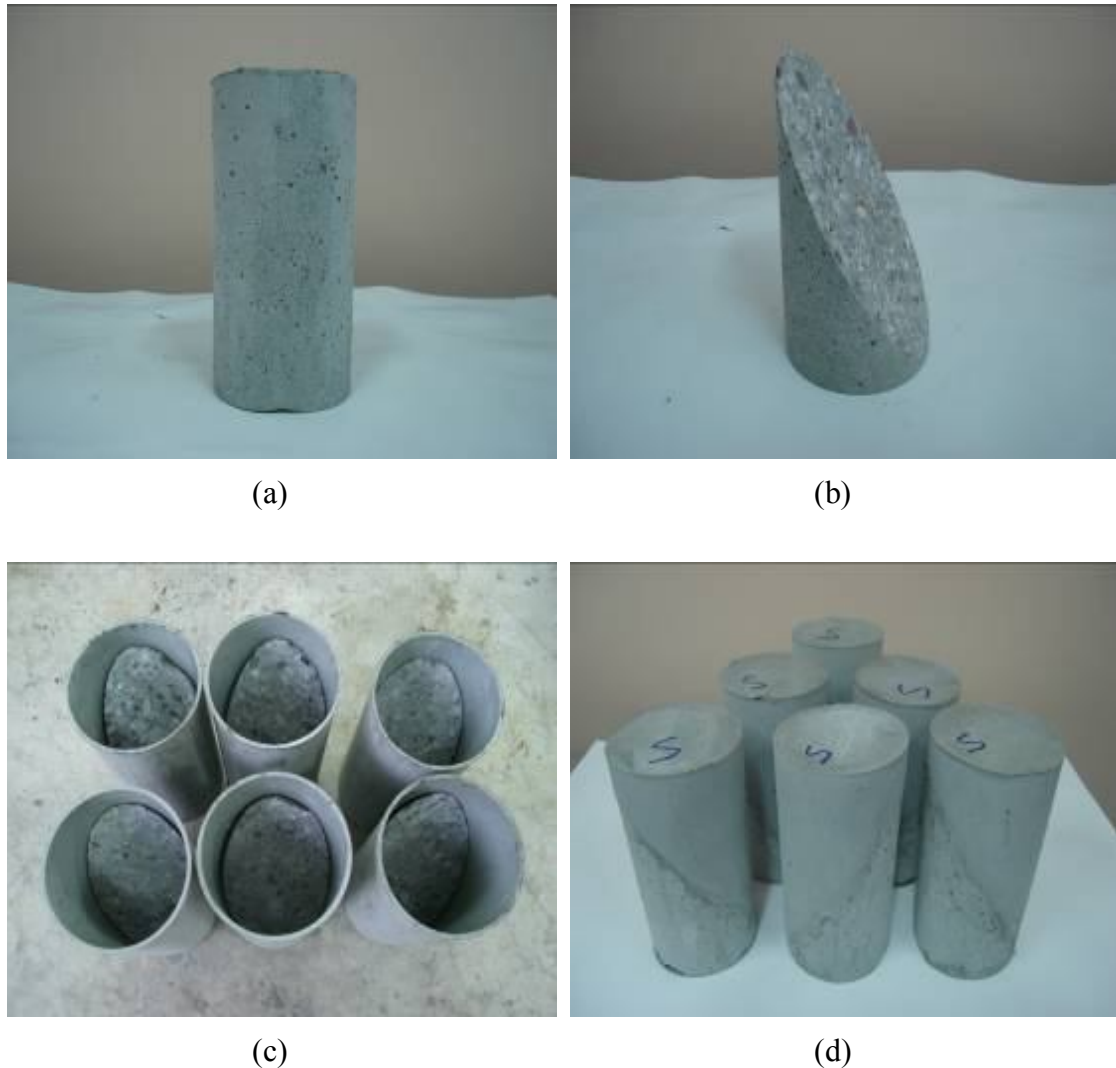
Figure 3.30 Preparation of composite cylinders for slant shear test

### 3.3.4.4 Splitting Prism Test

In the splitting test, a prism with rectangular cross-section is loaded along an interface plane to simulate a tensile load perpendicular to the plane. Tension stresses cause failure in a plane passing through upper and lower axes of loading and split the sample into two halves. This test method is similar to the ASTM C496 (2011) test for splitting tensile strength of cylindrical concrete specimens.

Figure 3.31 Slant shear test set-up

The first step in specimen preparation for splitting prism test was to cast the 76.2 mm x 81.3 mm x 406.4 mm base member (Figure 3.32). To obtain rough surface texture, no surface finish has been applied on the surface of the fresh substrate concrete. After demolding, the substrate blocks were cured in lime-saturated water at $23\pm2$ $^{o}$C for 4 weeks and then cured in laboratory environment for 5 months. The substrate concrete specimens for splitting prism test were prepared by cutting each substrate concrete block into sixteen pieces with a height of 30 mm (Figure 3.32) using a diamond saw. Two different situations were considered for the interface surface between the substrate and the added overlay layer to sight the effects of surface roughness on the bond strength. These are smooth and untreated rough surfaces. Figure 3.33 shows close-up view of smooth and untreated specimens' surface. From each prism specimen, eight pieces (below) were used for smooth surface repair sample and eight pieces (above) were used for untreated surface repair specimen. To prepare a repair specimen in the form of an overlay system, an 30 mm thick overlay layer (same as substrate) was cast against either the smooth surface or the untreated surface of the base concrete blocks (Figure 3.34). The prepared specimens were then moisture cured in plastic bags at $95\pm5$ % RH, $23\pm2$ $^{o}$C, until the age of testing. For each considered situation—surface treatment, and testing ages — eight splitting

62

prism specimens were cast. Three mixes of overlay materials (F_ECC, S_ECC and MSC) were used and as control, one continuous bond composed of only substrate concrete material were also cast to permit comparison of the results of overlaid samples with monolithic sample at the same time.
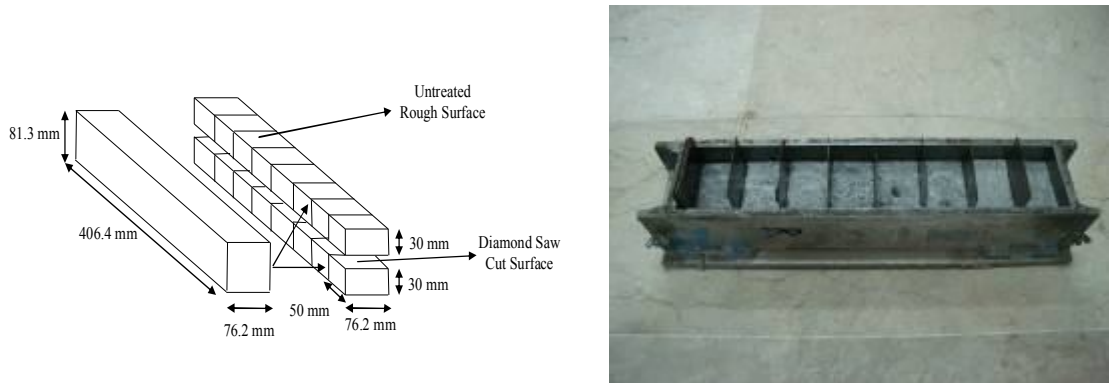


Figure 3.32 Specimen preparation: base concrete block (unit in mm); cutting of base concrete block; and casting with overlay materials



Figure 3.33 Typical close-up view of untreated rough and smooth concrete surfaces



Figure 3.34 Final view of splitting prism test samples

The splitting prism test setup is shown in Figure 3.35. The bond strength was calculated as Equation 3.1.

$$T = \frac{2P}{\pi A}$$

(3.2)

Where, T: bond strength, P: maximum load, A: area of the bonding plane.
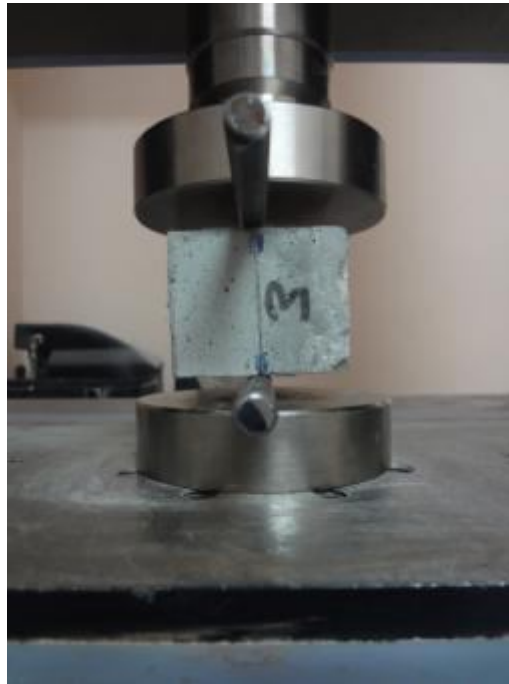


Figure 3.35 Splitting prism test set-up

## CHAPTER IV

## RESULTS AND DISCUSSIONS

## 4.1 Development of Engineered Cementitious Composites (ECC) with Locally Available Materials

Strain-hardening high performance fiber reinforced cementitious composites (patent-named as Engineered Cementitious Composites: ECC) is a promising and a new class of composite materials which are micro-mechanically designed to achieve high ductility and high durability. Unlike ordinary and fiber reinforced concrete (FRC), ECC strain-hardens after first cracking, similar to a ductile metal, and demonstrates a strain capacity about 300-500 times higher than normal concrete. Different from ordinary concrete and most FRC, ECC displays self-controlled crack widths under increasing load. Regardless of the ultimate tensile strain, average crack widths remain at about 60 μm or less. This behavior is the result of micro-mechanical tailoring of ECC, i.e. tailoring its micro-structure for achieving the desired mechanical performance from the composite. Moreover, by this superior behavior (the tight crack widths and high tensile ductility), this construction material shows also high durability.

For developing countries like Turkey, construction and concrete industry have a crucial importance on sustainable development. Even though lowering the cost of structural design and concrete reduces the initial cost, improper design of the structure, earthquake loads, severe exposure conditions, etc. increase the overall planned cost through early repairs, loss of time, man-power, materials and serviceability. The construction of the structures with a more ductile and durable material through the use of ECC, however, will reduce the need for material to be used in repair/strengthening and new constructions by increasing the service life of the structures. This, in turn, will enable to decrease the consumption of natural sources and energy used in the production process of the construction materials like cement and steel reinforcement. Moreover, the industrial by-product fly ash will

65

be re-cycled by using it very high volumes, and the hazard to the environment will be prevented.

In this section of thesis, it is aimed for sustainable development to produce ECC with locally available materials and with high volumes of mineral admixtures, to improve the performance and to lower the cost of the composites.

### 4.1.1 Compressive Strength

The compressive strength test results of the ECC mixtures incorporating different maximum aggregate size (MAS) and amount, and fly ash (FA) and slag contents, which are obtained from local resources, are shown in Table 4.1.

Table 4.1 Compressive strength test results of ECC mixtures

| Mix ID. | Compressive Strength (MPa) | | | |
|---|---|---|---|---|
| | 7 days | 28 days | 90 days | 180 days |
| FA1.2_0.36_400 (M45) | 40.1 | 69.3 | 75.8 | 78.6 |
| FA1.2_0.45_400 | 40.9 | 69.8 | 72.5 | 76.2 |
| FA1.2_0.55_400 | 37.4 | 62.6 | 67.6 | 73.8 |
| FA1.2_0.36_1000 | 37.4 | 60.8 | 65.5 | 71.4 |
| FA1.2_0.45_1000 | 40.0 | 63.5 | 66.8 | 71.9 |
| FA1.2_0.55_1000 | 41.6 | 69.4 | 72.7 | 77.3 |
| FA2.2_0.36_400 | 30.2 | 46.1 | 54.7 | 59.1 |
| FA2.2_0.45_400 | 29.0 | 45.8 | 56.8 | 62.3 |
| FA2.2_0.55_400 | 30.3 | 47.9 | 58.7 | 63.4 |
| FA2.2_0.36_1000 | 27.9 | 48.7 | 57.7 | 63.1 |
| FA2.2_0.45_1000 | 29.3 | 50.5 | 56.5 | 61.8 |
| FA2.2_0.55_1000 | 28.6 | 47.5 | 54.2 | 60.3 |
| S1.2_0.36_400 | 59.9 | 88.5 | 91.2 | 92.1 |
| S1.2_0.45_400 | 58.0 | 90.0 | 93.2 | 95.2 |
| S1.2_0.55_400 | 56.9 | 86.5 | 90.7 | 92.6 |
| S1.2_0.36_1000 | 60.0 | 89.6 | 92.2 | 95.1 |
| S1.2_0.45_1000 | 58.1 | 91.4 | 94.2 | 95.8 |
| S1.2_0.55_1000 | 58.5 | 87.9 | 91.1 | 94.3 |
| S2.2_0.36_400 | 51.8 | 76.3 | 80.3 | 83.7 |
| S2.2_0.45_400 | 50.6 | 78.5 | 88.7 | 88.9 |
| S2.2_0.55_400 | 52.8 | 81.5 | 86.6 | 88.6 |
| S2.2_0.36_1000 | 52.9 | 79.4 | 84.2 | 87.1 |
| S2.2_0.45_1000 | 50.4 | 78.0 | 88.1 | 89.6 |
| S2.2_0.55_1000 | 52.6 | 79.2 | 82.3 | 85.3 |

Compressive strength tests were performed at 7, 28, 90 and 180 days of age. Six cylinder specimens were tested at each age for each mixture. As seen from Table 4.1 and as expected, at same replacement level, especially at early ages, the ECC mixtures incorporating slag produced significantly greater compressive strengths than the FA. The greatest difference was observed at 7 days for the replacement level of 2.2, where the slag-ECC specimens achieved more than 70% higher compressive strengths than those containing FA. The higher early strength of slag-ECC specimens can be predicated to the predominant reaction of slag with alkali hydroxide during the early hydration period. This result is also partially a result of the higher rate in hydration of the slag due to its large specific surface area (425 $m^2$/kg) compared to that of FA (290 $m^2$/kg). High surface area provides more nucleating sites and $OH^-$ ions as well as alkalis into the pore fluid. All the mixtures, however, showed compressive strengths higher than 45 MPa at 28 days of age. This value could significantly exceed that of normal concrete strength (30 MPa), and fulfill engineering requirements in most projects.

The strength development characteristics of FA-ECC and slag-ECC with time were normalized as the ratio of average compressive strength data of ECC mixtures with same mineral admixture type and replacement level at various curing ages to those at 7 days and the normalized values were presented in Figure 4.1. Therefore, at each age, % compressive strength gain (relative to compressive strength at 7 days) versus age data could be plotted. Figure 4.1 indicated a continued increase in strength even after 28 days for ECC mixtures with FA while the compressive strength appeared to approach an asymptotic value after 28 days of age in the ECC mixtures with slag. The FA-ECC mixtures had significant strength gain from 28 days to 180 days, while the slag-ECC had already achieved more than 90% of their 180-day strength at 28 days. This finding was partially a result of the advances in hydration and pozzolanic reactions of the slag compared to that of ECC containing FA. However, from the strength gain observed in ECC mixtures it could be stated that significant improvements in the compressive strength and the rate of strength gain were obtained by increasing the volume of FA.

Table 4.1 tabulates the compressive strength dataset for all mixes. As seen from Table 4.1, an increase in the MAS and aggregate amount had no consistent effect in
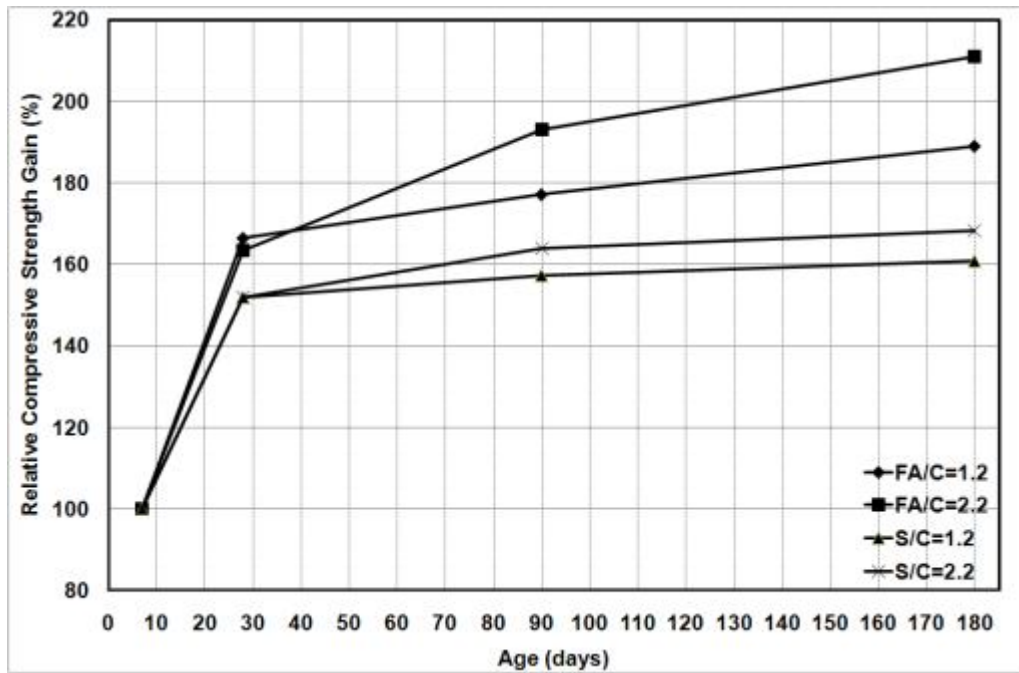
Figure 4.1 Compressive strength increase of ECC mixtures with the age

the compressive strength of ECC mixtures, and at same mineral admixture type and amount mixtures yielded very similar compressive strength test results. This behavior was consistent for all mineral admixture replacement level. This finding was likely the result of a limited supply of mix water available for hydration reactions or the hydration by-product required for pozzolanic reactions. If, for example, one examines mix S2.2_0.55_1000, shown in Table 4.1, which have the same W/B ratio and slag replacement rate as S2.2_0.36_1000 and less binder (S + C) content because of higher aggregate/binder ratio, one could deduce that the compressive strength of ECC mixtures with high cementing material was mostly influenced by the limited space suitable for hydration processes. This consequently would result in a high percentage of unhydrated particles in all ECC mixtures with a high binder content of more than 1100 kg/m$^3$. It was also known that conventional concrete strength was affected when the aggregate size becomes large or small. Smaller aggregate size, and consequently, higher surface area for a given aggregate content, resulted in lower bond stress at a given load level (Cetin and Carrasquillo, 1998). In addition, everything else being the same, the larger the aggregate size the higher the local W/C ratio in the interfacial transition zone and, as a result, the weaker the concrete (Mehta and Monteiro, 2006). Therefore, unlike conventional concrete, aggregate amount (0.36, 0.45 and 0.55 aggregate-binder ratios) and aggregate size (0.4 and 1.0 mm maximum particle sizes) did not influence the compressive properties in the case

68

ECC within the limited aggregate amount and size employed in the present experiments.

**4.1.2 Fracture Toughness**

Fracture toughness tests were performed on ECC matrix specimens (ECC without fiber) at 28, 90 and 180 days. Tests were carried out according to the ASTM E 399 (2003). The fracture toughness test results of the ECC mixtures incorporating different aggregate sizes and amount, and FA and slag contents were summarized in Table 4.2. Figure 4.2 illustrated the effects of FA, slag, MAS and aggregate amount on the fracture toughness of ECC matrixes as a function of the age of the matrix. The figure showed that the fracture toughness of the ECC matrixes containing slag was consistently higher than the fracture toughness of the ECC matrixes containing FA. This was mainly due to the enhanced matrix strength even at early ages caused by the presence of slag particles. Slag particles were most commonly activated by the hydration product of Portland cement, where calcium hydroxide formed during hydration was the principal activator. Slag hydration products lead to decreased porosity in the matrix, resulting in enhanced matrix strength and toughness. The pores in ECC matrix may act as stress concentrators and a reduction in their size will reduce the size of their stress intensity field. Therefore fracture toughness can be controlled by the total porosity and pore size distribution of the hardened ECC matrix. This result is consistent with that of the Mai and Cotterell who demonstrated a correlation between higher fracture toughness and lower porosity in cement mortar. In ECC composites, higher matrix toughness could be detrimental to achieving the desired mechanical properties, and reducing the margin to develop multiple-cracking in terms of toughness ratio (Li et al., 1995). Therefore, in order to satisfy the limits on the matrix toughness in slag-ECC, aggregate particle size had to be reduced or amount of slag replacement had to be increased, which consequently lead to a relatively low matrix fracture toughness values. Test results also indicated that the use of FA particles should be helpful for achieving strain-hardening behavior, as a lower fracture toughness value provided better opportunities for multiple cracking in the composite. It also demonstrated that fracture toughness was nearly constant as a function of age (in this case, for ages of 90 to 180 days).

Table 4.2 Fracture toughness test results of ECC matrix mixtures

| Mix ID. | Fracture Toughness (MPa×m$^{1/2}$) | | |
|---|---|---|---|
| | 28 days | 90 days | 180 days |
| FA1.2_0.36_400 (M45) | 0.536 | 0.662 | 0.683 |
| FA1.2_0.45_400 | 0.580 | 0.712 | 0.741 |
| FA1.2_0.55_400 | 0.627 | 0.788 | 0.799 |
| FA1.2_0.36_1000 | 0.624 | 0.700 | 0.723 |
| FA1.2_0.45_1000 | 0.649 | 0.721 | 0.738 |
| FA1.2_0.55_1000 | 0.707 | 0.772 | 0.807 |
| FA2.2_0.36_400 | 0.356 | 0.534 | 0.596 |
| FA2.2_0.45_400 | 0.424 | 0.551 | 0.619 |
| FA2.2_0.55_400 | 0.522 | 0.647 | 0.667 |
| FA2.2_0.36_1000 | 0.452 | 0.575 | 0.611 |
| FA2.2_0.45_1000 | 0.494 | 0.600 | 0.638 |
| FA2.2_0.55_1000 | 0.546 | 0.642 | 0.684 |
| S1.2_0.36_400 | 0.795 | 0.801 | 0.809 |
| S1.2_0.45_400 | 0.827 | 0.839 | 0.847 |
| S1.2_0.55_400 | 0.840 | 0.898 | 0.904 |
| S1.2_0.36_1000 | 0.778 | 0.817 | 0.848 |
| S1.2_0.45_1000 | 0.879 | 0.899 | 0.917 |
| S1.2_0.55_1000 | 0.873 | 0.944 | 0.961 |
| S2.2_0.36_400 | 0.712 | 0.728 | 0.748 |
| S2.2_0.45_400 | 0.715 | 0.756 | 0.766 |
| S2.2_0.55_400 | 0.747 | 0.795 | 0.811 |
| S2.2_0.36_1000 | 0.726 | 0.799 | 0.809 |
| S2.2_0.45_1000 | 0.753 | 0.807 | 0.821 |
| S2.2_0.55_1000 | 0.857 | 0.891 | 0.914 |
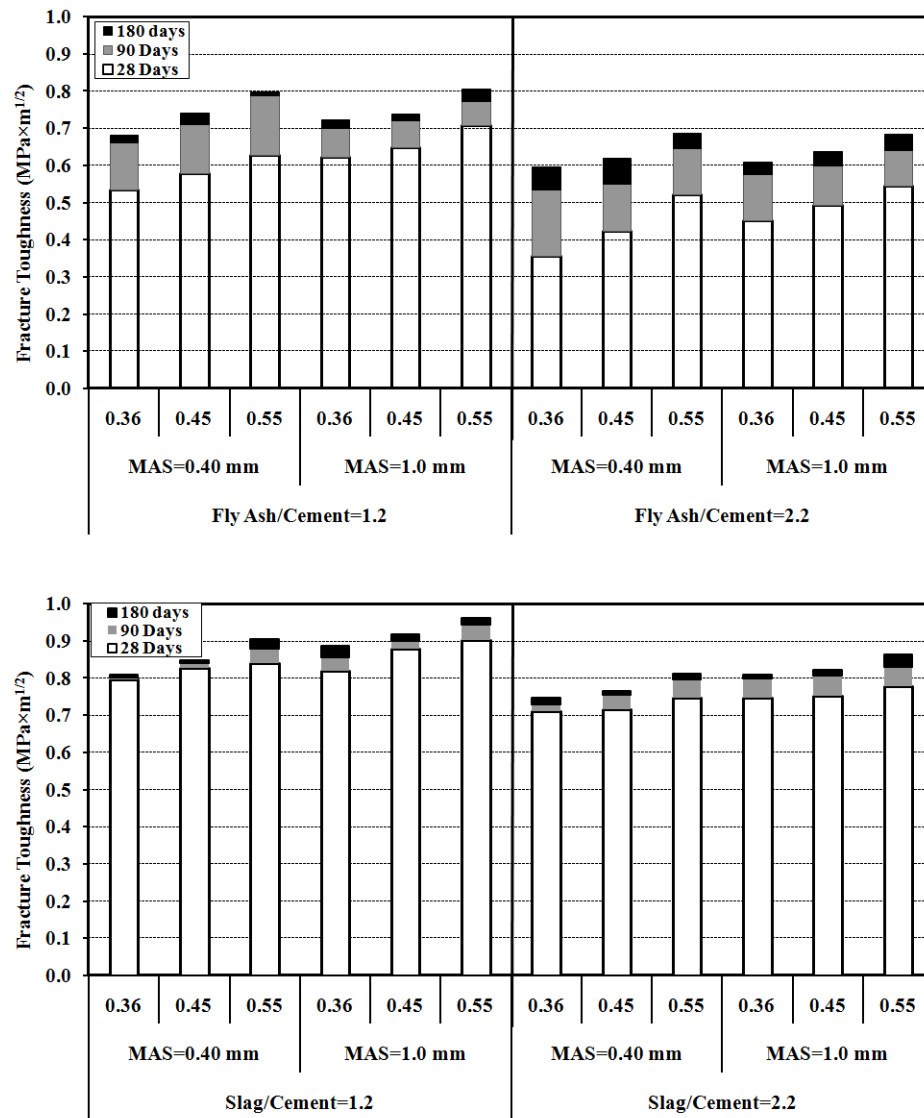
Figure 4.2 Matrix fracture toughness – $K_m$ as a function of the matrix age

The fracture energy of ECC matrixes (with the same replacement rate of mineral admixtures) increases significantly with the increase in aggregate-binder ratio and aggregate size. Especially at low strength level (for example, ECC mixtures with FA/C ratio of 2.2), matrix fracture toughness values significantly increased with the increase of aggregate amounts and sizes. It is well known that when concrete is loaded, cracks prefer to propagate along the weaker interfacial zone or larger pores in the matrix (Davis and Alexander, 1989; Davis and Alexander, 1992; De Larrard and Belloc, 1997). As the crack meets an aggregate particle, it is forced either to propagate through the tougher aggregate or deflect and travel around the aggregate-mortar interface. The interfacial zone is weaker than the aggregate for low strength concrete. Cracks prefer to propagate along the interfacial zone, while the aggregates

71

debond, and then deflect and bridge cracks. Thus, when aggregate volume increases, more aggregates debond and deflect cracks, resulting in more tortuous cracking path and more energy needed for cracking, and then higher values of fracture toughness. Moreover, the larger maximum size of aggregate, the more tortuous cracking path, also some snapped aggregate and the higher energy was required for overcoming interfacial bond (Chen and Liu, 2004). Especially for FA-ECC mixtures, rougher fracture surfaces were observed for ECC matrixes with maximum aggregate size of 1 mm. From the fractured surface, it was also determined that when the maximum aggregate size was small (0.4 mm for this study), the fracture surface of ECC matrix was smooth. While at high strength (for example ECC with slag), this effect was not as pronounced as in the low-strength matrix mixtures since the quality and porosity of the interfacial zone and matrix was greatly improved. At the range of the aggregate amount studied in this study, thus, more cracks passed through the aggregates in the case of high strength ECC (slag-ECC) while the effects of aggregate on bonding, deflecting and bridging cracks decreased.

### 4.1.3 Flexural Performance

The direct tensile test is considered to be the most accurate and effective method to confirm the strain-hardening behavior of a composite, as quasi-brittle fiber reinforced composites can potentially show apparent strain-hardening behavior under flexural loading, depending on the sample geometry. However, one of the principle concerns in designing concrete structures is the flexural performance of the concrete. Flexural strength test of ECC is also an indirect measure of direct tensile performance. Therefore it was decided to use four-point bending test to investigate the flexural strength and ductility by measuring mid-span beam deflection capacity of ECC mixtures. Previous studies also demonstrate that deflection capacity can be correlated with the tensile strain capacity when the material shows strain hardening behaviour (Qian and Li, 2007; Qian and Li, 2008).

The test results in terms of flexural strength (modulus of rupture – MOR) and ultimate mid-span deflection at the peak stress are displayed in Table 4.3, and the typical flexural stress-mid-span deflection curves for different aggregate amounts of the ECC mixtures are shown in Figure 4.3. To facilitate the comparison between the test results for different ECC mixtures, the same scales for both axes were used in

these figures. In the flexural load–deflection curves, the stress at the first drop associated with the first cracking is defined as the first cracking strength, the maximum stress is defined as the flexural strength (MOR), and the corresponding deflection is defined as the flexural deflection (mid-span beam deflection) capacity. The flexural performances of ECC mixtures were calculated by averaging the results of six four-point bending measurements. It is important to mark that the coefficient of variations of the flexural strength test results within each mix design is lower than 10%.

Table 4.3 Flexural strength test results of ECC mixtures

| Mix ID. | Deflection, mm | | | | Flexural Strength, MPa | | | |
|---|---|---|---|---|---|---|---|---|
| | 7 d. | 28 d. | 90 d. | 180 d. | 7 d. | 28 d. | 90 d. | 180 d. |
| FA1.2_0.36_400 | 5.68 | 4.83 | 4.49 | 4.41 | 8.48 | 12.73 | 12.80 | 12.91 |
| FA1.2_0.45_400 | 4.52 | 4.23 | 3.99 | 3.81 | 7.51 | 11.92 | 12.19 | 12.59 |
| FA1.2_0.55_400 | 4.09 | 3.97 | 3.84 | 3.71 | 7.69 | 11.41 | 12.42 | 12.87 |
| FA1.2_0.36_1000 | 5.11 | 4.59 | 4.12 | 3.98 | 7.88 | 11.63 | 12.04 | 12.44 |
| FA1.2_0.45_1000 | 4.38 | 4.14 | 3.79 | 3.67 | 7.96 | 11.12 | 11.98 | 12.18 |
| FA1.2_0.55_1000 | 3.54 | 3.15 | 3.07 | 3.01 | 8.52 | 12.17 | 12.62 | 12.93 |
| FA2.2_0.36_400 | 7.02 | 5.89 | 5.29 | 5.18 | 7.36 | 10.19 | 11.58 | 11.64 |
| FA2.2_0.45_400 | 6.25 | 5.56 | 4.85 | 4.74 | 7.04 | 10.79 | 11.23 | 11.78 |
| FA2.2_0.55_400 | 5.40 | 4.99 | 4.88 | 4.64 | 7.26 | 10.14 | 10.03 | 11.01 |
| FA2.2_0.36_1000 | 5.55 | 4.72 | 4.50 | 4.40 | 6.59 | 9.39 | 10.59 | 11.17 |
| FA2.2_0.45_1000 | 5.47 | 4.50 | 4.17 | 4.16 | 7.28 | 10.27 | 10.96 | 11.83 |
| FA2.2_0.55_1000 | 4.73 | 4.02 | 3.92 | 3.72 | 7.14 | 9.35 | 10.13 | 10.94 |
| S1.2_0.36_400 | 3.73 | 3.10 | 3.04 | 2.88 | 9.92 | 12.58 | 12.63 | 12.71 |
| S1.2_0.45_400 | 3.24 | 2.71 | 2.62 | 2.49 | 9.89 | 12.38 | 12.70 | 12.98 |
| S1.2_0.55_400 | 2.62 | 2.44 | 2.42 | 2.29 | 9.23 | 12.19 | 12.24 | 12.66 |
| S1.2_0.36_1000 | 3.60 | 2.94 | 2.74 | 2.61 | 9.78 | 12.04 | 12.36 | 12.87 |
| S1.2_0.45_1000 | 2.93 | 2.10 | 1.75 | 1.66 | 9.55 | 12.68 | 12.90 | 13.07 |
| S1.2_0.55_1000 | 2.51 | 2.14 | 1.71 | 1.66 | 9.11 | 12.50 | 12.51 | 12.87 |
| S2.2_0.36_400 | 4.31 | 3.98 | 3.44 | 3.31 | 8.44 | 11.50 | 11.78 | 12.02 |
| S2.2_0.45_400 | 3.66 | 3.22 | 3.18 | 2.95 | 8.69 | 11.89 | 11.73 | 12.11 |
| S2.2_0.55_400 | 3.23 | 2.55 | 2.21 | 2.05 | 8.45 | 11.42 | 11.35 | 11.63 |
| S2.2_0.36_1000 | 4.14 | 3.35 | 3.06 | 2.77 | 8.63 | 11.29 | 11.15 | 11.47 |
| S2.2_0.45_1000 | 3.55 | 3.10 | 2.73 | 2.60 | 8.73 | 11.73 | 11.46 | 11.88 |
| S2.2_0.55_1000 | 3.01 | 2.30 | 2.16 | 1.95 | 8.82 | 11.58 | 11.82 | 12.13 |
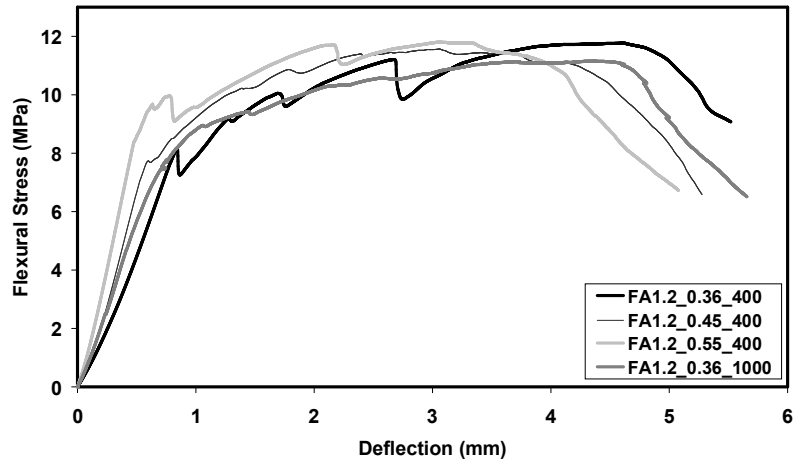
ECC with FA
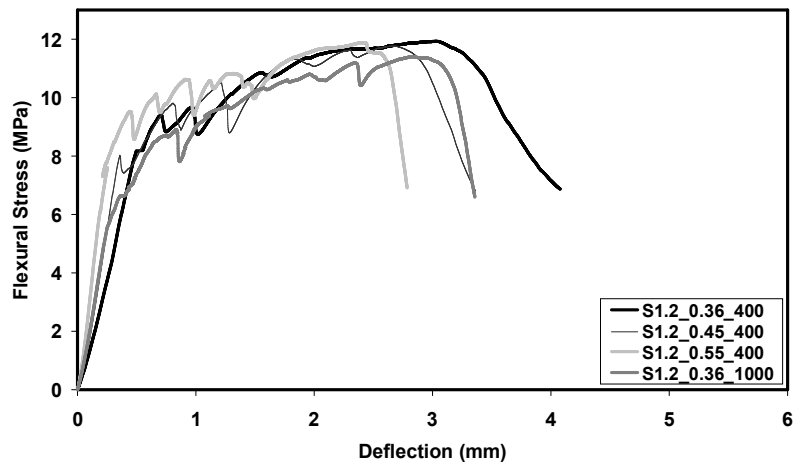


ECC with Slag

Figure 4.3 Typical flexural stress – mid-span deflection curves of ECC mixtures at age of 28 days

**4.1.3.1 Load-deflection Curves**

Typical load deflection curves for PVA-ECC incorporating 2 percent volume fraction of PVA fibers, different amount of aggregate content and MAS were presented in Figure 4.3 for comparison. As seen from the figure, under severe bending load, an ECC beam containing aggregate up to 1.0 mm MAS deforms similarly to a ductile metal plate through plastic deformation (Figure 4.4). Each specimen was examined using a portable microscope during and after the loading to determine the crack width and distribution. In all ECC specimens, the first cracks to appear were flexural cracks starting at the surface of the tension face. After first cracking, the load continues to rise accompanied by multiple cracking, which contributes to the inelastic deformation as stress increases. Shortly after initial

74

cracking, the crack width grows rapidly with an increase of deformation, and then stabilizes at a value between 40 to 90 μm while additional micro-cracks further improve. Microcracks developed from the first cracking point and spread out in the mid-span of the flexural beam as seen in Figure 4.4. Bending failure in ECC occurred when the fiber bridging strength at one of the microcracks was reached, resulting in localized deformation at this section (Figure 4.4) once the flexural strength is approached.
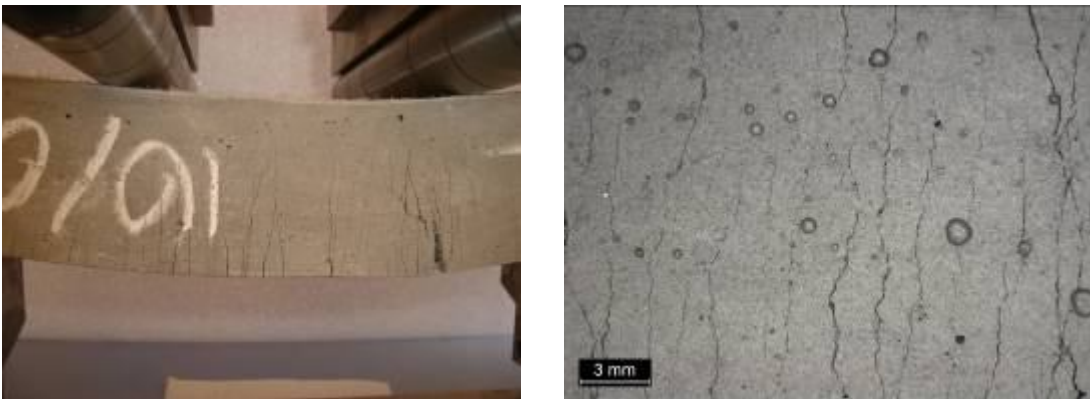


Figure 4.4 Typical cracking patterns of ECC beam specimen after flexure load applications (Mix ID.: FA1.2_0.55_1000)

The first crack strength was defined as the strength at which the strength-deformation response deviated from linearity. The average first crack strengths of ECC mixtures vary from 6.0 to 8.0 MPa in accordance with mineral admixture type (FA or slag) and replacement rate. The increase in FA (or slag)/C ratio from 1.2 to 2.2 reduces the first crack strength by an average of up to 20 percent. However, aggregate amount and MAS had little or no influence on the magnitude of the first crack loads of the ECC beams at constant mineral admixture replacement rate. The slope of the load-deflection curve represents the stiffness of the beams and it can be easily noted from Figure 4.3 that the slope increases significantly with replacement of slag and increasing aggregate content, and thereby indicating an increase in the stiffness of the ECC beams. This result is consistent with what is stated in the literature (Aïtcin and Mehta, 1990; Baalbaki et al., 1991; Cetin and Carrasquillo, 1998). Aggregate is known to be stiffer than mortar, the other component of ECC. Thus, inclusion of higher aggregate content makes the final product stiffer. As also shown in Figure 4.3, ECC with 0.4 or 1.0 mm maximum aggregate size had very similar stiffness for ECC mixtures containing same mineral admixture (FA or slag) and at all aggregate content levels. As a result, within the size range studied, elastic modulus appears to

be independent of MAS at a given aggregate content. This observation makes sense because; stiffness measurements were performed using the initial slopes of the load-deflection curves (generally up to 40 percent of the ultimate load). Bond strength is not likely to be a dominant factor to influence the test result at this load level (Cetin and Carrasquillo, 1998).

**4.1.3.2 Flexural Strength (Modulus of Rupture – MOR)**

The flexural strength values are shown in Table 4.3. As seen from Table 4.3, the average ultimate flexural strengths vary from 9.35 to 12.73 MPa at 28 days of age. Specimens which contained slag consistently developed slightly higher strength than specimens of identical mix proportions, but contained FA especially at the ages of 7 days, however similar values at later ages. It is also apparent that different from the compressive strength test results there is not a considerable influence of the FA or slag replacement rate on the flexural strength values especially at the ages of 28 days or later in the tested range. For instance, the flexural strength of ECC with FA/C ratio of 2.2 is about 85% that of the ECC mixtures with FA/C ratio of 1.2. This value is about 93% that of ECC mixtures with S/C ratio of 1.2. The MOR is likely limited by the fiber bridging capacity governed by the fiber/matrix bond and in turn by the mineral admixture replacement rate. However, even at about 70% replacement of cement by FA or slag (mineral admixture / cement ratio of 2.2), the flexural strength of ECC at 28 days was considerably higher than that of conventional concrete and fiber reinforced concrete. Moreover, flexural strength increased with age more slowly than compressive strength. As in the case of compressive strength test results, the aggregate content and MAS also appear to have a negligible effect on the flexural strength, at least within the parametric range investigated.

**4.1.3.3 Mid-span Beam Deflection**

The flexural deflection capacity of ECC mixtures, which reflects the material ductility, with different FA and slag contents, aggregate size and amount are summarized in Figure 4.5 and Table 4.3. As shown in Figure 4.5, the total deflection of ECC beam strongly depends on the type and amount of mineral admixture. The mixes of slag-ECC showed significantly lower deflection capacity when compared to the ductility of the mixes of FA-ECC. The reduced ductility can possibly be caused

by the higher fracture toughness, bond strength and friction between the slag-ECC matrix and the fibers compared with FA-ECC. The microstructural studies provide some assistance in evaluating the differences in macroscopic behavior between FA-ECC and slag-ECC. The SEM observation was made with specimens at the age of 28 and 180 days, respectively. The SEM observation of slag-ECC also showed that microstructure changed greatly with the incorporation of slag, and no unhydrated particles could be observed. The increase in fiber/matrix frictional bond strength with an addition of slag was also verified with SEM image observations (Figure 4.6), which may be detrimental to achieving sufficient multiple cracking and strain-hardening behavior. Differences in the matrix surrounding a fiber are seen between specimens containing FA and slag. Comparing Figure 4.6(a) with Figure 4.6(b), the fiber surfaces in slag-ECC have more attached matrix material compared to FA-ECC. For a fiber to be pulled out of the slag-ECC matrix, de-bonding at the fiber-interface or fracture of the hydrate product is required to overcome interlocking of the hydrate product (Gao and Van Zijl, 2004). Although slag-ECC mixtures exhibit smaller deformation capacity, their flexural deflection capacity is around or more than 2 mm at 28 days of age. The 2.0 mm deformation is nearly equivalent to 1.5% strain capacity on the tensile face of the beam. This deflection capacity remains almost 150 times higher than that in normal concrete and conventional fiber reinforced concrete.

From Figure 4.6, a trend of increased deformability – ductility – with mineral admixture content (FA or slag) beyond 55% could be detected. This effect was more pronounced in FA-ECC mixtures. The total deflection increased as the replacement level of FA increases, reaching as much as 7.02 mm at peak load at the ages of 7 days. The 7.02 mm deformation is more than 4% strain capacity on the tensile face of the beam. The deformation capacity measured after 7 days was lower than the 7-day deformation capacity for all ECC mixtures. However, the overall effect of this slight drop in long-term deformation capacity was minimal. Based on the similarity of test results up to 180 days, the flexural deformation capacity seemed to stabilize after 28 days. The time dependent deformation capacity change described above has been known for sometime and is ascribed to the increase in fiber/matrix interface characteristics and matrix toughness associated with the continued hydration process of binder (Wang and Li, 2007; Şahmaran and Li, 2009a).
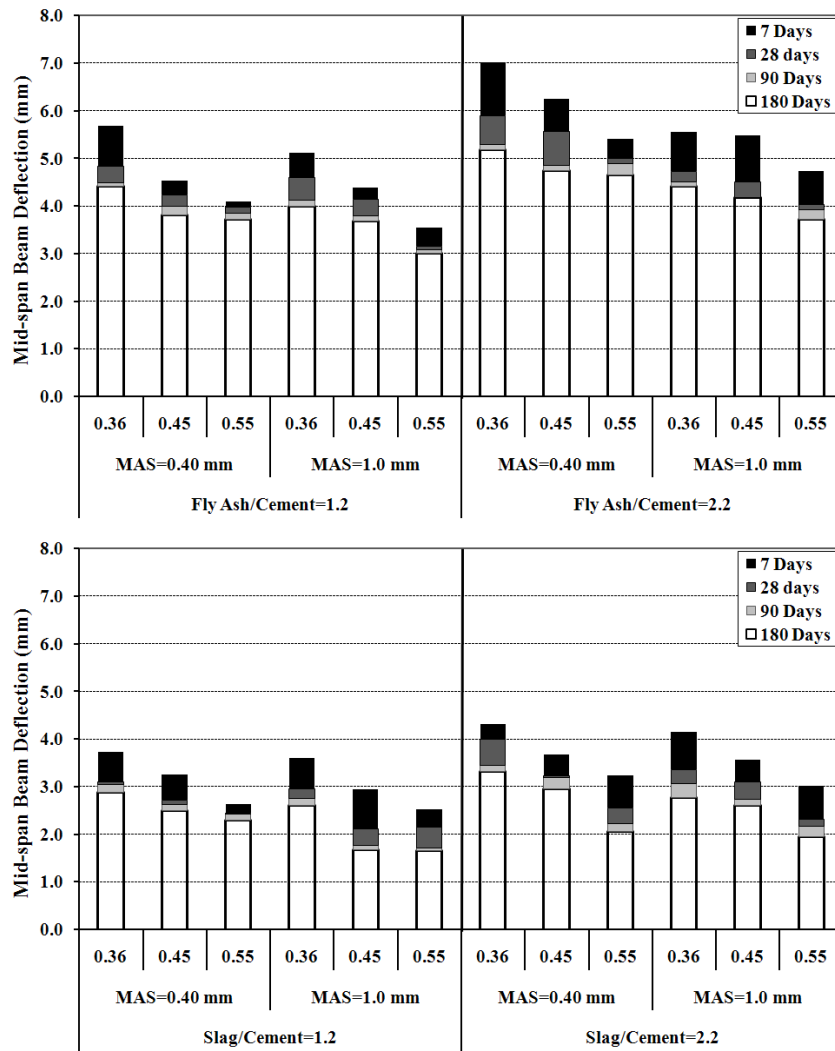
Figure 4.5 The influence of mineral admixture, aggregate size and amount on the deformability in flexure



(a) FA-ECC                                    (b) Slag-ECC
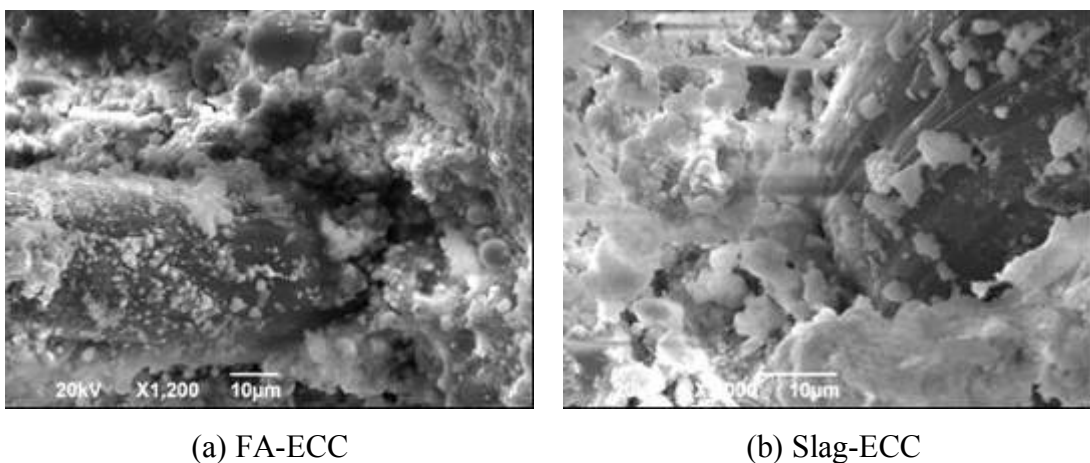
Figure 4.6 SEM image from the fractured surface

The better ductility performance of FA-ECC compared with slag-ECC is supported by several related observations. Figure 4.6(a) shows that there are numerous un-

78

hydrated spherical FA particles in the interfacial zone of FA-ECC mixtures both at the age of 28 and 180 days. It is apparent that the fiber was pulled out from the matrix, leaving a smooth interfacial surface. This is in agreement with the widely acknowledged fact that FA content beyond 30-40% does not participate in the hydration process since the amount of CH produced from the hydration of Portland cement will not adequate for the pozzolanic reaction of all FA particles, but could be seen as mere filler material, or aggregate. Thus, delayed hydration of FA did not set in and reduce the effective slippage mechanism in FA-ECC, which can also be clearly seen from Figure 4.5. In addition to fiber-pull-out from the matrix during flexural loading, the presence of unhydrated FA particles decreased matrix toughness and contributes to the crack pattern and eventual tortuous crack path of the localized, failing crack (Gao and Van Zijl, 2004). The use of FA is also expected to provide benefits in terms of improving the fiber dispersion, which is associated with enhanced workability. Therefore mineral admixture type, its chemical composition and physical and morphological properties play key roles in the resultant composite performance.

Adverse effects of increased size of aggregates on ductility performances of ECC are shown in Figure 4.5. This figure indicated that the increase in aggregate size and amount up to a certain volume fraction and 1 mm size results in a decrease in the ductility characteristics, total mid-span beam deflection of ECC. Test results also show that FA tend to perform significantly better than slag even at higher aggregate amount and sizes and was not affected to the same extent as those of slag-ECC mixtures. When the FA/C ratio was increased from 1.2 to 2.2, ECC mixtures with higher amount of aggregate and larger MAS showed higher deflection capacity to that of standard ECC beams (FA1.2_0.36_400, M45). The negative effects of increasing aggregate size at large aggregate content on ductility may be attributed to the corresponding damage to the uniform dispersion of fibers. The balling of fibers encouraged by coarser aggregates at constant aggregate content prevents sufficient coating of fibers by the matrix, and thus reduces the fiber-to-matrix bonding, which is an important factor influencing ductility (Soroushian et al.,1992). Moreover, for ECC with the larger aggregate size and volume, a higher degree of aggregate interlock is expected, resulting in higher matrix toughness and work-of-fracture during crack propagation. High matrix fracture toughness reduces the margin to

develop multiple according to the micromechanical model of steady state cracking, which is essential to achieving strain hardening behavior (Li et al., 1995; Li, 1997).

Test results also show that higher FA content tends to compensate the negative effect of higher aggregate amount and sizes on composite tensile ductility. When the FA/C ratio is increased from 1.2 to 2.2, ECC mixtures with higher amount of aggregate and larger MAS show deflection capacity almost as good as that of reference ECC beams (Figure 4.5).

The relationship between the matrix fracture toughness and composite deflection value obtained from four-point bending test for all mixes is shown in Figure 4.7. It can be seen that the deflection decreases linearly with an increase in fracture toughness (with an inverse linear correlation constant of 0.86). While the micromechanics of ECC predicts a tendency to lose composite ductility as matrix fracture toughness increases, this is the first time experimental correlation between composite ductility and matrix toughness is established with a large data set.
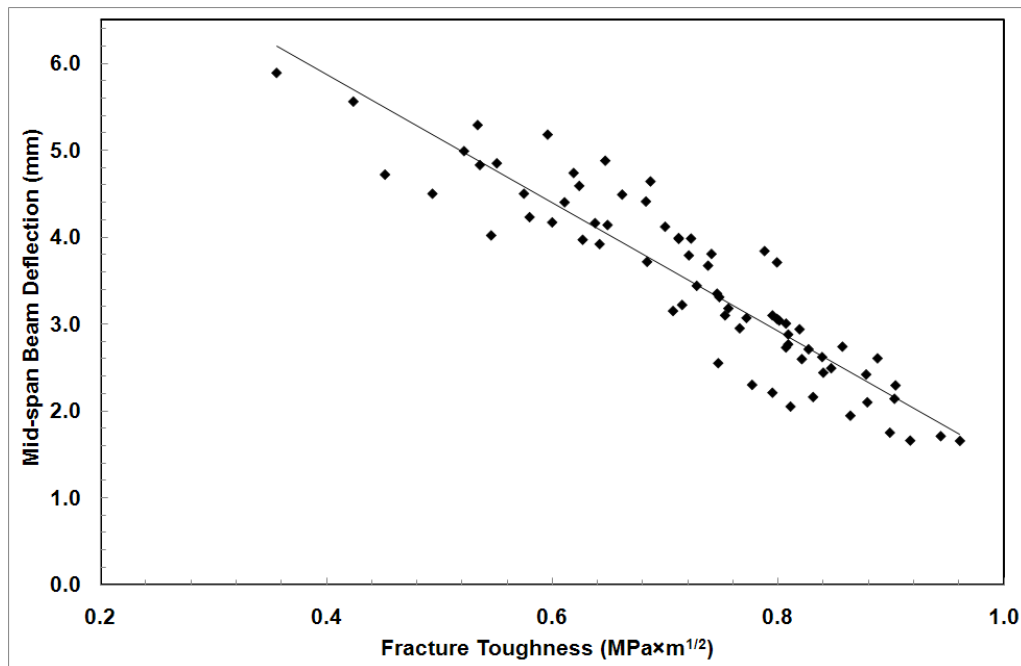


Figure 4.7 Correlation between fracture toughness versus mid-span beam deflection

#### 4.1.3.4 Crack Characterization

After unloading, multiple microcracks with a small average crack width, fine crack spacing and different amount of flexural strength tests were observed on all ECC

specimens tested under flexural loading. With crack width measurement on the surface of the specimens, it has been indicated that average crack width was lower than 90 μm in average for slag-ECC mixtures and 60 μm in average for FA-ECC mixtures. At the age of 180 days, this width has been reduced to lower than 70 μm by increasing the slag-cement ratio from 1.2 to 2.2. Similarly the crack width reduces significantly as FA content increases at all ages. At the age of 180 days, the residual crack width of ECC mixtures with FA/C ratio of 2.2 was about 40 μm with smaller crack spacing. The reason for this is not completely clear, but is likely associated with the enhanced fiber slippage due to spherical shaped FA particles along the fiber-matrix interface and more uniform distribution of fibers throughout the matrix. On the other hand, the use of aggregate up to 1.00 mm MAS and 0.55 aggregate/binder ratio did not influence the average residual crack width.

Crack width control is of primary importance for many reinforced concrete applications, since it is believed that there is a close relationship between the mean or maximum crack widths and the durability of the structure (Lepech and Li, 2005a; Şahmaran and Li, 2009a). Water flow, or permeability, is proportional to crack width cubed, which means ECC with multiple smaller cracks is less permeable than that with one large crack. Moreover, the lower magnitude of the crack width is expected to promote the self-healing behavior, and thus the transport properties in cracked composites (Yang et al., 2005; Lepech and Li, 2005b; Şahmaran et al.,2007a; Şahmaran and Li, 2009b). Consequently, in the serviceability limit state a mean or maximum crack width less than about 0.1 mm is usually prescribed (Evardsen, 1999; Reinhardt and Jooss, 2003).

### 4.1.4 Drying Shrinkage

The effects of MAS, aggregate amount, and mineral admixture type and replacement rate on the free shrinkage of ECC mixtures are evaluated with the goal of establishing guidelines to reduce cracking in ECC. The free drying shrinkage specimens were stored in a controlled environment at $23 \pm 2°C$ and $50 \pm 4$ percent relative humidity, and free shrinkage was recorded as the change in length over a gage length (distance between tips of gage studs) of 254 mm up to a period of 180 days. The results of drying shrinkage test at the age of 180 days are shown in Figure 4.8. Each value in Figure 4.8 represents the average drying shrinkage measurements

of three specimens. The ECC mixtures produced for this study had the same W/CM ratio, so varying water requirement was not a factor for drying shrinkage.
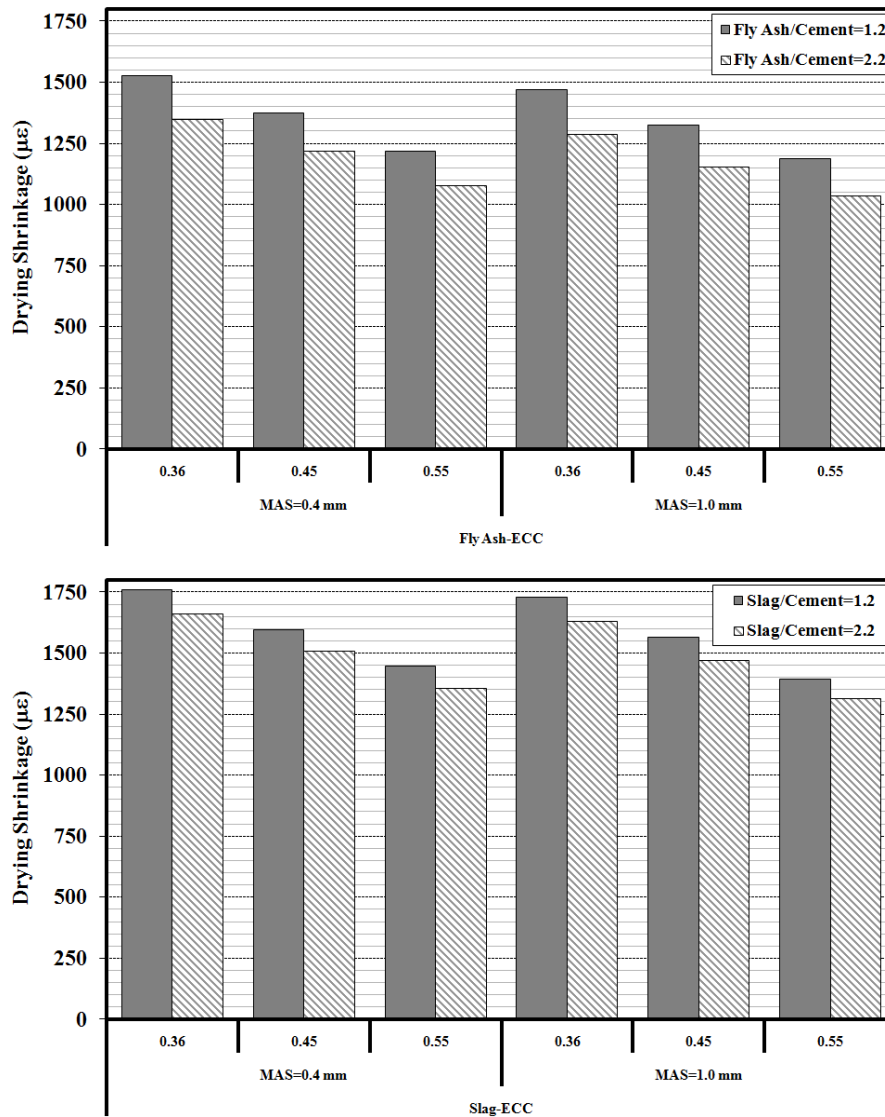


Figure 4.8 Drying shrinkage of ECC mixtures at 180 days

The drying shrinkage strains at the age of 180 days ranged between 1035 and 1761 micro-strain. ECC mixtures with S/C ratio of 1.2, aggregate/binder ratio of 0.36 (the lowest aggregate content) and MAS of 0.4 mm (S1.2_0.36_400) exhibited the highest drying shrinkage of 1761 µε at the end of 180 days. The general trend in Figure 4.8 shows that the increase in the mineral admixture content, especially FA, can effectively reduce free drying shrinkage deformation. Similar results have been reported for HVFA concrete (Şahmaran et al.,2007b; Şahmaran et al.,2009a). In the present study, a reduction between 11 to 13% of drying shrinkage depending on the aggregate size and amount was found when the FA/C ratio was increased from 1.2 to

2.2. A possible mechanism contributing to the reduction of drying shrinkage in ECCs is the matrix densification due to FA addition, which may prevent internal moisture evaporation (Maslehuddin et al., 1987). The matrix densification is typically attributed to the shape, pozzolanic property, and micro-filler effect of FA. An alternative mechanism is that unhydrated FA particles act as aggregates, which provide restraint to shrinkage, and the coarser pore structure, which results in decreased surface tension when a meniscus is formed and, thus, lower shrinkage forces exerted on the surrounding cement paste (Bisaillon et al., 1994; Zhang, 1995; Şahmaran et al.,2007b). On the other hand, compared with FA-ECC mixtures, the use of partial volume replacement of portland cement by slag without changing the MAS or aggregate content can lead to increase ultimate drying shrinkage between 15 to 27%. For example, mix S1.2_0.36_400 has similar mixture proportions as mix FA2.2_0.55_1000, while the shrinkage strain of mix S2.2_0.55_1000 at the age of 180 days is 1315 $\mu\varepsilon$, which is more than 27% higher than that of FA2.2_0.55_1000. The increase in the drying shrinkage of ECC might be due mainly to pozzolanic reaction and enhanced pore size refinement mechanism of slag especially at earlier ages. Typical pore size distribution curves are shown in Figure 4.9 for the FA-ECC and slag-ECC mixtures. As seen in Figure 4.9, the porosity of slag-ECC was much lower and has finer sizes than FA-ECC, which may proportionately increase free shrinkage. The total porosity and average pore diameter increased with an increase in the replacement of mineral admixture content. It was also observed that for a given aggregate content and size, a reduction up to 6% of drying shrinkage was found when the slag/C ratio was increased from 1.2 to 2.2.

It is clear from this experimental study that the effect of aggregate content was more pronounced than that of the aggregate size on the long-term drying shrinkage. Each 0.10 rate increase in the aggregate/binder ratio decreased the value of shrinkage in the order of almost 10%. This trend was consistent with different mineral admixture types and replacement rates. Shrinkage was lowest with the highest aggregate content (aggregate/binder ratio of 0.55). This is attributed, not only to the restraint provided by aggregates to shrinkage, but also to the reduction in paste content with the increase in aggregate content. Aggregates can also play the role of microcrack-arrestors in the matrix, further improving the composite behavior. On the other hand, for the range of maximum sizes from 0.4 mm to 1 mm studied, the differences in

drying shrinkage were so small as to be of little practical significance in most concrete applications.
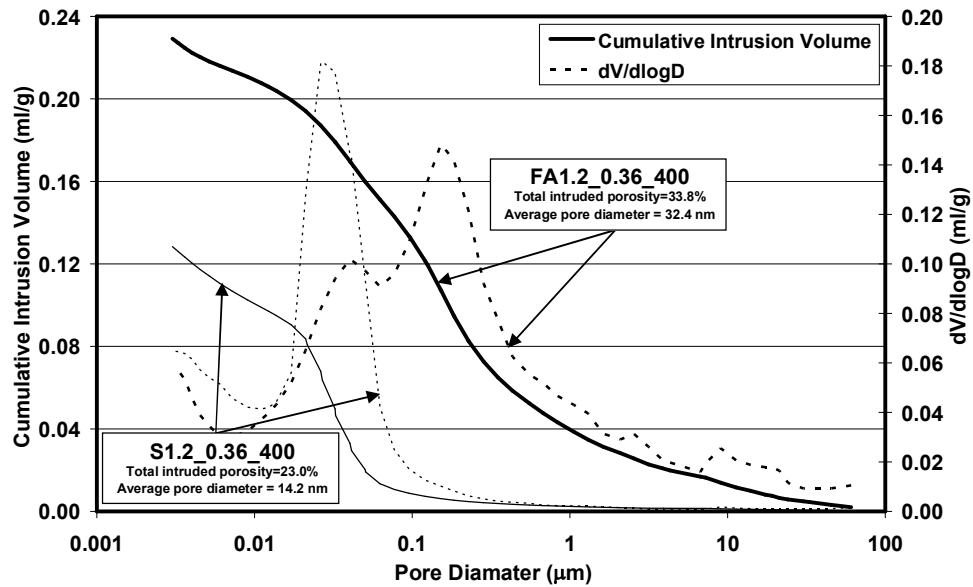


Figure 4.9 Comparison of pore size distribution of ECC mixtures with FA and slag at 28 days

The interference of aggregates with fiber dispersion, which tends to be more pronounced at higher volume fractions of larger aggregates (1 mm for this study), however, can reduce the composite performance. This effect is discussed in previous section to cause a reduction in flexural deflection capacity with increasing volume fraction of larger aggregates in ECC with 2 percent PVA fiber volume fraction. At such relatively moderate fiber volume contents, therefore, the negative effects of larger amount and size of aggregate on fiber dispersion, matrix and interface properties, and thus flexural ductility seem to be compensated by the positive effects of aggregates on the drying shrinkage of ECC mixtures, especially when incorporating FA.

### 4.1.5 Restrained Shrinkage Cracking

Shrinkage cracking is a major problem for concrete structures, especially for flat structures, like highway pavement, slabs and walls. Free shrinkage tests alone cannot offer sufficient information on the behavior of concrete structures because virtually every concrete structure is restrained in some way, either by reinforcement or by the boundary condition of the structure. In this study, the method of the ECC ring cast

next to a steel ring is used to simulate restrained shrinkage cracking. The ring specimens provide a simple test method in which the effect of restrained shrinkage cracking can be easily studied. Under the effect of restrained shrinkage, tensile stresses are developed. When they are greater than the tensile strength of the ECC mixtures, a crack appears. When a crack is formed in ECC, fibers that bridge the crack prevent it from opening more. With the action of shrinkage, fibers transmit forces through the crack and thus create tensile stresses along the ring (Mesbah and Buyle-Bodin, 1999). Since loads transmitted by fibers are high enough, as in ECC, then the second crack will form because the tensile stress transmitted across the crack is larger than the tensile strength of the matrix. Experimental results obtained in restrained shrinkage test confirm this tendency.

The typical development of an average crack width with time for restrained shrinkage specimens is shown in Figure 4.10. All of the ECC mixtures showed some degree of multiple cracking as seen in Figure 4.11. Basically, the width of a crack developed very fast in the first few days after crack formation. From then on the rate of development diminished its intension or stabilized. Figure 4.10 shows that slag-ECC mixtures began to crack after 3 to 4 days, and FA-ECC mixtures after 4 to 9 days in accordance with mineral admixture replacement rate and aggregate amount. The benefit of using FA was immediately obvious in the observed increase in the age of restrained shrinkage cracking (when compared with the mixture containing slag). In addition, the creation of the first crack was significantly delayed in time with an increase in aggregate content. The total crack widths for all the FA-ECC mixtures were significantly smaller than the cracks developed in slag-ECC mixtures. On increasing the volume of FA, further improvements were obtained in the potential for restrained shrinkage cracking behavior. On the other hand, the crack onset time was accelerated and the crack width was increased for slag-ECC specimens, and was not affected with the increase the volume of slag. As seen from Figure 4.10, the use of slag led to not only higher ultimate shrinkage capacity (as discussed in previous section) but also higher early age shrinkage. The higher early age shrinkage could lead to significant cracking because of low tensile strength of ECC at early age.

**4.1.6 Frost Durability of ECC Mixtures**

A proper air-void system must be maintained in normal concrete to achieve superior
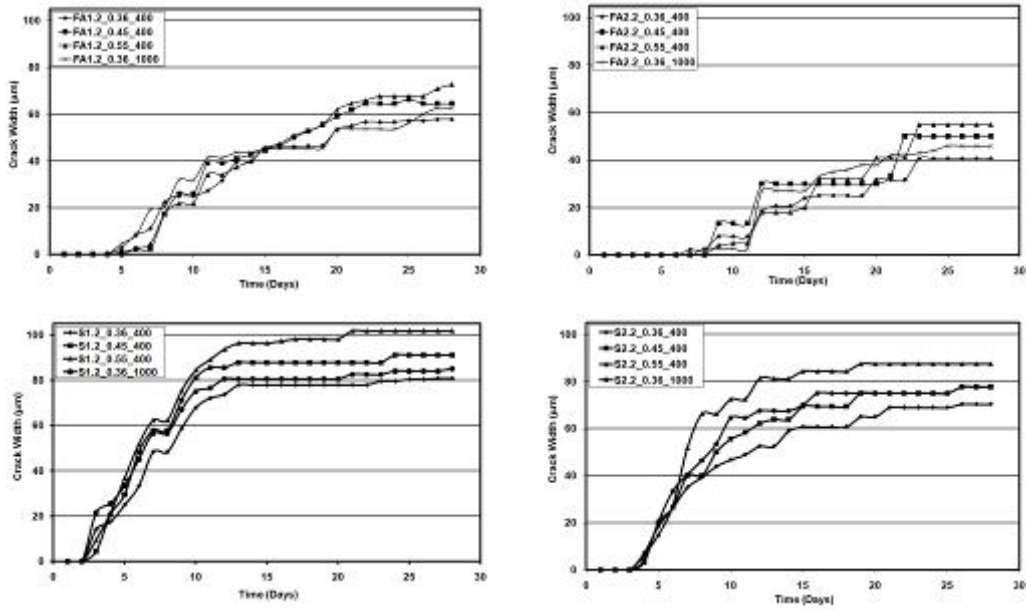
Figure 4.10  Development of crack width in restrained specimens with time



<div align="center">FA-ECC            Slag-ECC</div>
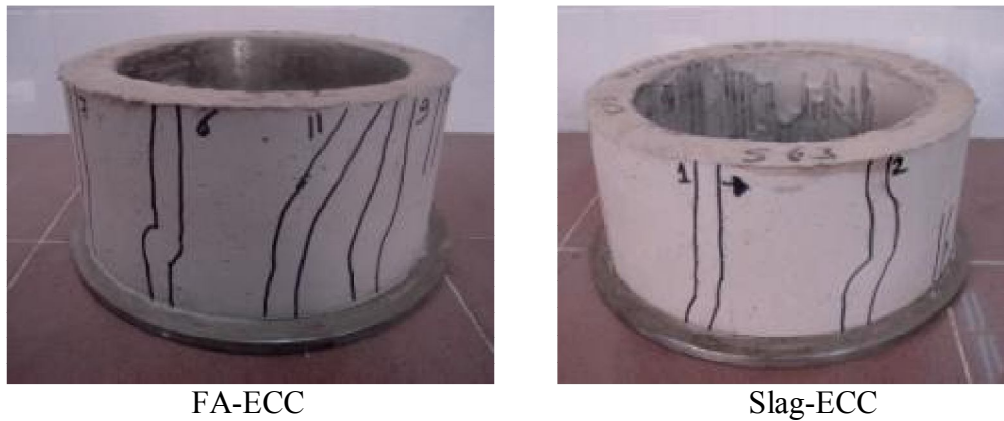
Figure 4.11  Typical restrained shrinkage cracking patterns of ECC mixtures

freezing and thawing resistance (Pigeon and Pleau, 1995). In the case of ECC, the available information is very limited, but it seems to indicate that in addition to the air-void system, other parameters such as high tensile strain capacity and strain hardening behavior are important for resisting cycles of freezing and thawing and are affected by the presence of micro-fibers.   In this section, the frost durability of selected non-air-entrained ECC mixtures (FA1.2_0.36_400, FA2.2_0.36_400, S1.2_0.36_400 and S2.2_0.36_400) was comprehensively investigated the freezing and thawing durability of ECC mixture (M45).

For some engineering applications, such as pavements and bridge decks in cold regions, the damage might occur through the double actions of mechanical load and freeze-thaw cycles (Mu et al., 2002). Cracking in ECC is fundamentally different

from that which occurs in concrete or reinforced concrete. ECC develops multiple micro-cracking in a strain-hardening response as a result of the bending preload. Due to multiple micro-cracking, it is important to test the pre-cracked ECC under freeze-thaw cycles, which is of great importance for critical assessment of the durability of ECC under comprehensive conditions. In this section, therefore, the durability performance of selected ECC mixtures when subjected to mechanical loading and freezing and thawing cycles was also studied. The resulting data is important in view of the growing use of ECC, especially for highway pavements, airport pavements and bridge decks in cold climate regions.

**4.1.6.1 Air-Void Characteristics of ECC Mixtures**

It is generally recognized that the air-void structure of cement based composites is a critical parameter for the durability of them subjected to frost action (Elsen, 2001). The air-void parameters of the non-air-entrained high volume slag and FA incorporated ECC mixtures are presented in Table 4.4 along with the fresh air content. For each mixture, only the average values obtained from two specimens are shown in the table. Although no air entraining admixture was added to ECC mixtures, air contents of these ECC mixtures in the fresh state as measured by ASTM C231 gave values between 6.3 and 7.3%, which seemed to be adequate for freeze-thaw durability. For this reason, no air-entrainment was applied to the ECC specimens in the freeze-thaw cycle tests. As seen in Table 4.4 that air content in fresh ECC and in hardened ECC revealed some differences. The total volume of air in hardened ECC was found to increase about 1% compared to fresh air content of ECC mixtures. Moreover, the air contents measured during the fresh and hardened states of the ECC mixtures showed that increasing the amount of FA or slag somewhat augmented the both fresh and hardened air contents. For instance, hardened ECC mixtures with 55% FA and slag had the 7.8% and 7.0% air contents at hardened state, respectively; however, these values became marginally high with increment of FA or slag content to 70% and reached to 8.2% and 7.2%, respectively. These fresh and hardened air contents seemed to be higher than those air contents of non-air-entrained normal concrete, most probably as a result of lack of coarse aggregate in ECC mixtures and the higher viscosity of the mortar matrix during the fresh state; the fine particles and high viscosity tend to prevent some of the air

bubbles from rising to the surface during placing operations (Şahmaran et al., 2009b; Powers, 1964a). Another reason of higher air content may be attributed to the proprietary hydrophobic oiling agent of 1.2% by mass coated on the surface of the PVA fibers to tailor the interfacial properties between fiber and matrix for strain-hardening performance. The proprietary coating chemical used on the surface of fibers may also entrain very small air bubbles, thus enhancing the freeze-thaw durability of ECC mixtures. Further study should be conducted to understand the reason of increase in air content with PVA fiber addition, which is beyond the scope of the study.

Table 4.4 Air-void characteristics of ECC mixtures

| | FA-ECC | | Slag-ECC | |
|---|---|---|---|---|
| | FA1.2_0.36_400 | FA2.2_0.36_400 | S1.2_0.36_400 | S2.2_0.36_400 |
| Fresh air content (%) | 6.9 | 7.3 | 6.3 | 6.6 |
| Hardened air content (%) | 7.8 | 8.2 | 7.0 | 7.2 |
| Specific surface $(mm^{-1})$ | 24.1 | 35.6 | 21.7 | 24.2 |
| Spacing factor($\mu$m) | 273 | 197 | 308 | 287 |

In the four non-air-entrained ECC mixtures, the specific surface value fluctuated between 21.7 $mm^{-1}$ and 35.6 $mm^{-1}$ and the spacing factor ranged between 197 $\mu$m and 308 $\mu$m. Though the spacing factor values generally exceed the generally accepted value of 0.200 mm and the specific surface values are less than the recommended minimum value of 25 $mm^{-1}$ (Powers, 1964b; Powers, 1965), this lack of an apparently ideal air-void system has not adversely affected the frost durability of ECC, as indicated in the following section. As also seen in Table 4.4, increasing the S/C or FA/C ratio from 1.2 to 2.2 increased the specific surface while decreased the spacing factor values significantly. For frost durability, the degree of hydration and thus the state of the microstructure at the moment of freezing is a decisive factor.

However, as it is well known that degree of hydration of mineral admixtures (especially FA) incorporated cement based composites are significantly low, especially at early ages, and depend on the content and quality of mineral admixtures and fineness of cement (Stark and Ludwig, 1997). Most probably, the degree of hydration of 55% slag or FA incorporated ECC mixtures was faster than that of the high volume (70%) slag or FA-ECC mixtures, and thus the microstructure clearly becomes denser, which becomes apparent through a decrease in hardened air content and specific surface.

## 4.1.6.2 Mass Loss and Pulse Velocity Measurement before and after Subjected to Freeze-Thaw Cycles

After subjected to the 300 freeze-thaw cycles, damage on pristine and mechanically preloaded ECC specimens was evaluated by means of mass loss and UPV changes. Even though the resonant frequency method was suggested by ASTM C666 for the assessment of internal damage due to frost action, in this study, UPV method was used due to the lack of resonance frequency measurement equipment. Previous studies have also shown that UPV test method can also be used to measure the deterioration of specimens during freeze-thaw cycles (Cohen et al., 1992).

Cracking in ECC is fundamentally different from that which occurs in concrete or reinforced concrete. ECC develops multiple micro-cracking in a strain-hardening response as a result of the bending preload. Due to multiple micro-cracking, it is important to test the pre-cracked ECC under freeze-thaw cycles. The mass of loss versus number of freezing–thawing cycles for pre-cracked ECC specimens is shown in Figure 4.12. The total mass loss of pristine ECC specimens exposed to freeze-thaw cycles is also included in this figure. As it is well known that mass variation during freeze-thaw cycles are due to water movements in and out of the specimens, surface scaling and cracking (Pigeon et al., 1987; Cohen et al., 1990). As seen from Figure 4.12, a slight mass gain was observed in all ECC mixtures up to 60 freeze-thaw cycles, however, it was generally less than 1%. The reason behind the mass gain is most probably due to the absorption of water and formation of reaction products in voids (Duchesne and Bérubét, 1995). However, beyond the 60 freeze-thaw cycles, a gradual decrease in mass started, and at the end of 300 cycles relative mass loss according to the initial mass of specimen varied between the 0.9 and 9.4%

depending on the pre-loading condition, mineral admixtures type and amount. It can also be observed from Figure 4.12 that the total mass loss after 300 cycles tends to increase with the mechanical pre-loading. The increase, however, is fairly insignificant for ECC specimens. This increase is somewhat more marked for FA2.2_0.36_400 mixture (9.4% after 300 cycles).
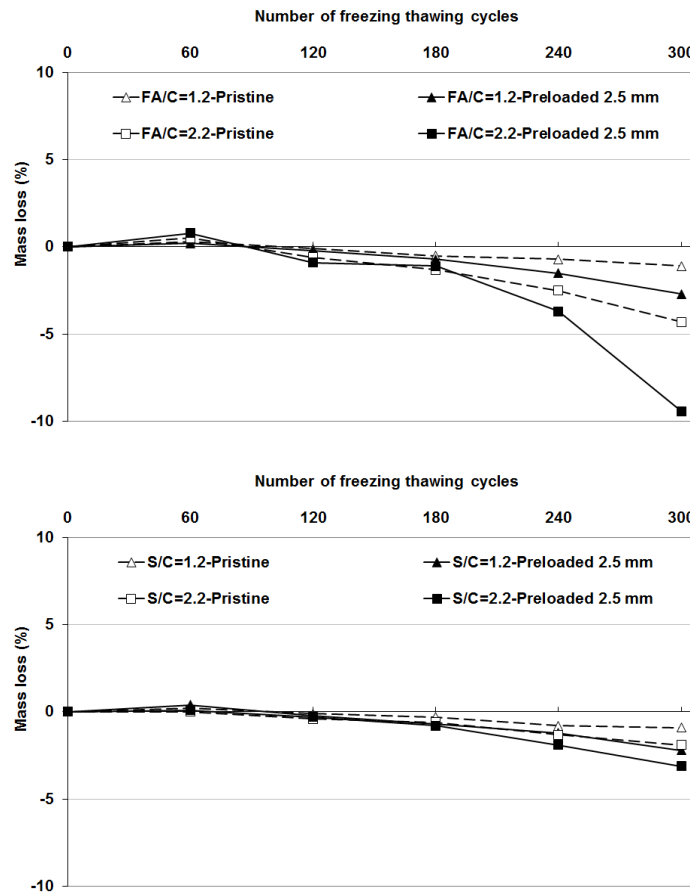


Figure 4.12 Relative mass loss changes as a function of number of freeze-thaw cycles

Figure 4.13 shows the data for the relative UPV change ($100*V_i/V_0$) due to the freeze-thaw action. $V_i$ is the UPV after certain number of freeze-thaw cycles, and $V_0$ is initial pulse velocity prior to any freeze-thaw cycles. Pre-loading of the specimens lead to microcracking on the tension surface of the specimens, so decreased the measured UPV value according to pristine specimens and relatively higher damage as a result of frost action. Moreover, higher the amount of slag and FA in the mixtures attributed to increase the amount of damage of ECC (higher reduction in UPV) mixtures as a result of frost action. As in the mass loss observation, this effect is more pronounced in the case of FA-ECC mixture. As seen in the figure, the

highest decrease in UPV value for both pristine and preloaded specimens was obtained in the case of ECC mixture with 70% FA content (FA2.2_0.36_400).
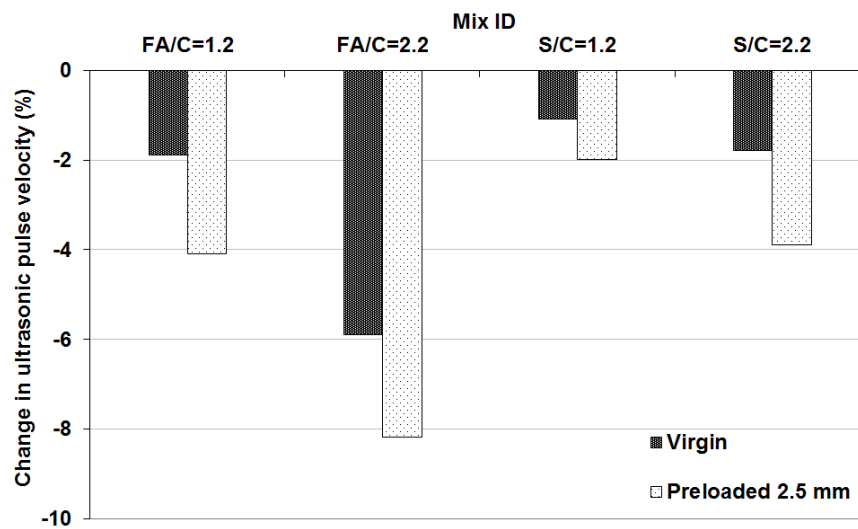


Figure 4.13 Ultrasonic pulse velocity change after 300 freeze-thaw cycles

Although FA-ECC mixtures show the highest deflection capacity and lowest residual crack width before freeze-thaw cycles (Table 4.5) due to four-point bending test, the highest variation both in mass loss and relative UPV after frost action were also observed on these mixtures. Moreover FA2.2_0.36_400 mixture has more deterioration than FA1.2_0.36_400 mixture, although FA2.2_0.36_400 mixture has a higher fresh air content (7.3%) and lower spacing factor than FA1.2_0.36_400 mixture (6.9%). FA-ECC specimens also exhibited some surface scaling at the conclusion of the freeze-thaw cycling, and increased surface scaling was observed on the pre-loaded specimens. Therefore, it is not possible on this figure to determine the critical air content and spacing factor for ECC, since no relation was found between frost durability and air-void characteristics of ECC mixtures. The scaling was, however, clearly confined to the surface layers of the test specimens, and had no effect on the integrity of the ECC mass. On the other hand, almost no surface scaling (almost no mass loss) was observed on both pristine and preloaded slag-ECC specimens after 300 cycles of freeze-thaw. Moreover, although slag-ECC mixtures had lower ductility and air contents, and higher spacing factors, at 300 cycles it had a higher average relative UPV and lower mass loss value than FA-ECC mixtures at the same number of freeze-thaw cycles. This was probably due to the greater maturity of the slag-ECC test specimens. When the compressive and flexural strengths before

91

freeze-thaw cycling (Tables 4.1 and 4.5) and mass loss (Figure 4.12) of the ECC mixtures due to the freeze-thaw cycling are evaluated together, it can be concluded that there is a powerful relation among them, high strength (especially compressive strength) lead to a less mass loss due to frost action. This result is in agreement with finding of the Sun et. al (1999) in which different strength grades of concrete under the simultaneous action of load and freeze-thaw cycles were studied and concluded that at the same stress ratio, concrete of higher strength could undertake more freeze-thaw cycles, and the dynamic elastic modulus decreased more slowly with freeze-thaw cycles. Therefore, FA-ECC needs sufficient time (maturity) to develop beneficial characteristics. Curing only 14 days in accordance with ASTM C666 prior to the first exposure to freeze-thaw cycles may have been insufficient for the hydration and self-desiccation to reduce the quantity of freezable water sufficiently in the case of FA-ECC mixtures. The benefits of using Class-F FA in ECC in terms of improved durability properties such as frost is usually manifested at later ages with the continuous supply of moisture (Şahmaran et al., 2007b).

Apart from the slight increase in mass loss, the results presented in this study largely confirm the durability performance of high volume FA/slag-ECC mixtures under freeze-thaw cycles, even in cases where the material experiences mechanical pre-loading that deforms it into the strain-hardening stage prior to exposure. This high frost durability can be attributed to the ECC's superior tensile properties and inherent air-void parameters. It is well known that upon freezing, water in capillary pores expands. If the required volume is greater than the space available, the pressure build-up could reach the tensile strength of the material, resulting in local micro-crack formation, brittle rupture and scaling. Therefore, the high tensile strength and ductility – and particularly fracture resistance in ECC – could lead to its higher frost resistant characteristic (Şahmaran et al., 2009b)

### 4.1.6.3 Flexural Performance of ECC Mixtures after Subjected to Freeze-Thaw Cycles

Table 4.5 shows the test results of pristine and preloaded ECC specimens in terms of ultimate deflection capacity, flexural strength, stiffness and residual crack width after subjected to 300 freeze-thaw cycles. Each reading represents the average value of

Table 4.5 Flexural properties of ECC mixtures

| | Mix. ID | Pre-loading deformation (mm) | Mid-span deflection (mm) | Flexural strength (MPa) | Residual crack width (µm) | Flexural stiffness (MPa/mm) |
|---|---|---|---|---|---|---|
| Cured 14 days moist curing | FA1.2_0.36 | 0.0 | 5.36 | 11.06 | ~60 | 11.1 |
| | _400 | 2.5 | 3.31 | 10.58 | ~60 | 8.8 |
| | FA2.2_0.36 | 0.0 | 6.27 | 9.27 | ~40 | 8.6 |
| | _400 | 2.5 | 4.40 | 9.11 | ~40 | 7.6 |
| | S1.2_0.36_ | 0.0 | 3.44 | 11.31 | ~90 | 14.8 |
| | 400 | 2.5 | 1.33 | 10.88 | ~90 | 10.5 |
| | S2.2_0.36_ | 0.0 | 4.16 | 10.07 | ~70 | 13.4 |
| | 400 | 2.5 | 2.18 | 9.94 | ~70 | 10.0 |
| After 14 days moist curing, subjected to 300 freezing and thawing cycles | FA1.2_0.36 | 0.0 | 4.33 | 9.63 | ~80 | 10.7 |
| | _400 | 2.5 | 3.18 | 8.53 | ~80 | 8.0 |
| | FA2.2_0.36 | 0.0 | 4.23 | 7.18 | ~80 | 7.8 |
| | _400 | 2.5 | 3.05 | 6.24 | ~80 | 5.7 |
| | S1.2_0.36_ | 0.0 | 3.08 | 10.86 | ~120 | 14.6 |
| | 400 | 2.5 | 1.45 | 9.11 | ~120 | 10.3 |
| | S2.2_0.36_ | 0.0 | 3.55 | 9.28 | ~120 | 12.7 |
| | 400 | 2.5 | 2.01 | 8.29 | ~120 | 9.1 |

three specimens. As seen from Table 4.5, it is noticeable that both of the flexural strength and deflection capacities of all ECC mixtures reduced due to the 300 freeze-thaw cycles, however, the impression of frost action is considerably low. After subjected to freeze-thaw cycles, under flexural loading, all ECC specimens demonstrate the strain-hardening behavior and multiple cracking. As in the non-frost deteriorated specimens, the first crack started inside the mid-span at the tensile face. The flexural stress increased at a slower rate, along with the development of multiple cracks with small crack spacing and tight crack widths. Micro-cracks developed from the first cracking point and spread out in the mid-span of the flexural beam. Bending

failure in the ECC occurred when the fiber-bridging strength at one of the micro-cracks was reached; resulting in localized deformation once the modulus of rupture was approached.

Figure 4.14 demonstrates variation of flexural strength and deflection capacity of ECC mixtures before and after subjected to frost action. As seen in the figure, contrary to the expectations, drop in flexural strength and deflection values for the pristine and pre-loaded specimens were not distinctive from each other; mechanical pre-loading of the ECC specimens did not significantly influence residual mechanical properties of the frost deteriorated ECC specimens. Percent decrement in the deflection and flexural strength values for the pristine and preloaded specimens due to the frost action was intimate. For instance, percent decrease in deflection values of pristine and preloaded FA2.2_0.36_400 specimens due to frost action were 32.5 and 30.6%, respectively, and percent decrease in flexural strength of pristine and preloaded specimens for the same mixture were 13.0 and 19.4%, respectively. This result suggests that between the time of inducing pre-cracking and the time of testing, after freeze-thaw cycles, slight healing of the micro-cracks has also occurred in the ECC specimens. This can be attributed primarily to the high cementitious material content and relatively low water-binder ratio within the ECC mixture. As a result of the formation of micro-cracks due to mechanical loading, unhydrated cementitious particles are easily exposed to the water during the thawing period, which leads to the development of further hydration processes. Finally micro-cracks under conditions of a damp environment were partially healed by newly formed products. Therefore, self-healing phenomenon is only valid for the pre-cracked specimens. These observations are in good agreement with those discussed in the literature (Loukili et al., 1998; Granger et al., 2007). These investigations indicated that the formation of re-hydration products in micro-cracks is possible during freeze-thaw cycles . In ECC, the re-healing process is especially aided by the innately tight crack width.

Table 4.5 summarizes the average deflection capacity of ECC specimens exposed to 300 freeze-thaw cycles. The deflection capacity reported for these specimens does not include the residual deflection from the pre-cracking deformation. By neglecting this residual deflection, the large variability in material relaxation during unloading

94
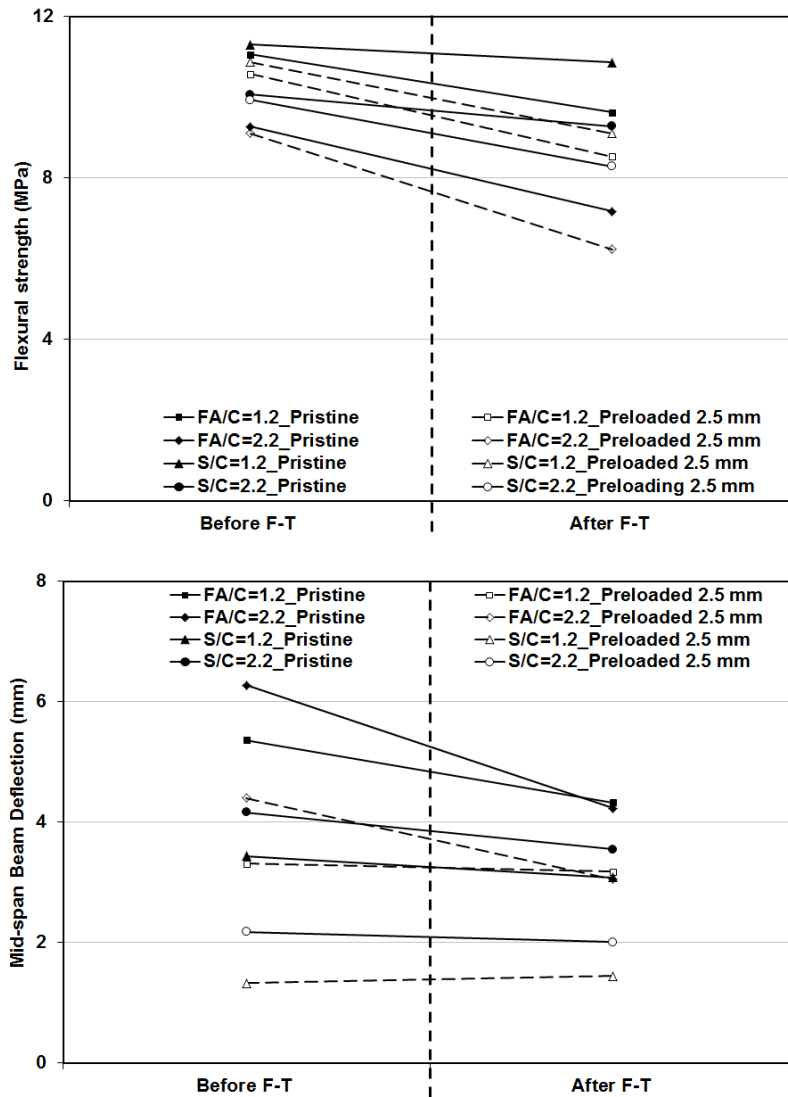
Figure 4.14 Variation in flexural parameters of ECC mixtures due to freeze-thaw cycles (F-T)

is avoided, and a conservative estimation for ultimate deformation capacity of the material is presented. The deflection capacity of virgin and pre-cracked ECC specimens exposed to 300 freeze-thaw cycles range from 1.45 to 4.33 mm. The effect of pre-loading on the deflection capacities before freeze- thaw cycles was more prominent than the effect of frost action.  For instance, FA2.2_0.36_400 mixture had the 6.27 mm and 4.40 mm mid-span beam deflection capacities for the pristine and 2.5 mm preloaded specimens at the ages of 14 days, however, after 300 freeze-thaw cycles, 6.27 mm deflection capacity of pristine specimen was decreased to 4.23 mm.  For the flexural strength, behavior is not like to deflection, as a result of 2.5 mm pre-loading, average flexural strength of pristine specimens decreased from 9.27 MPa to 9.11 MPa for the same mixture, but after subjected to 300 freeze-thaw

cycles, average flexural strength of pristine specimens drop to 7.18 MPa. Reduction in flexural strength was around 2% due to the pre-loading and 23% due to 300 freeze-thaw cycles for the FA2.2_0.36_400. This may be attributed to the effects of damage on the fiber/matrix interface and matrix micro-cracking as a result of frost deterioration. As expected, when the dual effect of pre-loading and freeze-thaw cycles examined, flexural strength of the FA2.2_0.36_400 mixture decreased from 9.27 MPa (average flexural strength of pristine specimens before freeze-thaw cycles) to 6.24 MPa (average flexural strength of preloaded specimens after freeze-thaw cycles); rate of reduction was around 33%.

As mentioned earlier, the slope of the initial part of the load-deflection curve represents the flexural stiffness of the beams. Table 4.5 shows that the slope decreases with the frost deterioration, thereby indicating a reduction in the stiffness of the ECC mixtures. Figure 4.15 pointed out the reduction in relative stiffness of both pristine and preloaded specimens due to frost action. Stiffness of pristine specimens before freeze-thaw cycling and pre-loading accepted as 100% (stiffness of pristine specimens at 14 days) and the change in stiffness due to the pre-loading and frost action was exhibited in this figure. As seen in this figure, reduction in relative stiffness due to frost action was slight (not more than 9% at extreme deterioration) and at tolerable range for pristine specimens, however, detrimental for preloaded specimens. As in the other measured properties, the highest reduction was monitored in high volume FA incorporated ECC mixture (FA2.2_0.36_400) and followed by high volume slag incorporated ECC mixture (S2.2_0.36_400). Relative stiffness of the preloaded specimens after 300 freeze-thaw cycles was very close to each other and around 70%. These results revealed that the presence of microcracks due to mechanical stresses or time dependent effects (e.g., shrinkage, creep, etc.) is one of the major factors which can influence durability and serviceability of cement based composites in terms of freeze-thaw cycles (Granger et al., 2007).

Table 4.5 shows the residual crack width of ECC mixtures after subjected to the 300 freeze-thaw cycles. The residual crack width of virgin and pre-cracked specimens exposed to 300 freeze-thaw cycles is wider than that of non-frost deteriorated virgin specimens, but remains less than 120 μm. As in the non-frost deteriorated ECC specimens' residual crack width, slag incorporated ECC mixtures, after subjected to
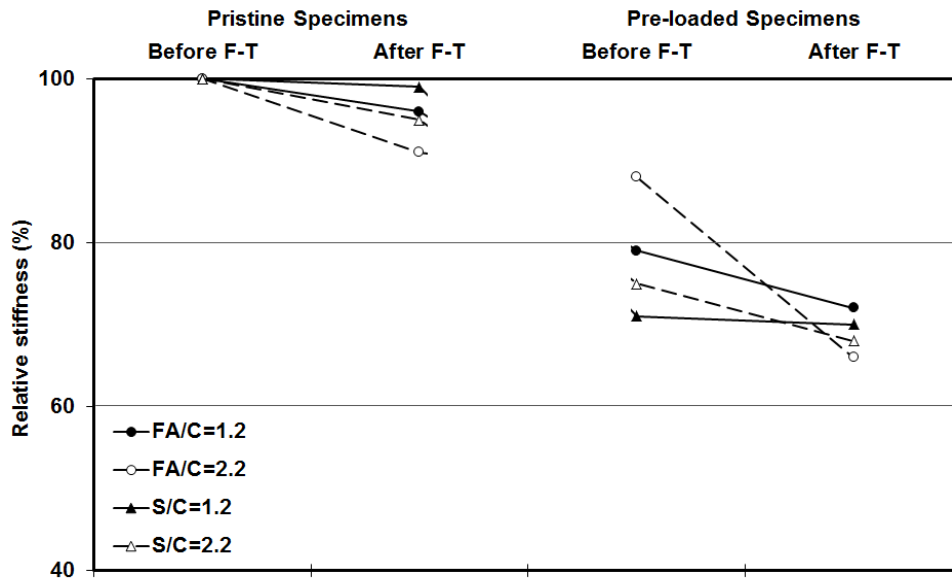
Figure 4.15 Variation of relative flexural stiffness due to freeze-thaw cycles and mechanical pre-loading

freeze-thaw cycles, had wider residual crack width than those of the FA incorporated ECC mixtures. Before exposure to frost deterioration, although a clear diverseness of the residual crack width was monitored by the increase of mineral admixture replacement rate, it was disappeared after subjected to freeze-thaw cycles. In other words, the residual crack width of the preloaded and pristine specimens became equal for the different replacement rate of FA or slag, and beneficial effect of high volume slag or FA usage on residual crack width evanesced. More experimental studies on a micro-mechanical scale are necessary to clearly understand the mechanisms behind the increased crack width, and are beyond the scope of this study.

It should be noted that the flexural properties of frost deteriorated ECC beams provide a conservative estimate of their residual flexural properties in actual structures. These accelerated deterioration periods are equivalent to a time span of many years in real structures, even those located in regions with harsh winters. This difference in accelerated and normal frost deterioration periods should have a significant influence on the residual flexural properties of ECC because in the long term, deterioration in ECC as a result of freeze-thaw cycles can more effectively be closed due to a self-healing process (Şahmaran and Li, 2007). Thus the flexural performances of ECC summarized in Table 4.5 are underestimated.

97

**4.2 Performance of ECC Mixtures as Overlay Materials**

In recent years, the use of rigid concrete overlays has become increasingly popular. The main purpose of an overlay is to extend the service life of the structure, and increasing structural performance and durability of wearing surface. Moreover, the overlay provides adequate load bearing capacity. The superior ductility and improved durability characteristics of Engineered Cementitious Composites (ECC) suggest that they could be used as an attractive alternative to conventional concrete overlay materials. In this section, the performance of ECC mixtures as an overlay material is investigated by laboratory experiments. Two different ECC-overlay mixture designs were selected for the comparison of overlay performances: one with high strength and moderate ductility (S1.2_0.36_400 – after now called as S_ECC), and the other with moderate strength and high ductility (FA1.2_0.36_400 – after now called as F_ECC). Layered ECC/concrete beams were cast with three different ECC layer thicknesses, namely 25, 35 and 50 mm. After measuring the basic mechanical properties and dimensional properties of monolithic overlay specimens, layered ECC-concrete beam in which a layer of ECC was applied beneath a layer of substrate concrete under four point-bending tests were carried out to investigate the reflective cracking and flexural performances. The influences of ECC's strength and ductility, and layer thickness on the strength and ductility of the layered beam were discussed in experimental aspects. By measuring the basic mechanical properties and dimensional stability test results of ECC mixtures again, the repeatability of basic mechanical properties and dimensional stability test results of ECC mixtures was investigated. The bond strength properties of layered beam which was composed by two types of materials such as old concrete substrate and ECC overlay material were also evaluated. During the experimental study, microsilica concrete (MSC), one of the most commonly used type of overlay mixtures, was also cast and tested as control overlay materials.

**4.2.1 Basic Mechanical Properties and Dimensional Stability of Monolithic Overlay Specimens**

**4.2.1.1 Compressive Strength**

At the ages of 1, 7, 28 and 90 days, compressive strength tests for cylinder specimens

were applied following ASTM C39 (2003) procedures. Table 4.6 tabulates the average of compressive strength results as determined from six cylinder specimens. As it is seen from Table 4.6, for the first 1 day of curing, strength gain in the MSC specimens was significantly higher compared to the ECC mixtures. At the ages of 7 days of curing, the compressive strength test results were similar for both S_ECC and MSC mixtures. However, the strength gain was more pronounced for S_ECC beyond 7 days of curing. Between the ages of 28 days and 90 days high amount of strength gain was achieved by F_ECC mixture, but still it has the lowest compressive strength at all ages. The effect of mineral admixture type on the compressive strength properties of ECC mixtures has already been discussed in Section 4.1.1. The slight difference of compressive strength test results reported in the previous section and this section may be attributed to the specimen size effect.

Table 4.6  Compressive strength of overlay materials

| Mix ID | Compressive Strength (MPa) | | | | Modulus of Elasticity (GPa) |
|--------|------|------|-------|-------|-----------------------------|
|        | 1 d. | 7 d. | 28 d. | 90 d. |                             |
| **F_ECC** | 17.1 | 31.1 | 53.8 | 65.6 | 19.7 |
| **S_ECC** | 24.6 | 44.1 | 71.2 | 74.1 | 24.9 |
| **MSC**   | 32.8 | 46.3 | 68.7 | 72   | 35.2 |

**4.2.1.2 Flexural Performance of Overlay Materials**

The test results in terms of flexural strength (MOR) and ultimate mid-span beam deflection at the peak stress at the end of 1, 7, 28 and 90 days are displayed in Table 4.7. Typical bending test results are displayed in Figure 4.16 in terms of flexural stress–deflection diagrams for different kinds of overlay materials at the age of 28 days. The flexural performances of overlay materials mixtures were calculated by averaging the results of six specimens. As seen from Table 4.7, even though MSC mixture has the highest compressive strength at early ages, and similar compressive strength at later ages, the ECC prisms show a substantially higher ultimate flexural strength in comparison with that of the MSC prisms. MOR of ECC mixtures values varied from 11.51 to 12.04 MPa showing that increase in the values of flexural strength of S_ECC was not that of drastic compared to the values of F_ECC for the first 28 days as in the compressive strength test results. Moreover, for all specimens,

no significant flexural strength gain was observed beyond the age of 28 days. The most probable reason for this trend may be attributed to the fact that flexural strength is governed by more complex material properties, such as tensile first cracking strength, ultimate tensile strength and tensile strain capacity, particularly in the case of strain hardening cementitious materials (Qian et al., 2009).

Table 4.7 Flexural properties of overlay materials

| Mix ID | Flexural Strength (MPa) | | | | Deformation (mm) | | | |
|--------|------|-------|-------|-------|------|------|------|------|
| | 1 d. | 7 d. | 28 d. | 90 d. | 1 d. | 7 d. | 28 d. | 90 d. |
| F_ECC | 5.35 | 8.80 | 11.51 | 11.82 | 4.18 | 4.78 | 4.43 | 3.99 |
| S_ECC | 6.74 | 10.89 | 12.04 | 12.58 | 3.18 | 3.23 | 3.05 | 2.94 |
| MSC | 4.97 | 6.30 | 7.00 | 7.56 | 0.55 | 0.41 | 0.28 | 0.27 |

Ultimate mid-span beam deflection capacity, which reflects the material ductility, of the mixtures ranged between the values of 0.28 and 4.43 mm for the first 28 days. As seen from Figure 4.16, MSC mixture is a brittle material with sudden fracture failure, on the other hand, F_ECC and S_ECC samples have significantly higher deformation capability than MSC at all testing ages. Among the ECC mixtures, F_ECC showed the highest deflection capacity, therefore ductility, at all ages. The improvement in the mid-span beam deflection capacity with the use of Class-F FA can be attributed to the fact that the addition of FA has a tendency to reduce PVA fiber/matrix interface chemical bond and matrix toughness while increasing the interface frictional bond, in favor of attaining high tensile strain capacity (Wang and Li, 2007; Şahmaran and Li, 2009a). The overall decrease in the mid-span beam deflection capacity for S_ECC specimens might be associated with higher lime content and reactivity of slag which in turn causes enhanced fracture toughness, bond strength and the chemical bond between mortar matrix and fibers. Although S_ECC mixtures exhibit smaller deformation capacity, their flexural deflection capacity is still around or more than 3 mm at 28 days of age. The 3.0 mm deformation is nearly equivalent to almost 2.0% strain capacity on the tensile face of the beam. This deflection capacity remains almost 200 times higher than that in normal concrete and conventional fiber reinforced concrete (Qian and Li, 2008).
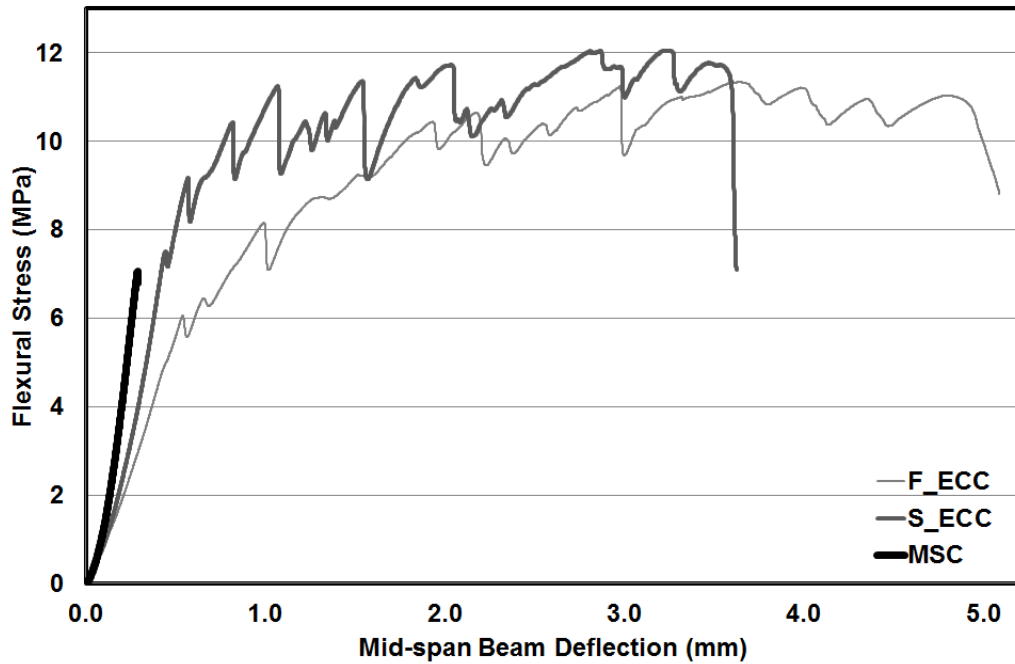
Figure 4.16 Flexural strength – mid-span beam deflection curve of overlay materials at 28 days of age

### 4.2.1.3 Drying Shrinkage

Free drying shrinkage tests were conducted on ECC and MSC (reference) prism specimens. The free drying shrinkage specimens were stored in a controlled environment at 23 ± 2 °C and 50 ± 5% relative humidity, and free shrinkage was recorded as the change in length over a gage length (distance between tips of gage studs) of 254 mm up to a test at the age of 180 days. The results of drying shrinkage test at the age of 180 days are shown in Figure 4.17. Each value in Figure 4.17 represents the average drying shrinkage measurements of three specimens. The ECC mixtures produced for this study had the same W/CM ratio, so varying water requirement was not a factor for drying shrinkage test results of ECC overlay materials.

The drying shrinkage strains of overlay materials at the age of 180 days ranged between 451 and 1548 micro-strain. ECC mixtures with slag exhibited the highest drying shrinkage of 1548 με at the end of 180 days. While by using FA with ECC can effectively reduce free drying shrinkage deformation. A possible mechanism contributing to the reduction of drying shrinkage in F_ECC has already been discussed in Section 4.1.4. The experimental results revealed also that the drying

101
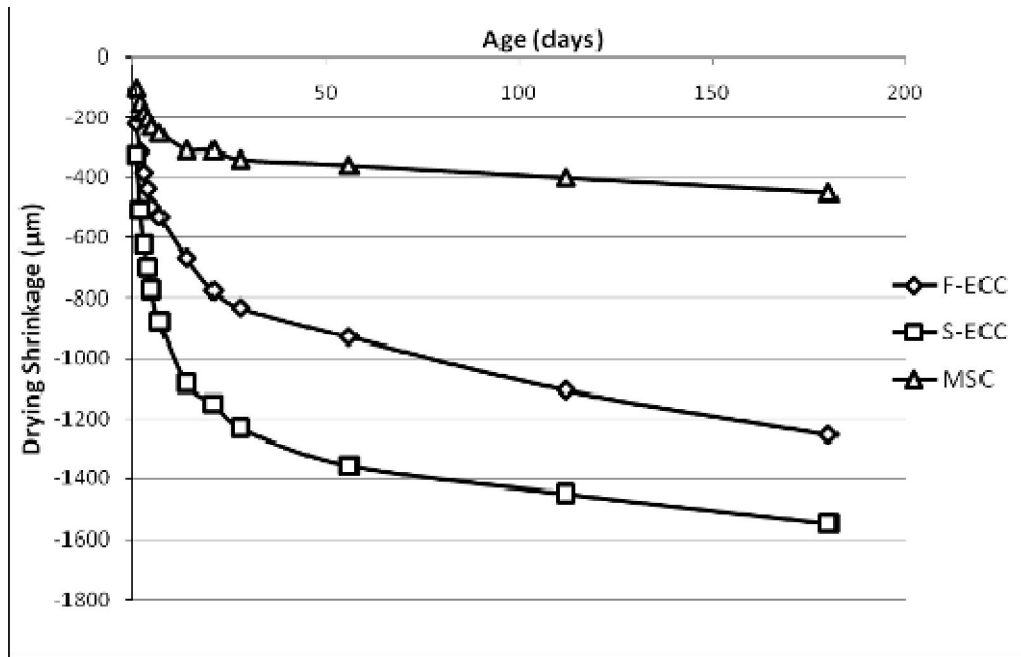
Figure 4.17 Drying shrinkage of overlay mixtures

shrinkage of ECC overlay materials is above triple that of the MSC reference overlay mixture. This is due to the very high cementitious materials (Portland cement and mineral admixture) content, and absence of large volume of coarse aggregates. The previous results showed that the restraining effect of the micro-silica sand in the ECC mixtures was too small to contribute significantly to drying shrinkage (Şahmaran et al., 2009c).

**4.2.1.4 Restrained Shrinkage**

Shrinkage cracking is a major problem for concrete structures, especially for flat structures, such as highway pavement, slabs and walls. Free shrinkage tests alone cannot offer sufficient information on the behavior of concrete structures because virtually every concrete structure is restrained in some way, either by reinforcement or by the boundary condition of the structure. In this study, the method of the ECC and MSC rings cast next to a steel ring is used to simulate restrained shrinkage cracking. Once exposed to the ambient relative humidity and temperature conditions, the drying shrinkage deformation of the F_ECC, S_ECC and MSC, when restrained by the steel ring, results in internal radial pressure. Consequently, the overlay material layers are subjected to a circumferential tensile stress state that can cause cracking. The cracking pattern, crack number and crack width were measured as a function of age with a portable microscope. Measurements were taken at three

102

different locations along each crack and the average value was plotted. From each overlay material, two specimens were tested.

Crack numbers occurred on the F_ECC, S_ECC and MSC mixtures, and average, minimum and maximum crack widths are presented in Table 4.8. For the MSC control specimens, two cracks were observed in each specimen. The average and maximum crack width of the two specimens were 165μm and 280 μm at 28 days. For F_ECC and S_ECC specimens, 7 and 8 cracks were formed at 28 days, respectively. The average crack widths at the end of 28 days were 78 μm and 108 μm for F_ECC and S_ECC specimens, respectively. The crack width of these ECC microcracks was significantly lower than the crack width of MSC localized cracks, and the former retains its load carrying capacity after crack formation. Restrained ring shrinkage tests results during 28 days period after casting are shown in Figure 4.18. Because of significant differences between these two crack widths, only maximum crack width of MSC specimens were considered in Figure 4.18. As seen in Figure 4.18, both ECC mixtures showed some degree of multiple cracking. Basically, the width of a crack developed very fast in the first few days after crack formation. From then on the rate of development diminished its intension or stabilized. On the other hand, the crack width of MSC mixture still want to go upward after 28 days.

Wang et al. (1997) reported that as crack width increases from 100 μm to 500 μm, the permeability coefficient increases nearly seven orders of magnitudes from 1.0 x $10^{-11}$ m/sec to 1.0 x $10^{-4}$ m/sec. However, for crack widths under 100 μm, the permeability coefficient remains nearly identical to that of uncracked concrete, suggesting that for crack widths below this threshold there is no significant increase in permeability after cracking. Crack widths under 100 μm were also found to have same effective chloride diffusion coefficient as uncracked concrete (Sahmaran et al., 2007a). Taking these into account, the test results show that ECC overlay materials has significantly greater resistance to restrained shrinkage cracking than MSC, despite its higher drying shrinkage value. This is due to the large tensile strain capacity of ECC overlay materials, which leads to a negative shrinkage cracking potential and great dimensional compatibility with existing concrete.

Table 4.8 Restrained shrinkage crack characterization of overlay mixtures

| Mixtures | Crack Width (μm) | | | Crack Number |
|---|---|---|---|---|
| | Average | Minimum | Maximum | |
| F_ECC | 78 | 40 | 100 | 7 |
| S_ECC | 108 | 80 | 125 | 8 |
| MSC | 165 | 50 | 280 | 2 |
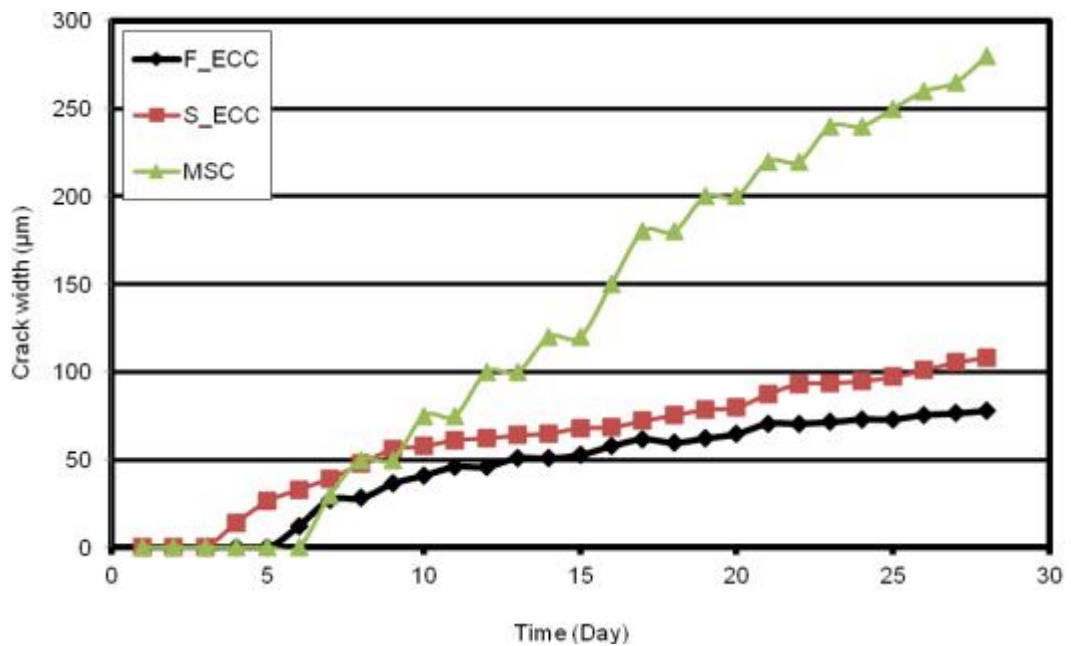


Figure 4.18 Crack width-time relations of overlay mixtures under restrained shrinkage

### 4.2.1.5 Rapid Chloride Permeability Test

Chloride ion permeability test results of the specimens for overlay mixtures at 28 and 90 days are presented in Figure 4.19. They are expressed in terms of the total electrical charge in coulomb, which provides an indirect measure of the resistance of F_ECC, S_ECC and MSC mixtures to chloride ion penetration. The classification ranges given in the ASTM C1202 are also illustrated graphically in Figure 4.19 by horizontal gridlines. The data presented in Figure 4.19 shows that F_ECC, S_ECC and MSC mixtures exhibited sufficient resistance to chloride ion penetration with the total charge exceeding 2863 coulomb, 878 coulomb and 212 coulomb, respectively, at the age of 28 days. Although, all of these values are acceptable for chloride ion

penetrability, MSC and S_ECC mixtures show better performance than F_ECC mixture as very low chloride ion penetrability.
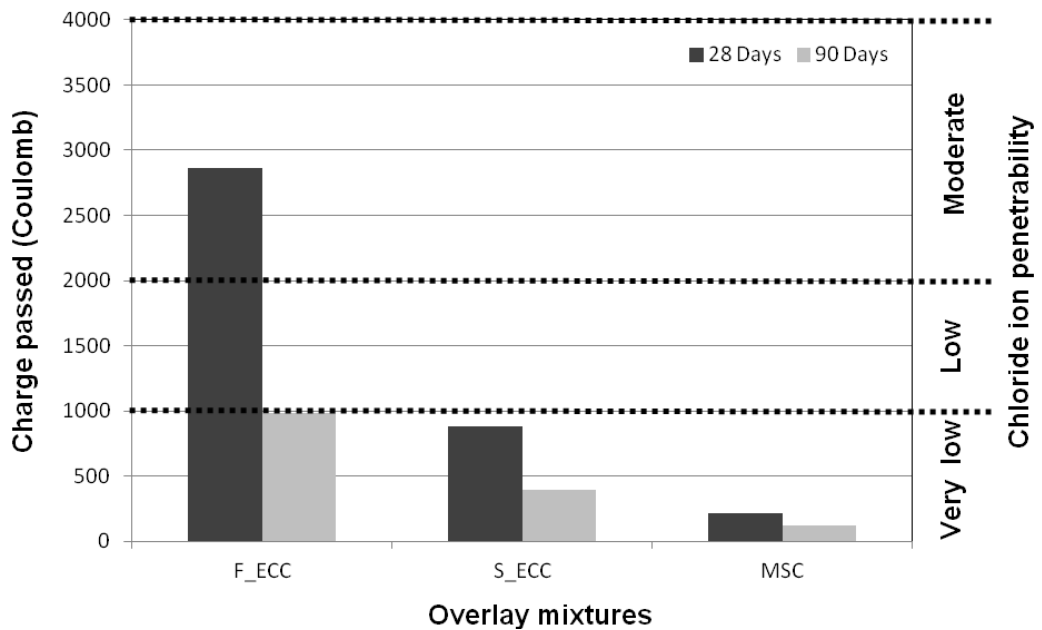


Figure 4.19 Chloride ion penetrability of overlay mixtures with charge passed

### 4.2.1.6 Modulus of Elasticity Test

Modulus of elasticity values of F_ECC, S_ECC and MSC mixtures are presented in Table 4.6. Three cylinder specimens of each overlay mixture were used to determine these values. The experimental results revealed also that the modulus elasticity of ECC overlay materials is lower than that of the MSC reference overlay mixture. This is due to the very high cementitious materials (Portland cement and mineral admixture) content, and absence of large volume of fine and coarse aggregates. It is important to note that cracking due to the lack of the dimensional compatibility of the repair material with substrate can be reduced/eliminated by one, or a combination, of the following factors: low shrinkage, high creep, low modulus of elasticity, high tensile strength, and high tensile strain of the repair material (Morgan, 1996; Li and Stang, 2004; Li and Li, 2009).

### 4.2.2 Performances of Overlaid (Overlay + Substrate Concrete) Specimens

### 4.2.2.1 Flexural Performance of Overlaid Specimens

The layered specimens' flexural tests were conducted with three different overlay

materials, namely F_ECC, S_ECC and MSC. Three overlay thicknesses of 25 mm, 35 mm and 50 mm were used for each material. Maximum flexural stress (or modulus of rupture) of F_ECC, S_ECC and MSC composite beams after four point bending test are summarized in Table 4.9. The MSC test results serve as a reference for assessing the flexural performance of ECC overlaid specimens. The average flexural strength of substrate concrete beam was 5.0 MPa at the ages of 28 days. Test results show that ECC overlaid specimens were superior to MSC overlaid specimens in terms of flexural strength regardless of the thickness of overlay. Among the ECC specimens, S_ECC composite beam has the highest flexural strength for each pavement overlay thickness and testing age. For 28 days of age the overlaying with 25 mm F_ECC, S_ECC or MSC on the diamond saw smooth interface offers respectively 9.46, 10.88 and 6.07 MPa in the flexural stress of layered specimen. The percentage of strength improvement relative to the monolithic substrate concrete member is 89.2% for F_ECC, 117.6% for S_ECC and 21.4% for MSC overlay materials. The failure flexural stress is measured at 9.46 to 11.98 MPa treating the ECC overlay as an original monolithic ECC beam without the concrete substrate. Based on the results, it can be concluded that the addition of ECC layer could significantly improve the maximum flexural stress. Moreover, when the thickness of pavement overlay increases, the percentage of improvement with the use of ECC increased. It is important to note that, the maximum flexural load carrying capacities of 35 mm thickness ECC composite beams have a higher maximum flexural load carrying capacity than MSC composite beam with the thickness of 50 mm. In other words, in terms of load carrying capacity under flexural loading, ECC overlay materials with 35 mm thickness is preferable to MSC overlay with 50 mm thickness.

Figure 4.20 demonstrates the typical flexural stress – mid-span beam deflection curves of the MSC, F_ECC and S_ECC pavement overlay composite beams with different overlay thicknesses as 25 mm, 35 mm and 50 mm at the ages of 28 days. As seen from Figure 4.20, in addition to the flexural strength improvement, the use of ECC layer can also result in significant ductility improvement for the layered beams. Strain-hardening behavior is observed in every test case of F_ECC and S_ECC composite beams. On the other hand MSC composite beams show the behavior of brittle material. The F_ECC and S_ECC composite beams generally show increase in the amount of strain hardening, when the pavement overlay

106

Table 4.9  Flexural strengths of F_ECC, S_ECC and MSC composite beams after four-point bending test

| Mix ID | Thickness (mm) | Flexural Strength, MPa | | |
|---|---|---|---|---|
| | | 1 day | 7 days | 28 days |
| **F_ECC** | | 4.83 (0.17)[*] | 7.55 (0.31) | 9.46 (0.37) |
| **S_ECC** | 25 | 6.30 (0.24) | 8.94 (0.34) | 10.88 (0.41) |
| **MSC** | | 4.64 (0.16) | 5.33 (0.20) | 6.07 (0.22) |
| **F_ECC** | | 5.12 (0.19) | 8.12 (0.31) | 9.98 (0.36) |
| **S_ECC** | 35 | 6.31 (0.24) | 9.90 (0.37) | 11.00 (0.41) |
| **MSC** | | 4.80 (0.18) | 5.59 (0.21) | 6.22 (0.23) |
| **F_ECC** | | 5.29 (0.19) | 8.50 (0.32) | 11.31 (0.41) |
| **S_ECC** | 50 | 6.58 (0.24) | 10.48 (0.40) | 11.98 (0.42) |
| **MSC** | | 4.85 (0.17) | 6.11 (0.23) | 6.51 (0.24) |

*Numbers in parenthesis are the standard deviations

thickness increases. For 25 mm MSC composite beam, the average deflection capacity at ultimate stress was about 0.26 mm. With the addition of a 25 mm layer of S_ECC, this value increased to an average value of 2.2 mm, with a 746% increase as compared to that of micro-silica concrete. For the same overlay thickness, this value reached about 3.0 mm for F_ECC composite beam, which corresponds to an increase of about 1054%. If the thickness of pavement overlay increases to 35 mm, these values also increased as seen in Figure 4.20. The average deflection at ultimate load was about 0.27 mm, 3.0 mm and 3.5 mm for MSC, S_ECC and F_ECC, respectively. Therefore, the rise percentages of deflection at ultimate load were 1011% for S_ECC and 1196% for F_ECC. Also, for 50 mm pavement overlay thickness, the average deflection at ultimate load was about 0.29 mm for MSC, 3.5 mm for S_ECC with a 1106% increase and 4.1 mm for F_ECC with a 1313% increase. The increase in deflection capacity with the use of ECC, which reflects materials' ductility, is related to change in the failure mode. The crack propagations of MSC, S_ECC and F_ECC composite beams after four point bending test can be seen in Figure 4.21. For MSC composite beam, there is only one major crack propagating from the bottom of the

beam (Figure 4.21-a). For S_ECC and F_ECC composite beams, multiple fine cracks are formed in the ECC layer first (Figure 4.21-b and c). Finally, one of these cracks will open more widely than the others and propagate into the concrete layer. Multiple cracking permits large straining in the ECC layer until its failure, therefore leading to a higher ultimate deflection value and a ductile failure mode. Similar results were obtained from the previous work by using poly-ethylene fiber-reinforced ECC (Lim and Li, 1997; Kamada and Li, 2000; Zhang and Li, 2002). It is also important to note that both ECC overlay systems failed without delamination for all studied thicknesses in these experiments (Figure 4.21-b and c). However, regardless of the thickness of overlay, slight delamination between the substrate concrete and MSC overlay materials was observed (see Figures 4.21-a). Therefore, the deformation capacity of the material used in the overlay construction should be high enough to prevent the delamination type of failure in rehabilitated structures.

**4.2.2.2 Reflective Cracking Test of Overlaid Specimens**

Table 4.10 summarizes the maximum flexural loads of F_ECC, S_ECC and MSC composite beams with three different pavement overlay thicknesses as 25 mm. 35 mm and 50 mm according to reflective cracking test. As seen from Table 4.10, as in the flexural strength test results of overlaid specimens, S_ECC composite beam has the highest and MSC composite beam has the lowest maximum flexural load for each pavement overlay thickness and testing age. In the ECC overlay system, in accordance with the type of ECC and overlay thickness, the ultimate load is approximately 1.1 to 2.0 times larger than that of the MSC overlay system. For 28 days of age and 25 mm overlay thichness, the maximum flexural load of MSC composite beam was 1278 N. For F_ECC composite beam this value increased to 1414 N, which is about 11 % increase. For S_ECC composite beam, this value reached about 1839 N, which is about 44% increase. The tests results also show that there is a direct relationship between maximum flexural load and overlay thickness. When the thickness of pavement overlay increases as 35 mm and 50 mm, the percentages of increase are about 50% for F_ECC, 73% for S_ECC, and 82% for F_ECC, 103% for S_ECC, respectively. If pavement overlay thicknesses are compared, maximum flexural load of 35 mm thickness S_ECC composite beam has a higher maximum flexural load than MSC composite beam with the thickness of 50
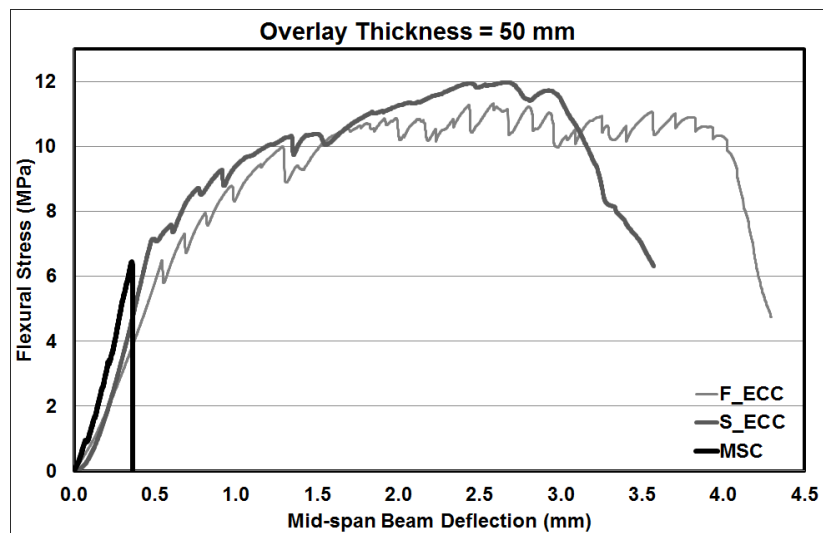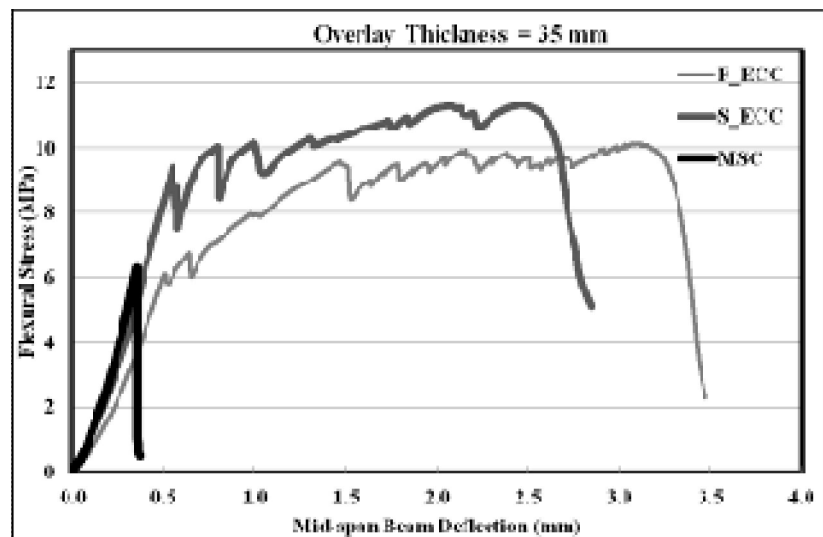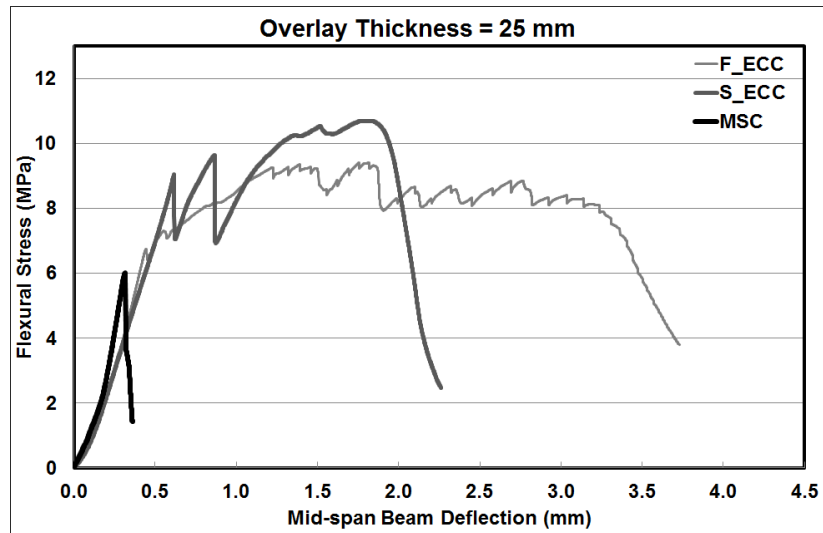
Figure 4.20 Flexural stress vs. deflection curves of composite beams with different thicknesses obtained from four-point bending test at the age of 28 days

a) MSC composite beam after four point bending test



b) S_ECC composite beam after four point bending test



c) F_ECC composite beam after four point bending test

Figure 4.21 Crack propagations of layered composite beams after four-point bending test

mm. Therefore, as in the flexural performances, S_ECC mixture with the thickness of 35 mm can be used instead of 50 mm thick MSC mixture in accordance with the reflective cracking test results.

Table 4.10 Maximum flexural loads of composite beams obtained from reflective cracking test

| Mix ID | Thickness (mm) | Maximum Flexural Load (N) | |
| --- | --- | --- | --- |
| | | 7 days | 28 days |
| F_ECC | | 1066 (40.1)[*] | 1414 (53.5) |
| S_ECC | 25 | 1409 (50.7) | 1839 (66.8) |
| MSC | | 959 (38.9) | 1278 (51.1) |
| F_ECC | | 2330 (82.0) | 2857(108.9) |
| S_ECC | 35 | 3219 (122.0) | 3652 (136.5) |
| MSC | | 1903 (71.7) | 2108 (81.5) |
| F_ECC | | 4096 (158.1) | 5486 (212.1) |
| S_ECC | 50 | 5469 (221.1) | 6780 (270.2) |
| MSC | | 3144 (119.3) | 3334 (128.8) |

*Numbers in parenthesis are the standard deviations

The overall flexural load-deflection behaviors as a result of reflective cracking testing in the three different overlay systems with different overlay thicknesses as 25 mm, 35 mm and 50 mm are illustrated in Figure 4.22. For the deflections at peak load, which reflect the system ductility and energy absorption capacity, the F_ECC and S_ECC composite beams are considerably larger than MSC composite beam. These results are in aggrement with the previous results (Lim and Li, 1997; Kamada and Li, 2000; Zhang and Li, 2002). Besides, it is clear from Figure 4.22 that the energy absorption capacity in the F_ECC and S_ECC overlay systems are much enhanced when it is compared with MSC overlay system. The area under the load-deflection curve of the ECC overlay system is more than hundred times larger than that of the MSC overlay system. This meaningful improvement in ductility and energy absorption capacity of the F_ECC and S_ECC overlay systems are expected to improve the durability of repaired structures by resisting brittle failure. In many cases, the high ductility might be more important than the strength. The causes of failure in many infrastructures might be excessive uneven deflection in structures or

imposed straining. The superior deflection capacity of the ECC overlay system can provide good serviceability without any major failure. According to the reflective cracking test results, when the pavement overlay thickness increases, the deflection values at ultimate load of F_ECC and S_ECC composite systems slightly decrease. This could be the effect of compression zone because in reflective cracking test, ECC overlay section of the composite beam face with compression zone unlike four point bending test of composite beams. For all pavement overlay materials and thicknesses, F_ECC overlay system has the highest deflection capacity at ultimate load and MSC overlay system has the lowest deflection capacity at ultimate load, as seen in Figure 4.22. There is also a huge gap between the deflection values at ultimate load of ECC composite systems and MSC composite system. For instance, the deflection at ultimate load was about 0.3 mm for MSC composite beams, and the deflection at ultimate load was 4.9 mm and 3.6 mm for F_ECC and S_ECC composite beams, respectively for 25 mm pavement overlay thickness. This gap is related to change in the failure mode (Figure 4.23).

A typical crack patterns at failure of the composite beams with different overlay materials (F_ECC, S_ECC and MSC) are shown in Figure 4.23. The most significant differences in external appearance after testing between the ECC overlay systems and the MSC overlay system are the number of cracks and the crack width. In the MSC composite beams, only one crack at the initial notch in the overlay systems is found and this crack opening is the final failure of the MSC overlay system. The fractured halves of the specimens separated completely at the end of the test. However in the ECC overlay systems with smooth surface, for both ECC mixtures, multiple microcracks are developed on both sides of the initial notch increasing with the deflection of specimens (see Figure 4.23-a and b). This means that the ECC overlay system was able to redistribute the load and utilize more material to resist the final failure. Multiple cracking also enables large deformation under flexural loading in the ECC layer before its failure, therefore leading to a higher ultimate deflection value and a ductile failure mode without direct crack reflection. It is also important to note that both the MSC and ECC overlay systems failed without delamination in these experiments (Figure 4.21).
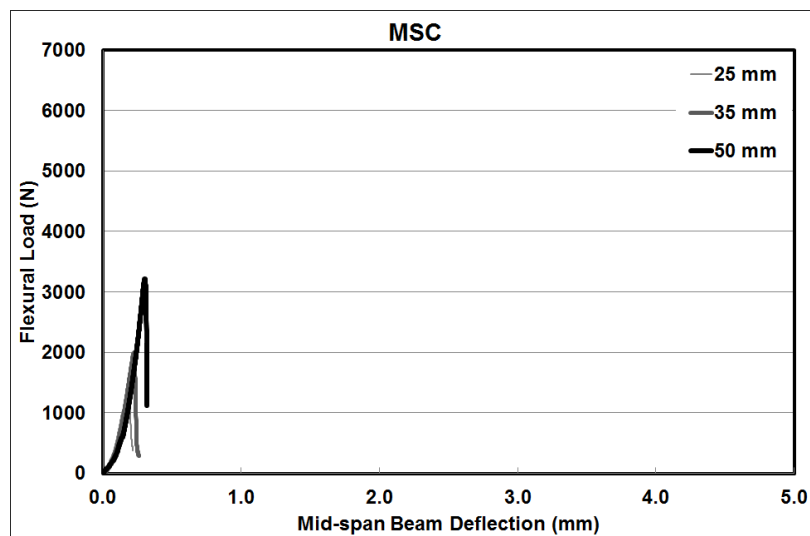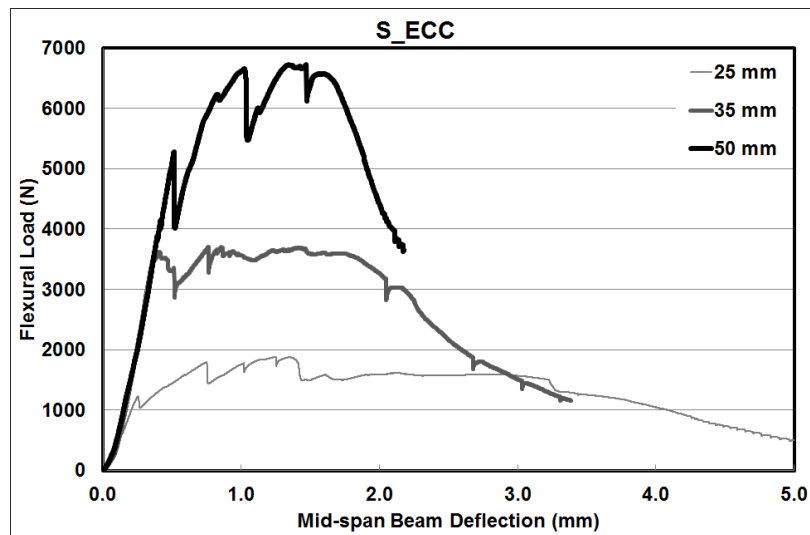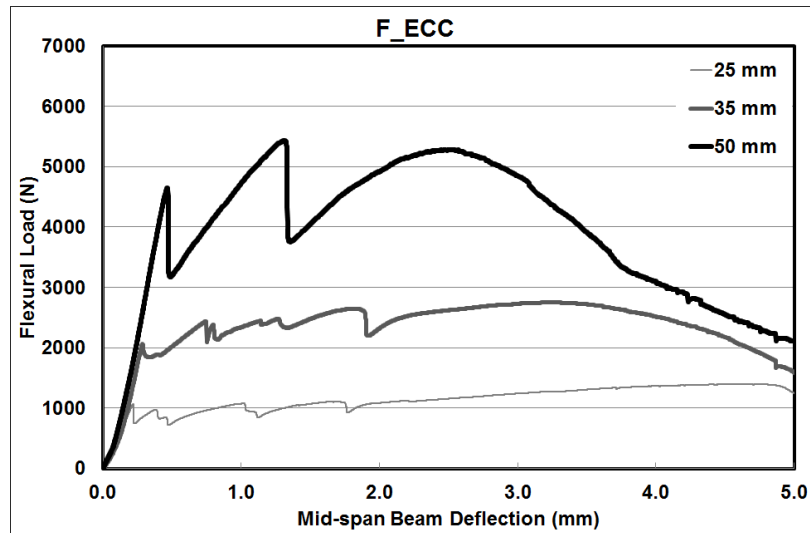
Figure 4.22 Flexural load vs. deflection graph of composite beams with different thicknesses obtained from reflective cracking test at the age of 28 days

a) S_ECC composite beam



b) F_ECC composite beam



Reflective cracking
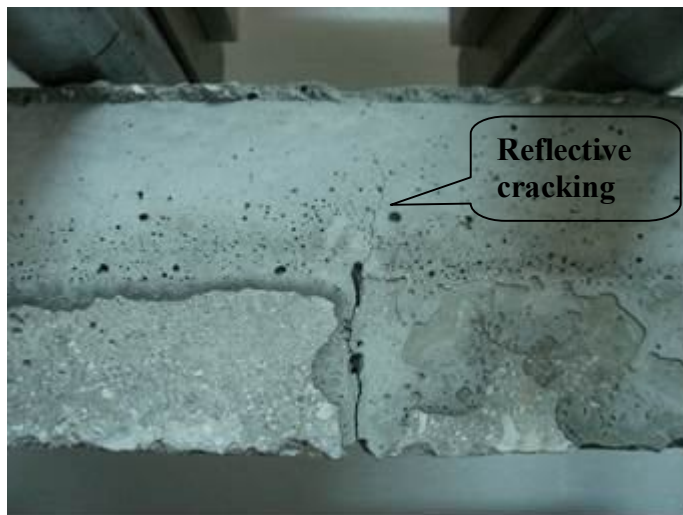
c) MSC composite beam

Figure 4.23  Crack patterns at failure of overlay materials after reflective cracking test

The most significant differences in external appearance after testing between the F_ECC overlay system and the S_ECC overlay system are the crack number and the crack intervals. More multiple cracks are observed in the case of F_ECC with much closer spacing. These observations are consistent with test results given in previous sections.  Also the crack width in the ECC overlay systems (20 - 100 μm) is much smaller than the other overlay system (sub-millimeter for MSC) at the peak load. This is one of the outstanding characteristics of ECCs. Crack width control is of primary importance for many reinforced concrete applications, since it is believed that there is a close relationship between the mean or maximum crack widths and the durability of the structure.  Moreover, the lower magnitude of the crack width is expected to promote the self-healing behavior, and thus the transport properties in cracked composites (Lepech and Li, 2005b; Yang et al.,2005; Şahmaran et al., 2007a; Şahmaran and Li, 2009b).  Consequently, in the serviceability limit state a mean or maximum crack width less than about 0.1 mm is usually prescribed (Evardsen, 1999; Reinhardt and Jooss, 2003).

### 4.2.3 Bond Strength Performances of Overlay Materials

### 4.2.3.1 Slant Shear Test

The slant shear test is as one of the most promising test methods for bond assessments in which the interface is subjected to the shear and compression at the same time. The bond strength for the slant shear test was calculated by dividing the maximum load at failure obtained from compression loading by the elliptical area of the bonded interface. Table 4.11 shows the results of bond tests of F_ECC, S_ECC, and MSC bi-layer composite cylinder specimens including the modes of failure. The loading rate was 0.25 MPa/second for all the test specimens. As previously discussed, from each mixture 18 slant shear specimens were cast with smooth surface texture for all testing ages. The strength result at each testing age represents the average of six cylinders.  The average coefficient of variation (COV) of all the test results was less than 9% indicating consistent result throughout the test. ACI specified a bond strength range to select the repair materials in "Concrete Repair Guide (ACI 546R)" in accordance with slant shear test results (ACI Committee 546, 2004). As seen from Table 4.11, all the overlay materials have considerably greater bond strength than the bond strength range specified by the ACI for all testing ages.

Table 4.11 Slant shear bond strength test results and failure mode

| Mix. ID | Bond Strength (MPa) | | | Failure Mode |
| | 1 Day | 7 Days | 28 Days | 28 Days |
| --- | --- | --- | --- | --- |
| **F_ECC** | 7.1 (0.31)[*] | 14.7 (0.68) | 21.7 (0.92) | All through substrate |
| **S_ECC** | 8.3 (0.39) | 17.4 (0.75) | 24.3 (1.14) | All through substrate |
| **MSC** | 10.4 (0.49) | 14.1 (0.68) | 15.6 (0.77) | 4 through slanted interface 2 through a monolithic rupture |
| **ACI bond strength range** | 2.8 to 6.9 | 6.9 to 12.4 | 13.8 to 20.1 | - |

*Numbers in parenthesis are the standard deviations

The slant shear test results of MSC serve as a reference for assessing the bond performance of ECC mixtures. As seen from Table 4.11, for the 1 day of curing, bond strength gain in the MSC specimens was higher compared to the ECC mixtures. The reason for this was the difference in maturity of the overlay materials (please see 1-day compressive strength test results of overlay materials). At the relative young ages of testing used in this research, full hydration of neither the ECC mixtures incorporating large volumes of mineral admixture (fly ash and slag) has been reached. However, with increased curing ages, significant strengthening in slant shear resistance is found in ECC mixtures. For example, the 1-day bond strength of F_ECC is roughly half the 7 day strength and the bond strength capacity of MSC and F_ECC specimens are approximately equal at the age of 7 days. The S_ECC specimens resulted bond strength that are approximately 20%, higher than the MSC and F_ECC specimens. This finding was partially a result of the advances in hydration and pozzolanic reactions of the slag due to its large specific surface area (425 $m^2$/kg surface area) compared to that of fly ash (290 $m^2$/kg). Due to the smaller average particle size of slag than that of cement, it can well fill the space among the cement grains (filler effect), improving the particle distribution of cementitious system, and forming dense microstructure. Moreover, high surface area of slag provides more nucleating sites and $OH^-$ ions as well as alkalis into the pore fluid (Roy and Idom, 1983). This high strength should be correlated not only to the fineness but also to the self-cementitious activity of slag. The predominant reaction

of slag with alkali hydroxide especially during the early hydration period seems to contribute to the strength of ECC mixture. Between the ages of 7 days and 28 days, high amount of bond strength gain was achieved by both ECC mixtures. At the age of 28 days, test results show that ECC slant shear test specimens are superior to MSC overlaid specimens in terms of bond strength. Among the ECC specimens, S_ECC composite cylinder has the highest bond strength. For 28 days of age the overlaying with F_ECC, S_ECC or MSC on the diamond saw smooth interface offers respectively 21.7, 24.3 and 15.6 MPa. The percentage of bond strength improvement relative to the monolithic substrate concrete member's shear strength (15.9 MPa at the ages of 28 days) is 36.4% for F_ECC, 52.8% for S_ECC and -1.9% for MSC overlay materials. Based on the results, it can be concluded that the addition of ECC layer could significantly improve the bond stress measured by slant shear test. This result indicates that bond strength is greatly dependent on the type of overlay materials.

During slant shear test, visual observations were also made at the age of 28 days regarding whether the cylinder failed along the shear plane or if failure was due to significant cracking in the overlay material or substrate concrete. The mode of failure provides valuable information about the appropriateness of the overlay system. The failure modes are described in Table 4.11. Three different failure modes were observed in this slant shear test. The failure type for MSC/SUBC specimens was interface debonding or monolithic rupture. In 4 specimens out of total of 6 MSC specimens, the failure plane passed entirely through the bond line (interface). Figure 4.24-a displays a typical interface failure of MSC. In two of the MSC specimens, a monolithic rupture mode occurred with the propagation of cracks through the MSC (Figure 4.24-b). On the other hand, despite the absence of surface roughness, in all cases of ECC-substrate bi-layer specimens, the failure plane occurred preferentially through the substrate, for both types of ECC mixtures (Figure 4.24 (c-d)). Only in one of the F_ECC specimen, a slight interface splits, though the final failure mechanism resulted from cracking failure through the substrate concrete was observed. This is due to the effectiveness of the ECC with its high adhesion strength that did not allow the interface to fail. Failure through the substrate concrete is always desirable, because failure through the substrate concrete demonstrated that the existing substrate is the weakest component of the ECC/SUBC system. This can

(a) MSC – interface failure          (b) MSC – monolithic rupture
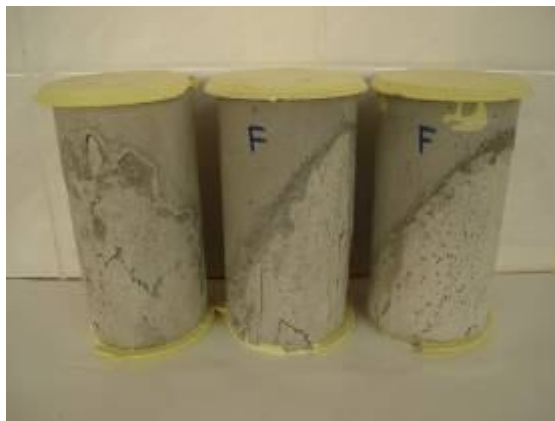
(c) F_ECC – substrate failure          (d) S_ECC – substrate failure

Figure 4.24 Failure types of slant shear test

be attributed to chemical reactions between the active silicon dioxide of fly ash and slag in the ECC and the $Ca(OH)_2$ in the substrate concrete to form secondary C-S-H. It can be, therefore, inferred that the microstructure of the interface zone can be improved further with time in consequence of a secondary reaction between the $Ca(OH)_2$ present there and pozzolana, thus leading to a even denser interface zone with a better durability. The presence of coarse aggregate also seems to play an important role in the bond strength, as lack of coarse aggregate in ECC mixture increase the contact area between substrate and overlay where chemical reactions take place. The improvement of the bond strength by using fly ash and slag is not only the consequence of chemical reaction but also of the ability of the very small fly ash and slag particles to ''fit in'' between cement particles and pores on the surface of substrate. The noticeable improvement in the microstructure led to a significant increase of the intermolecular force and mechanical interlocking. Consequently, the bond strength increased greatly as shown in Table 4.11.

**4.2.3.2 Splitting Prism Test**

The bond strength in tension was assessed with the splitting prism test based on ASTM C496 (2011). Overlaying with F_ECC, S_ECC or MSC, have been applied separately on the top of the smooth interface substrate and untreated rough interface substrate. Rough surface refers to the surface with no treatment on it, and smooth surface refers to the diamond saw cut surface. Eight splitting prism specimens were tested for each testing age and surface texture. The final splitting prism samples were 76.2 mm wide x 50 mm long x 30 mm high yielding a bond surface area 50 mm x 76.2 mm. Load was applied at the rate of 50 kN/min., approximately the minimum rate specified for cylindrical specimens by ASTM C 496. Assuming a uniform tensile stress across the bond plane, and the splitting tensile strength was calculated, accordingly.

Table 4.12 summarizes the test results, including the compressive strength of substrate concrete and overlay materials, and average splitting test results of F_ECC, S_ECC and MSC composite specimens for the two different surface textures. The coefficient of variance (COV) values for the entire splitting prism test ranged from 5.30-12.07%. The values are reasonable considering the variability of production of cementitious composites. The narrow range of COV values in the present study is an indication of the consistent repeatability of the splitting prism test method. As seen from Table 4.12, the tensile bond strength of MSC increased rapidly until 7 days after casting and remained almost at a constant level beyond the 7 days of curing. From the experimental data, it is also possible to observe that the splitting tensile strength for MSC overlay is relatively low in comparison with the results for F_ECC and S_ECC, meaning that the type of overlay material plays a role in the response, and increasing the compressive strength of the overlay does not lead to an increase in the bond strength. S_ECC mixture attained larger average bond strengths than the other overlay materials tested. For 28 days of age, the bond strength of MSC was 2.96 MPa. For F_ECC composite beam this value increased to 3.20 MPa, which is about 8% increase. For S_ECC composite beam, this value reached about 3.43 MPa, which is about 16% increase. These bond strength values on the rough interface are respectively improved by 12, 10 and 5 % compared to those of the smooth interface. This is likely because bond failure mechanism is primarily affected by the area of

contact between the substrate and overlay material. The rough surface specimens provide higher surface contact area and in turn greater bond strength than the smooth surface.

Table 4.12  Performance of composite prisms under splitting prism test

| Mix ID | Compressive strength substrate concrete 28 d. (MPa) | Compressive strength overlay 28 d. (MPa) | Bond Strength (MPa) | | |
| --- | --- | --- | --- | --- | --- |
| | | | 1 day | 7 days | 28 days |
| F_ECC-S[*] | 31.9 (1.6)[**] | 53.8 (2.3) | 1.82 (0.15) | 2.88 (0.25) | 3.20 (0.28) |
| F_ECC-R[*] | 31.9 | 53.8 | 2.00 (0.18) | 3.15 (0.28) | 3.58 (0.30) |
| S_ECC-S | 31.9 | 71.2 (3.1) | 2.00 (0.17) | 3.02 (0.26) | 3.43 (0.29) |
| S_ECC-R | 31.9 | 71.2 | 2.17 (0.19) | 3.34 (0.28) | 3.75 (0.32) |
| MSC-S | 31.9 | 68.7 (3.2) | 2.12 (0.20) | 2.77 (0.25) | 2.96 (0.26) |
| MSC-R | 31.9 | 68.7 | 2.40 (0.22) | 2.91 (0.26) | 3.11 (0.28) |
| Continuous | 31.9 | - | - | - | 3.22 (0.15) |

*S: Smooth surface texture, R: Rough surface texture
**Numbers in parenthesis are the standard deviations

In order to compare the results of repaired specimens with a monolithic sample (continuous samples) which represent the substrate repairing, substrate specimens were cast in a single stage, so there is no predefined interface plane. An equivalent bond strength for these specimens was calculated by dividing the applied force by the corresponding non continuous bond area values. The bond strength for the continuous samples at the age of 28 days is given in Table 4.12. The bond strength value of continuous sample is important because the value of each test can only be judged in terms of its ability to predict the strength of a continuous sample tested under the same conditions. As seen from Table 4.12, because the bond strength of both ECC mixtures is stronger than the equivalent bond strength of continuous substrate concrete, no failures occurred within the ECC section. We notice the substrate material broken and adhesive with ECC material as shown in Figure 4.25 (a-b), which point to the high bond of the ECC. On the other hand, the failure mode

observed for MSC/SUBC composite prism was bond failure (Figure 4.25-c). Therefore in such applications, the use of ECC materials results in bond strengths that represent better than a monolithic structure.

Smooth surface texture                    Rough Surface texture



F_ECC



S_ECC



MSC

Figure 4.25 Failed splitting prism test samples

# CHAPTER V

# CONCLUSIONS

## 5.1 Development of Engineered Cementitious Composites (ECC) with Locally Available Materials

First part of this thesis described the influence of aggregate size and amount on the mechanical performances and dimensional stability of ECC with mineral admixture. ECC mixtures contain mineral admixture (fly ash or slag) with mineral admixture/cement ratio of 1.2 or 2.2, aggregate with maximum grain sizes of 0.4 or 1.0 mm and aggregate/binder ratio of 0.36, 0.45 and 0.55. For comparison purpose, standard ECC mixture with FA/C ratio of 1.2, micro silica sand with an aggregate to binder ratio (A/B) of 0.36 (Mix. ID: FA1.2_0.36_400 – M45) were also produced. The following conclusions can be drawn from this study.

1. Increase in mineral admixture (FA and slag) replacement rate lead to a reduction in fracture toughness of matrix, and compressive and flexural strengths of composites whereas ductility increases. The ECC ductility, by measuring mid-span beam deflection capacity, strongly depends on the type and amount of mineral admixture. The mixture of slag-ECC showed significantly lower deflection capacity when compared to the ductility of the mixture of FA-ECC. The reduced ductility can possibly be caused by the higher fracture toughness, matrix and bond strength and friction between the slag-ECC matrix and the fibers compared with FA-ECC mixtures.

2. For a given mineral admixture type and content, fracture toughness of specimens produced without PVA fiber significantly affected while there was no definite change in compressive and flexural strength as aggregate size and amount increases. Moreover, increase in the percentage of aggregate size and its amount, adversely influenced ductility of ECC specimens. The ductility of ECC could be improved

through the addition of coarse aggregate with the quantity more than used in the standard ECC mixture. This was true as long as the maximum size and content of aggregates did not exceed certain limits, beyond which aggregates start to increase matrix fracture toughness to a limit value, interfere with the uniform dispersion of fibers and negatively influence the composite ductility. The negative effects of aggregates on fiber dispersion were particularly pronounced in composites with lower mineral admixture replacement rate (especially slag) when relatively large contents of coarser aggregates (1 mm MAS for this study) are used. The negative effects of aggregates on fiber dispersion and matrix toughness can be eliminated or minimized by increasing mineral admixture content (replacing cement). In this study, the FA-ECC mixtures produced with higher maximum aggregate sizes and amount exhibit strain-hardening behavior with deformation capacities better than the standard ECC mixtures. This was true for all aggregate amount and sizes used in the production of ECC in this study.

3. There is a strong correlation between the deflection capacity and the matrix fracture toughness. As the matrix fracture toughness decreases, the deflection capacity increases.

4. After unloading, multiple microcracks with a small average crack width, fine crack spacing and different amount were observed on all ECC specimens tested under flexural loading. With crack width measurement on the surface of the specimens, it has been indicated that average crack width was lower than 90 $\mu$m for slag-ECC mixtures and 60 $\mu$m for FA-ECC mixtures. In slag ECC, cracks were also spaced further apart than in FA-ECC. On the other hand, the use of aggregate up to 1.00 mm MAS and 0.55 aggregate/binder ratio did not influence the average residual crack width. Crack width control is of primary importance for many reinforced concrete applications, since it is believed that there is a close relationship between the mean or maximum crack widths and the durability of the structure. Moreover, the crack width of ECC mixtures (less than 90 $\mu$m) is very important for self-healing process. Because, the various findings on self-healing in ECC have been revealed that there is crack width limit (90 $\mu$m) that can be healed. Therefore, ECC can be accepted as a virtually 'crack-free' concrete.

5. Cement replacement with FA and increase in aggregate content have a significant influence on the drying shrinkage and restrained shrinkage cracking when compared with the slag-ECC. The ultimate drying shrinkage and restrained shrinkage cracking performance of ECC further improve with further increase in the FA content. Test results also suggests that, within the limited aggregate size employed in the present experiments, no significant role of size of aggregate on the ultimate shrinkage is observed for a given aggregate content. The ultimate drying shrinkage of ECC slightly decreases with increase in the size of aggregate from 0.4 mm to 1.0 mm. In comparison, ECC with identical replacement of cement with slag resulted in significantly higher drying shrinkage and a decrease in the age of restrained shrinkage cracking.

6. ECC specimens exposed to freeze-thaw cycles show decreases in UPV, flexural strength, deformation capacity and stiffness, and increase in the mass loss compared with the non-frost deteriorated specimens. Furthermore, the crack width increase to around 1.5 times compared with that of air curing specimens. This phenomenon suggests possible change in the fiber/matrix interface bond properties after accelerated freeze-thaw cycles. For the pre-loaded ECC specimens, the applied pre-loading deformation was found to have detrimental effect on the frost durability of ECC mixtures. This effect is more pronounced in the case of FA-ECC mixtures. Moreover increase in FA content in ECC production can further exacerbate the deterioration caused by freeze-thaw cycles.

Finally, the results presented in this study provide a preliminary database for the suitability of locally available aggregate in the production of ECC, and indicate that locally available aggregate with relatively higher nominal aggregate size and aggregate amount can also be successfully used to produce an ECC having similar or better mechanical properties than corresponding ECC made with micro-silica aggregate. These conclusions are confined to the ECC defined herein, and are based on the experimental results described in this study.

## 5.2 Performance of ECC Mixtures as Overlay Materials

Second part of this thesis explained the performance of selected ECC mixtures (F_ECC and S_ECC) as overlay materials. Also, MSC mixture was produced as

control overlay mixture for the comparison of ECC mixtures. Firstly, basic mechanical properties and dimensional stability of overlay materials were determined by using monolithic overlay specimens. After that, performances of overlaid (overlay + substrate concrete) specimens were investigated with flexural and reflective cracking tests. Finally, bond strength performances of overlay materials were determined by slant shear and splitting prism tests.

### 5.2.1 Basic Mechanical Properties and Dimensional Stability of Monolithic Overlay Specimens

This section explains basic mechanical properties and dimensional stability of monolithic overlay specimens. Compression test, flexural test, drying shrinkage test, restrained shrinkage test and rapid chloride permeability test were performed on monolithic overlay specimens. The following conclusions can be drawn from these tests.

F_ECC mixture has the lowest compressive strength and S_ECC mixture has the highest compressive strength at 28 days of age. Even though MSC mixture has the highest compressive strength at early ages, and similar compressive strength at later ages, the ECC prisms show a substantially higher ultimate flexural strength in comparison with that of the MSC prisms. Moreover, for all specimens, no significant flexural strength gain was observed beyond the age of 28 days. For deformation properties, MSC mixture is a brittle material with sudden fracture failure, on the other hand, F_ECC and S_ECC samples have significantly higher deformation capability than MSC at all testing ages. The drying shrinkage of ECC overlay materials is above triple that of the MSC overlay mixture. But, it is important that the results of restrained shrinkage test showed that the crack width of ECC microcracks was significantly lower than the crack width of MSC localized cracks, and the former retains its load carrying capacity after crack formation. According to rapid chloride permeability test, MSC and S_ECC mixtures show better performance than F_ECC mixture as very low chloride ion penetrability.

### 5.2.2 Performances of Overlaid (Overlay + Substrate Concrete) Specimens

This section of the study examines, on the basis of experimental results, the feasibility of using ultra-thin Engineered Cementitious Composites (ECC) overlay

for the rehabilitation of rigid pavements. Two different ECC-overlay mix designs are investigated: one with high strength and moderate ductility, and the other with moderate strength and high ductility. The rehabilitation work should desirably produce an overlaid pavement which has an improved resistance to reflective cracking, and a load-carrying capacity equal to or higher than the most effective and and generally used as overlay material for rigid pavement overlay – microsilica concrete. The experiments were designed to study the properties of ECC overlays in two aspects: (i) the flexural performances of ECC overlaid specimens with different thicknesses, and (ii) the reflective cracking characteristics of ECC overlaid specimens. The findings of these experiments are summarized below.

Examining the performances of overlaid specimens under four-point flexural loading, significant differences between MSC overlay and ECC overlays with different thicknesses can be noted. First, it is clear that the flexural strength of the layered specimens is significantly increased by using the ECC material in the overlay (above 100% of the value of MSC overlaid beam), and the degree of improvement increased with the increase of ECC thickness applied. Second, the deformation capacity, represented by midpoint deflection at peak load of the beams and energy absorption capacity, represented by the area under the load-deflection curve, with ECC overlaid are obviously increased in comparison to that of MSC overlaid beams. The difference between MSC and ECC overlaid beams on the deformability is due to the single cracking behavior of MSC in bending and the multiple cracking behavior of ECC in bending, respectively. The superior ductility of ECC is a desirable characteristic for it to replace MSC to suppress brittle failure. Third, the increase in deformability in the form of microcracking totally eliminates reflective cracking observed in substrate concrete overlaid with microsilica concrete. The ECC overlay system can also prevent the delamination type of failure in rehabilitated infrastructures. Finally, on the basis of the results of the test programme presented, ECC overlay with 35 mm thick is superior to MSC overlay with 50 mm thick for rehabilitating concrete pavements. The superior performance of ultra-thin ECC overlay system under mechanical loading will be expected to prolong the service life of the structure under traffic loading and to reduce the costs in the rehabilitation work.

The tests reported in this study do not provide a complete simulation of the actual loading, geometry and environmental conditions experienced by field situations. To increase confidence in predicting the behavior of ultra-thin ECC overlay system, however, the field-scale application of ECC as a repair material is needed to be carried out to obtain realistic and consistent results. The results reported in this thesis provide a preliminary database of with ultra-thin ECC overlay behavior under flexural loading.

### 5.2.3 Bond Strength Performances of Overlay Materials

In this section, bond strength performances of overlay materials were explained. Slant shear test and splitting prism test were conducted on the prepared overlay materials' specimens. The following conclusions can be drawn in the light of these tests.

At the age of 28 days, slant shear test results show that ECC specimens are superior to MSC overlaid specimens in terms of bond strength. Among the ECC specimens, S_ECC composite cylinder has the highest bond strength. The failure type for MSC/SUBC specimens was interface debonding or monolithic rupture. On the other hand, despite the absence of surface roughness, in all cases of ECC-substrate bi-layer specimens, the failure plane occurred preferentially through the substrate, for both types of ECC mixtures. From the splitting prism test data, it is observed that the splitting tensile strength for MSC overlay is relatively low in comparison with the results for F_ECC and S_ECC, meaning that the type of overlay material plays a role in the response, and increasing the compressive strength of the overlay does not lead to an increase in the bond strength. S_ECC mixture attained larger average bond strengths than the other overlay materials tested. The rough surface specimens provide higher surface contact area and in turn greater bond strength than the smooth surface as expected.

### 5.3 Recommendations for Future Work

In the present study, the overlay performances of ECC mixtures were investigated under flexural loading condition. However, the fatigue performance of pavement overlays is a very important parameter because of the repeated traffic loads.

Therefore, the performance of ECC mixtures should be performed to determine the behavior of ECC mixtures as pavement overlay under fatigue loading condition.

Rigid overlays can be used to rehabilitate for both flexible and rigid pavements. In this thesis ECC mixtures were used as a pavement overlay material to rehabilitate rigid pavements. Thus, the overlay performances of ECC mixtures can be investigated for flexible pavements.

This thesis investigated three major deterioration mechanisms in concrete overlays: overlay reflective cracking, interfacial delamination due to flexural loading and bond performance between overlay and existing pavement. However, there are other deterioration mechanisms that need to be better understood in the future, such as alkali silica reaction, salt-scaling and spalling in concrete overlays. Furthermore, combined loading states consisting of mechanical and environmental loads, instead of single deterioration mechanisms, need to be more comprehensively considered in future studies of concrete overlay durability and service life estimations.

Although, as a result of this research ECC mixtures has a high performance as a pavement overlay material according to the laboratory studies, it will be important to analyze ECC mixtures in real field conditions. Also it is important that especially reflective cracking and flexural mechanisms should still be valid for large or full scale ECC overlaid concrete pavement. Therefore, ECC mixtures can be applied on a part of a highway to investigate the overlay performance of full scale ECC in field conditions.

**REFERENCES**

Aïtcin, P.C. and Mehta, P.K. (1990). Effect of Coarse Aggregate Characteristics on Mechanical Properties of High-Strength Concrete. *ACI Materials Journal*, **87**, 103-107.

Alaee, F.J, Karihaloo, B.L. Retrofitting of RC beams with CARDIFRC (2003). *ASCE J Comp Const*, **7**, 174-186.

Aleis, K.A. (2004). *Evaluation of the Interlayer Stress-Absorbing composite (IS AC) to Mitigate  Reflective Cracking in Asphaltic concrete Overlays.* Wisconsin Department of Transportation, Report Number: WI-09-04.

Alexander M.G., Stanish K. (2005). Durability design and specification of reinforced concrete structures using a multi-factored approach. *CONMAT'05*, pp.10.

Alhassan, Muhammad A. (2007). *Performance-based aspects and structural behavior of high performance fibrous bonded concrete overlays.* Ph.D. Thesis. University of Illinois, Chigago, Illunois.

American Concrete Pavement Association (ACPA-1990a). *Guidelines for Bonded Concrete Overlays.* Technical Bulletin TB-007P. American Concrete Pavement Association, Arlington Heights, IL.

American Concrete Pavement Association (ACPA-1990b). *Guidelines for Unbonded Concrete Overlays.* Technical Bulletin TB-005P. American Concrete Pavement Association, Arlington Heights, IL.

ASTM Standard C1202 (1997). Standard Test Method for Electrical Indication of Concrete's Ability to Resist Chloride Ion Penetration. *American Society for Testing and Materials,* Philadelphia, USA.

ASTM Standard C157 (2004). Standard Test Method for Length Change of Hardened Hydraulic-Cement Mortar and Concrete. *American Society for Testing and Materials,* Philadelphia, USA.

ASTM Standard C39 (2003). Standard Test Method for Compressive Strength of

Cylindrical Concrete Specimens. *American Society for Testing and Materials,* Philadelphia, USA.

ASTM Standard C457 (1998). Standard Test Method for Microscopical Determination of Parameters of the Air-Void System in Hardened Concrete. *American Society for Testing and Materials,* Philadelphia, USA.

ASTM Standard C469 (2010). Standard Test Method for Static Modulus of Elasticity and Poisson's Ratio of Concrete in Compression. *American Society for Testing and Materials,* Philadelphia, USA.

ASTM Standard C496 (2011). Standard Test Method for Splitting Tensile Strength of Cylindrical Concrete Specimens. *American Society for Testing and Materials,* Philadelphia, USA.

ASTM Standard C618 (2003). Standard Specification for Coal Fly Ash and Raw or Calcined Natural Pozzolan for Use in Concrete. *American Society for Testing and Materials,* Philadelphia, USA.

ASTM Standard C666. (1991). Standard Test Method for Resistance of Concrete to Rapid Freezing and Thawing. *American Society for Testing and Materials,* Philadelphia, USA.

ASTM Standard C672. (2001). Standard Test Method Scaling Resistance of Concrete Surfaces Exposed to De-icing Chemicals. *American Society for Testing and Materials,* Philadelphia, USA.

ASTM Standard C882 (2012). Standard Test Method for Bond Strength of Epoxy-Resin Systems Used With Concrete. *American Society for Testing and Materials,* Philadelphia, USA.

ASTM Standard C989 (2009). Standard Specification for Slag Cement for Use in Concrete and Mortars. *American Society for Testing and Materials,* Philadelphia, USA.

ASTM Standard E399 (2003). Standard Test Method for Linear-Elastic Plane-Strain

Fracture Toughness $_{Ic}$ of Metallic Materials. *American Society for Testing and Materials,* Philadelphia, USA.

Atkinson, Harold N. (2003). *Highway materials, soils and concretes (4$^{th}$ ed.)*. USA: Prentice Hall.

Baalbaki, W., Benmokrane, B., Chaallal, O. and Aïtcin, P.C. (1991). Influence of Coarse Aggregate on Elastic Properties of High Performance Concrete. *ACI Materials Journal*, 499-503.

Bisaillon, A., Rivest, M. and Malhotra, V.M. (1994). Performance of high-volume fly ash concrete in large experimental monoliths. *ACI Materials Journal*, **91,** 178-187.

Blankenship P. (2007). *Reflective Cracking Relief Interlayer for Composite Pavement*, Asphalt, Vol. 22 No.2 Asphalt Institute.

Button J.W. (1989). *Overlay Construction and Performance Using Geotextiles*. Texas Transportation Institute, Transportation Research Record, 1248.

Cable, J.K. and Hart, J. (1998). Evaluation of bond between ultra-thin PCC and asphaltic concrete. *Crossroads 2000 Proceedings*, Iowa State University, Ames Iowa, August.

Carlson, R.W. and Reading, T.J. (1988). Model study to shrinkage cracking in concrete building walls. *ACI Materials Journal,* **85,** 395–404.

Cetin, A. and Carrasquillo, R.L. (1998). High-performance concrete: Influence of coarse aggregates on mechanical properties. *ACI Material Journal,* **95,** 252–261.

Chen, B. and Liu, J. (2004). Effect of aggregate on the fracture behavior of high strength concrete. *Construction and Building Materials*, **18**, 585- 590.

Cho, Yoon-Ho. (1995). *Asphalt Overlay Design Methods for Rigid Pavements Considering Rutting, Reflection Cracking and Fatigue Cracking*. PhD Thesis, University of Texas, Austin.

Cleveland G.S., Button J.W., Lytton R.L. (2002). *Geosynthetics in Flexible and Rigid Pavement Overlay Systems to Reduce Reflection Cracking.* Research Report 0-177701, Texas Transportation Institute.

Cohen, M.D., Olek, J., and Dolch, W.L. (1990). Mechanism of plastic shrinkage cracking in Portland cement and Portland cement-silica fume paste and mortar. *Cement and Concrete Research*, **20**, 103–119.

Cohen, M.D., Zhou, Y., and Dolch, W.L. (1992). Non-air-entrained high strength concrete—is it frost resistant? *ACI Materials Journal*, **89**, 406–415.

Concrete Research and Education Foundation Strategic Development Council (2002). Roadmap 2030: The US Concrete Industry Technology Roadmap. *Concrete Research and Education Foundation*, pp. 27

Davis, D.E. and Alexander, M.G. (1989). *Properties of Aggregate in Concrete (Part 1)*. Hippo Quarries Technical Publication, Sandton, South Africa.

Davis, D.E.and Alexander M.G. (1992). *Properties of Aggregate in Concrete (Part 2)*. Hippo Quarries Technical Publication, Sandton, South Africa.

De Larrard Francois and Belloc Albert. (1997). The influence of aggregate on the compressive strength of normal and high-strength concrete. *ACI Material Journal,* **94,** 417–425.

Duchesne, J., and Bérubét, M.A. (1995). Effect of supplementary cementing materials on the composition of cement hydration products. *Advanced Cement Based Materials*, **2**, 42–53.

Elsen, J. (2001). Automated air void analysis on hardened concrete Results of a European inter comparison testing program. *Cement and Concrete Research*, **31**, 1027–1031.

Emmanuel, B.O.A., Lev K. and Leslie, T. G. (1998). Mechanistic-based model for predicting reflective cracking in asphalt concrete-overlaid pavements. *Transportation Research Record*, **1629**, 234–241.

Engineers Canada. (2008). *Adapting to climate change: Canada's first national engineering vulnerability assessment of public infrastructure.* pp.250.

Evardsen, C. (1999). Water permeability and autogenous healing of cracks in concrete. *ACI Materials Journal*, **96,** 448-454.

Fwa, T.F. and Paramasivam, P. (1990). Thin steel fibre cement mortar overlay for concrete pavement. *Cement&Concrete Composites*, **12**, 175-184.

Gao, Song and Van Zijl, G.P.A.G. (2004). Tailoring ECC for commercial application. *Fibre-Reinforced Concretes (BEFIB'2004), RILEM Pro039*, 1391–1400.

Granger, S., Loukili, A., Pijaudier-Cabot, G., and Chanvillard, G. (2007). Experimental characterization of the self-healing of cracks in an ultra-high performance cementitious material: Mechanical tests and acoustic emission analysis. *Cement and Concrete Research*, **37**, 519–527.

Inaguma, H., Seki, M., Suka, K. and Rokugo, K. (2005). *Experimental study on crack-bridging ability of ECC for repair under train loading.* Proc. Of Int'l Workshop on HPFRCC in Structural Applications, Honolulu, Hawaii, USA., 499-508.

Jacob, T.R. (1990). Design Parameters for Use of Reinforced Stress-Absorbing Membrane Interlayers. *Transportation Research Record*, 1272.

Kallas, B.F. (1983). *Pavement Maintenance and Rehabilitation.* ASTM Publication Code Number (PCN) 04-881000-08, Philadelphia.

Kamada, T. and Li, V.C. (2000). The effects of surface preparation on the fracture behavior of ECC/concrete repair system. *Cement&Concrete Composites*, **22 (6)**, 423-431.

Kanda T., Li V.C. (1999). A new micromechanics design theory for pseudo strain-hardening cementitious composite. *ASCE Journal of Engineering Mechanics,* **124(4)**, 373-381.

Kendall, A., Lepech, M.D. and Keoleian, G.A. (2008). Materials design for

sustainability through life cycle modeling of Engineered Cementitious Composites. *Materials and Structures*, **41**, 1117-1131.

Kim, Y.Y., Kong, H.J. and Li, V.C. (2003). Design of Engineered Cementitious Composite (ECC) suitable for wet-mix shotcreting. *ACI Materials Journal,* **100,** 511-518.

Kong, H.J., Bike, S. and Li, V.C. (2003). Development of a Self-Consolidating Engineered Cementitious Composite Employing Electrosteric Dispersion / Stabilization. *Journal of Cement and Concrete Composites*, **25,** 301-309.

Kraai, P.P. (1985). Proposed test to determine cracking potential due to drying shrinkage of concrete. *Concrete Construction*, **30,** 775–778.

Kunieda M, and Rokugo, K. (2006). Recent Progress on HPFRCC in Japan. *Journal of Advanced Concrete Technology*, **4(1)**, 19-33.

Lepech, M. and Li, V.C. (2005a). *Durability and Long Term Performance of Engineered Cementitious Composites*. In Proceedings of International RELIM Workshop on HPFRCC in Structural Applications, Honolulu, Hawaii, pp. 165-174.

Lepech, M. and Li, V.C. (2005b). Water *Permeability of Cracked Cementitious Composites.* In: Proceeding of Eleventh International Conference on Fracture*,* Turin, Italy, pp. CD-Paper 4539.

Lepech, M. and Li, V.C., (2008). Large Scale Processing of Engineered Cementitious Composites. *ACI Materials Journal,***105(4)**, 358-366.

Li, M. and Li, V. C. (2007). Durability of HES-HPFRCC repair under mechanical and environmental loading conditions. *High Performance Fiber Reinforced Cement Composites*, 399-408.

Li, M. and Li, V.C. (2009). Influence of material ductility on performance of concrete repair. *ACI Materials Journals*, **106**, 419-428.

Li, V.C. (1993). From micromechanics to structural engineering – the design of cementitious composites for civil engineering applications. *JSCE J. Struc. Mech. & Earthquake Engineering*, **10 (2)**, 37-48.

Li, V.C. (1997). HPFRCC - Tailored Composites Through Micromechanical Modeling in Fiber Reinforced Concrete: Present and the Future, Banthia, N. A., Bentur and Mufti, A. Editor. *Canadian Society for Civil Engineering*, 64-97.

Li, V.C. (1998). ECC – tailored composites through micromechanical modeling. *Fiber Reinforced Concrete: Present and the Future*, CSCE, Montreal, 64-97.

Li, V.C. (2003a). On Engineered Cementitious Composites (ECC) – A review of the material and its applications. *Advanced Concrete Technology*, **1 (3)**, 215-230.

Li, V.C. (2003b). Durable Overlay Systems with Engineered Cementitious Composites (ECC). *International Journal for Restoration of Buildings and Monuments*, **9 (2)**, 1-20.

Li, V.C. and Lepech, M.D., (2004). Crack Resistant Concrete Material for *Transportation Construction, Transportation Research Board 83rd Annual Meeting Compendium of Papers, Paper* No. 04-4680, Washington, DC, USA.

Li, V.C. and Leung, C.K.Y. (1992). Theory of steady state and multiple cracking of random discontinuous fiber reinforced brittle matrix composites. *ASCE Journal of Engineering Mechanics*, **118,** 2246–2264.

Li, V.C., Fischer, G., Kim, Y.Y., Lepech, M., Qian, S., Weimann, M. and Wang, S. (2003). Durable link slabs for jointless bridge decks based on strain-hardening cementitious composites. *Report for Michigan Department of Transportation* RC-1438.

Li, V.C., Lepech, M., Wang, S., Weimann, M., and Keoleian, G., (2004). Development of Green ECC for Sustainable Infrastructure Systems. *Proc., Int'l Workshop on Sustainable Development and Concrete Technology,* Beijing, China, 181-192.

Li, V.C., Mishra, D.K. and Wu, H.C. (1995). Matrix Design for Pseudo Strain-Hardening Fiber Reinforced Cementitious Composites. *RILEM Journal of Materials and Structures*, **28,** 586-595.

Li, V.C., Wang S. and Wu C. (2001). Tensile strain-hardening behavior of PVA-ECC. *ACI Materials Journal*, **98 (6)**, 483-492.

Li, V.C., Wu C., Wang S., Ogawa A., Saito T. (2002). Interface tailoring for strain-hardening polyvinyl alcohol-Engineered Cementitious Composite (PVA-HPFRCC). *ACI Materials Journal*, **99(5)**, 463-472.

Lim Y.M. and Li V.C. (1997). Durable repair of aged infrastructures using trapping mechanism of engineered cementitious composites. *Cement&Concrete Composites*, **19(4)**, 373-385.

Lin, Z., Kanda, T. and Li, V.C. (1999). On interface property characterization and performance of fiber reinforced cementitious composites. *Concrete Science and Engineering, RILEM,* **1,** 173-184.

Loukili, A., Richard, P., and Lamirault, J. (1998). A study on delayed deformations of an ultra high strength cementious material. *ACI Recent Advances in Concrete Technology*, **179**, 929–949.

Maalej, M., Hashida, T. and Li, V.C., (1995). "Effect of Fiber Volume Fraction on the Off Crack-Plane Fracture Energy in Strain-Hardening Engineered Cementitious Composites", *Journal of the American Ceramic Society*, **78(12)**, 3369-3375.

Malhotra V.M. (1998) Role of supplementary cementing materials in reducing greenhouse gas emission. *CANMET Report MTL* 98-03, 16 pp.

Malhotra, V.M. (1970). Concrete ring for the determination of tensile strength of concrete. *ACI Materials Journal,.* **77,** 354–357.

Markovic I., Walraven J.C., van Mier J.G.M. (2004). Tensile behaviour of high performance hybrid fibre concrete. *Fracture Mechanics of Concrete Structures*, 1113-1120.

Marlowe I. (2003). *Emission factors programme Task 4(b): Review of cement sector pollution inventory.* Report No: 1425, Abingdon, Oxon.

Marshall, D.B. and Cox, B.N. (1988). A J-integral method for calculating steady-state matrix cracking stresses in composites. *Mechanics of Materials*, **8,** 127–133.

Maslehuddin, M., Saricimen, H. and Al-Mani, A. (1987). Effect of fly ash addition on the corrosion resisting characteristics of concrete. *ACI Materials Journal*, **84,** 42-50.

Mather B., Warner J. (2003). Why do concrete repairs fail. *<http://aec.engr.wisc.edu/resources/rsrc07.html>*.

McGhee, K.H. (1994). Portland Cement Concrete Resurfacing. NCHRP Synthesis of Highway Practice 204. *Transportation Research Board*, Washington, DC.

Mehta P.K. (1998). Role of pozzolanic & cementitious by-products in sustainable development of the concrete industry. *6th CANMET/ACI/JCI Conference: Fly Ash, Silica Fume, Slag & Natural Pozzolans in Concrete.*

Mehta P.K. (2001). Burrows R.W.. Building durable structures in the 21st century. *Conc Int*, **23(3)**, 57-63.

Mehta P.K. and Monteiro P.J.M. (2006). *Concrete: Structure, Properties, and Materials*. Third Edition, McGraw Hill, New York.

Mesbah, H.A. and Buyle-Bodin, F. (1999). Efficiency of polypropylene and metallic fibres on control of shrinkage and cracking of recycled aggregate mortars. *Construction and Building Materials,* **13**, 439–447.

Michigan Department of Transportation, (2009). *MDOT Bridge Design manual.*

Miller, John S.and Bellinger, William Y.(2003). *Distress identification manualfor the long-term pavement performance program.* US Department of Transportation, Federal Highway Administration.

Mindess S., Young J.F., Darwin D. (2003). *Concrete.* 2$^{nd}$ Ed., Prentice Hall, NJ.

Mokarem, D.W., Lane, D.S., Özyıldırım, H.Ç. and Sprinkel, M.M. (2008). *Measurement of early age shrinkage of Virginia concrete mixtures.* Final Report, VTRC 08-R9.

Morgan D.R. (1996). Compatibility of concrete repair materials and systems. *Construction of Building Materials*, **10(1)**, 57-67.

Mu, R., Miao, C., Luo, X. and Sun, W. (2002). Interaction between loading, freeze–thaw cycles, and chloride salt attack of concrete with and without steel fiber reinforcement. *Cement and Concrete Research*, **32**, 1061–1066.

Mukhtar, M.T. (1996). *Interlayer stress absorbing composite (ISAC) for mitigating reflection cracking in asphalt concrete overlays*. Department of Civil Engineering University of Illinois at Urbana-Champaign.

Ostro B. (1994). Estimating the health effects of air pollutants: A method with an application to Jakarta. *Policy Research Working Paper 1301*, World Bank, Policy Research Department, Washington, D.C.

Özyıldırım, Ç. and Gomez, J.P. (1999). *High-performance concrete in a bridge in Richlands, Virginia*. Final Report, VTRC 00-R6.

Pigeon, M. and Pleau, R. (1995) *Durability of Concrete in Cold Climates*. Chapman & Hall, London.

Pigeon, M., Gagne, R. and Foy, C. (1987). Critical air void spacing factors for low water cement ratio concretes with and without silica condensed silica fume. *Cement and Concrete Research*, **17**, 896–906.

Powers, T. C. (1964a). Frost Resistant Concrete. *Journal of the PCA Development Laboratories*, pp.19.

Powers, T. C. (1964b). Topics in Concrete Technology 3: Mixtures Containing Intentionally Entrained Air. *Journal of the PCA Development Laboratories*, **6**, 19–42.

Powers, T. C. (1965). Topics in Concrete Technology 3: Characteristics of Air-Void Systems. *Journal of the PCA Development Laboratories*, **7**, 23–41.

Qian, S. (2007). *Influence of Concrete Material Ductility on the Behavior of High Stress Concentration Zones*. Thesis (Ph.D.). University of Michigan: Ann Arbor.

Qian, S. and Li, V.C. (2007). Simplified inverse method for determining the tensile strain capacity of strain hardening cementitious composites. *Journal of Advanced Concrete Technology,* **5,** 235–246.

Qian, S. and Li, V.C. (2008). Simplified inverse method for determining the tensile properties of strain hardening cementitious composites. *Journal of Advanced Concrete Technology,* **6 (2) ,** 353–363.

Qian, S., Zhou, J., Rooij, M.R., Schlangen, E., Ye, G. and Breugel, K.V. (2009). Self-healing behavior of strain hardening cementitious composites incorporating local waste materials. *Cement&Concrete Composites*, **31**, 613–621.

Ramm W. and Biscoping M. (1998). Autogenous healing and reinforcement corrosion of water-penetrated separation cracks in reinforced concrete. *Nuclear Engineering and Design*, **179**, 191-200.

Raupach M. (2006). Concrete repair according to the new European standard EN-1504, *RWTH Aachen*.

Reinhardt, H.W. and Jooss, M. (2003) Permeability and self-healing of cracked concrete as a function of temperature and crack width. *Cement and Concrete Research*, **33,** 981-985.

Risser, R.J., LaHue, S.P., Vogit, G.F. and Mack, J.W. (1993). Ultra-thin concrete overlays on existing asphalt pavement. *Proceedings of the Fifth International Conference on Concrete Pavement Design and Rehabilitation*, 2, Purdue University, West Lafayette, Indiana, 247-254.

Rossi P. and Parant E. (2005). Mechanical behaviours of a multi-scale fibre reinforced cement composite (MSFRCC) subjected to severe loading conditions. *Proceedings of ConMat'05*.

Roy, D.M. and Idorn, G.M. (1983). Hydration, structure, and properties of blast furnace slag cements, mortars, and concrete. *ACI Journal*, **79(6)**, 445-457.

Sahmaran M., Li M. and Li V. (2007). Transport properties of HPFRCC under chloride exposure. *ACI Materials Journal*, **104**, 604-611.

Şahmaran, M. and Li, V.C., (2009a). Durability properties of micro-cracked ECC containing high volumes fly ash. *Journal of Cement and Concrete Research*, **39**, 1033-1043.

Şahmaran, M. and Li,V.C. (2009b). Influence of Microcracking on Water Absorption and Sorptivity of ECC. *RILEM-Journal of Materials and Structures*, **42**, 593-603.

Şahmaran, M., and Li, V.C. (2007). De-icing Salt Scaling Resistance of Mechanically Loaded Engineered Cementitious Composites. *Cement and Concrete Research*, **37**, 1035–1046.

Şahmaran, M., Lachemi, M., and Li, V.C. (2009b). Assessing the Durability of Engineered Cementitious Composites under Freezing and Thawing Cycles. *Journal of ASTM International*, **6**, 1–6.

Şahmaran, M., Lachemi, M., Hossain K.M.A. and Li, V.C. (2009a). Internal Curing of Engineered Cementitious Composites for Prevention of Early Age Autogenous Shrinkage Cracking. *Cement and Concrete Research*, **39**, 893-901.

Şahmaran, M., Lachemi, M., Hossain, K. M. A., Ranade, R. and Li, V. C. (2009c). Influence of Aggregate Type and Size on the Ductility and Mechanical Properties of Engineered Cementitious Composites. *ACI Materials Journal*, **106 (3)**, 308-316.

Şahmaran, M., Li, M. and Li, V.C. (2007a). Transport properties of Engineered Cementitious Composites under chloride exposure. *ACI Materials Journal*, **104**, 604-611.

Şahmaran, M., Yaman, İ. Ö. and Tokyay, M. (2007b). Development of High Volume Low-Lime and High-Lime Fly-Ash-Incorporated Self Consolidating Concrete. *Magazine of Concrete Research,* **59**, 97-106.

Sherman, George (1982). *Minimazing reflection cracking of pavement overlays.* National Cooperative Research Program Synthesis of Highway Practice 92.

Sikdar, P.K., Jain, S.S., Bose, S., and Kumar, P. (1999). Premature cracking of flexible pavements. *Indian Roads Congress*, Paper No. 461, **60** (3), 355-398.

Smith, K.D., Yu, H.T. and Peshkin, D.G. (2002). *Portland Cement Concrete Overlays: State of the Technology Synthesis*. Federal Highway Administration, Report No: DTFH61-00-P-00507.

Soroushian, P., Nagi, M. and Hsu, J. (1992). Optimization of the use of lightweight aggregates in carbon fiber reinforced cement. *ACI Materials Journal*, **89**, 267-276.

Sprinkel, M. (2000). *Evaluation of latex-modified and silica fume concrete overlays placed on six bridges in Virginia*. Final Report, VTRC 01-R3.

Sprinkel, M. (2003). *Evaluation of corrosion inhibitors for concrete bridge deck patches and overlays*. Final Report, VTRC 03-R14.

Sprinkel, M. (2004). *Performance specification for high performance concrete overlays on bridges*. Final Report, VTRC 05-R2.

Stang, H. and Li, V.C. (1999). Extrusion of ECC-material. *In Proc. Of High Performance Fiber Reinforced Cement Composites 3 (HPFRCC 3)*, pp. 203-212.

Stark, J., and Ludwig, H.M. (1997). Freeze-Thaw and Freeze-Deicing Salt Resistance of Concretes Containing Cement Rich in Granulated Blast Furnace Slag. *ACI Materials Journal*, **94**, 47–55.

Sun, W., Zhang, Y.M., Yan, H.D., Mu, R. (1999). Damage and damage resistance of high strength concrete under the action of load and freeze-thaw cycles. *Cement and Concrete Research*, **29**, 1519–1523

Suthiwarapirak, P., Matsumoto, T. and Kanda, T. (2002). Flexural fatigue failure characteristics of an Engineered Cementitious Composite and Polymer Cement Mortars. *Materials, Conc. Struc. Pavements*, **57**, 121-134.

Turkish Cement Manufacturers' Association (TCMA), (2009). <*http://tcma.org.tr/ENG/*>.

Vaysburd A., Brown C., Bissonnette B., Emmons P. "Realcrete" vs. "Labcrete" *Conc Int*, 26(2), 2004, 90-94.

Vecchio F., Bucci F. (1999). Analysis of repaired reinforced concrete structures. *ASCE Str Eng*, **125(6)**, 644-652.

Von Quintus, H.L. (2007). *Techniques for Mitigation of Reflective Cracking*. Applied Research Associates, Inc., Champaign, IL, USA.

Wang, K., Jansen, D, Shah, S., Karr, A. (1997). Permeability Study of Cracked Concrete. *Cement and Concrete Research*, **27(3)**, 381-393.

Wang, S. and Li, V.C. (2004). Tailoring of pre-existing flaws in ECC matrix for saturated strain hardening. *Proceedings of FRAMCOS-5*, Vail, Colorado, USA, pp. 1005–1012.

Wang, S. and Li, V.C. (2007). Engineered Cementitious Composites with highvolume fly ash. *ACI Materials Journal*, **104**, 233–241.

Weimann, M.B. and Li, V.C. (2003a). Hygral behavior of engineered cementitious composites (ECC). *International Journal for Restoration of Buildings and Monuments*, **9**, 513-534.

Weimann, M.B. and Li, V.C., (2003b). Drying Shrinkage and Crack Width of ECC, *Seventh International Conference on Brittle Matrix Composites*, Warsaw, Poland, pp. 37-46.

Yang Y., Lepech M.D., Yang E., Li V.C. (2009). Autogenous healing of Engineered Cementitious Composites under wet–dry cycles. *Cement and Concrete Research*, **39(5)**, 382-390.

Yang, Y., Lepech, M.D. and Li, V.C. (2005). Self-healing of ECC under cyclic wetting and drying. *Proceedings of Int'l Workshop on Durability of Reinforced Concrete under Combined Mechanical and Climatic Loads*, Qingdao, China, 231-242.

Zhang, H., Keoleian, G.A. and Lepech, M.D. (2008). An integrated life cycle assessment and life cycle analysis model for pavement overlay systems. *First International Symposium on Life-Cycle Civil Engineering*, Varenna, Lake Como, Italy: CRC Press/Balkema.

Zhang, J. and Li, V.C. (2002). Monotonic and fatigue performance in bending of fiber reinforced Engineered Cementitious Composite in overlay system. *Cement and Concrete Research*, **32**, 415-423.

Zhang, M.N. (1995). Microstructure, crack propagation, and mechanical properties of cement pastes containing high volumes of fly ashes. *Cement and Concrete Research*, **25**, 1165-1178.

## PERSONAL INFORMATION

| | |
|---|---|
| Name and Surname | : Hasan Erhan YÜCEL |
| Nationality | : T.C. |
| Birth place and date | : Antakya/1981 |
| Marital status | : Married – 1 child |
| Phone number | : 530 608 07 89 / 342 317 24 52 |
| Fax | : 342 360 11 07 |
| E-mail | : yucel@gantep.edu.tr |

## EDUCATION

| Degree | Graduate School | Year |
|---|---|---|
| Master | University of Gaziantep | 2007 |
| Bachelor | University of Gaziantep | 2004 |
| High School | Kahramanmaraş Super High School | 1999 |

## WORK EXPERIENCE

| Year | Place | Enrollment |
|---|---|---|
| 2005-2006 | Nigde University | Research Assistant |
| 2006-Present | University of Gaziantep | Research Assistant |
| 2012 (May-July - 3months) | Vicolocorto Association, Italy | Project Participant |

## PUBLICATIONS

### A. International Journals

**A1.** Şahmaran, M., Lachemi, M., Erdem, T. K. and **Yücel, H. E.** "Use of Spent Foundry Sand and Fly ash for the Development of Green Self-Consolidating Concrete," *RILEM-Journal of Materials and Structures*, **44 (7)**, 1193-1204 (2011).

**A2.** Şahmaran M., Özbay, E., **Yücel, H. E.**, Lachemi, M. and Li, V. C. "Effect of Fly Ash and PVA Fiber on Microstructural Damage and Residual Properties of Engineered Cementitious Composites Exposed to High Temperatures," *ASCE Journal of Materials in Civil Engineering,* **23 (12),** 1735-1745 (2011).

**A3.** Şahmaran M., Özbay, E., **Yücel, H. E.**, Lachemi, M. and Li, V. C. "Frost Resistance and Microstructure of Engineered Cementitious Composites: Influence of Fly Ash and Micro Poly-Vinyl-Alcohol Fiber," *Cement and Concrete Composites*, **34 (2),** 156-165 (2012).

**A4**. Şahmaran M., **Yücel, H. E.**, Demirhan, S., Arik, M.T., and Li V. C. "Combined Effect of Aggregate and Mineral Admixtures on the Tensile Ductility of ECC," *ACI Materials Journal*, **109 (6)**, 627-638 (2012).

**A5**. **Yücel, H. E.**, Jashami, H., Şahmaran, M., Guler, M. and Yaman, I.O. "Thin ECC Overlay Systems for Rehabilitation of Rigid Concrete Pavements", *Magazine of Concrete Research*, **65 (2)**, 108-120 (2013).

**A6**. Ozbay E., Şahmaran, M., Lachemi M. and **Yücel, H. E.**, "Self-Healing of Microcracks in High Volume Fly Ash Incorporated Engineered Cementitious Composites," *ACI Materials Journal*, **110 (1)**, 33-44 (2013).

**A7.** Şahmaran, M., Bilici, Z., Özbay, E., Erdem, T. K., **Yücel, H. E.**, and Lachemi, M. "Improving the Workability and Rheological Properties of Engineered Cementitious Composites using Factorial Experimental Design," *Composites: Part B*, **45 (1)**, 356-368 (2013).

**A8**. Ozbay E., Şahmaran, M. Lachemi M. and **Yücel, H. E.**, "Effect of Microcracking on the Frost Durability of High Volume Fly Ash and Slag Incorporated ECC," *ACI Materials Journal*, Accepted for Publication (2013).

**A9**. Ozbay E., Şahmaran, M., **Yücel, H. E.**, Erdem, T. K. and Lachemi, M. "The Effect of Sustained Flexural Loading on Self-Healing of Engineered Cementitious Composites," Journal of Advanced Concrete Technology, Accepted for Publication (2013).

**B. International Congress, Conference and Symposium**

**B1**. Şahmaran, M., Yıldırım, G. and **Yücel, H. E.** "Green Engineered Cementitious Composites: A Durability Point of View" *2nd International Conference on Microstructure Related Durability Properties of Cementitious Composites*, Amsterdam, Netherland, 11-13 April 2012.

**B2**. Şahmaran, M., Yıldırım, G., Ahmed, K., **Yücel, H. E.** and Ozbay, E. "Effects of Different Environmental Exposures on Self-Healing Capacity of Cementitious Composites" *10th International Congress on Advances in Civil Engineering*, 17-19 October 2012, Middle East Technical University, Ankara, Turkey.

**B3**. Şahmaran, M., **Yücel, H. E.**, Al-Emam, M., Yaman, I. O. and Guler M. "Bond Characteristics of Engineered Cementitious Composites Overlays," *92th Annual Meeting of Transportation Research Board*, Washington D.C., USA, 13-17 January, 2013.

**C. National Congress, Conference and Symposium**

**C1.** M. Şahmaran, **H.E. Yücel**, E. Özbay, ve T.K. Erdem "Uçucu Kül Kullanım Oranının Yüksek Performanslı Çimento Esaslı Kompozitlerin Donma-Çözülme Dayanıklılığına Etkisi," *8. Ulusal Beton Kongresi*, 277-287, İzmir, 5-7 Ekim, 2011.

**RESEARCH PROJECTS**

**1.** Sürdürülebilir Kalkınma için Mikro-mekanik Olarak Tasarlanmış Şekil Değiştirme Sertleştirmesi Gösteren Yüksek Performanslı Lif Donatılı Çimento Esaslı Kompozitler, TÜBİTAK - MAG-108M495, **Scholar**, 2009-2012.

**2.** Sürdürülebilir Karayolu Üstyapı Kaplamaları için Çatlaksız ve Sünek Beton Tasarımı, University of Gaziantep, BAP, MF.10.09, **Researcher**, 2010-2012.